2018

Mechanosensing By The Nuclear Lamina: From Embryonic Development To Aging

Sangkyun Cho
University of Pennsylvania, chosangkyun89@gmail.com

Mechanosensing By The Nuclear Lamina: From Embryonic Development To Aging

Abstract
'Nuclear mechanosensing' encompasses a wide range of biophysical pathways that are emerging as key processes in the regulation of cell function and fate. Many of these mechanisms involve the main structural protein of the nucleus, lamin-A, which is abundant in stiff and mechanically stressed tissues such as striated muscle, but is comparatively low in soft tissues such as the brain. Lamin-A's increase with tissue stiffness correlates strongly with elevated levels of collagen-I fibers in the extracellular matrix (ECM), but mechanisms and functional consequences of any matrix-nucleus interplay remain unclear. Here, in the first set of studies, we show that lamin-A and collagen-I exhibit tightly coupled mechano-sensitivity in the first functional vertebrate organ, the beating embryonic heart, following a mechanism for tension-suppressed turnover that confers mechano-protection against DNA damage. Lamin-A and collagen-I increase together as the heart stiffens daily in embryogenesis, but their levels are found here to be modulated within 1-2 hours by rapid and reversible perturbations of actomyosin contractility or ECM mechanics. In both intact hearts and in isolated cardiomyocytes, suppression of lamin-A – combined with high contractile stress – results in i) increased nuclear envelope rupture, ii) cytoplasmic mis-localization of DNA repair factors, and iii) accumulation of DNA damage, which ultimately causes arrythmia. Embryonic cardiomyocytes on stiff collagen-coated gels show increased lamin-A levels compared to those on soft gels, suggesting a cell-intrinsic protective mechanism against DNA damage. Interphase phosphorylation of lamin-A emerges as a key posttranslational modification that gives rise to such mechano-sensitivity, as phosphorylation and subsequent degradation of lamin-A are suppressed with myosin-II-dependent cell spreading. This mechanism of tension-suppressed turnover is further examined in a second set of studies, which focuses on the aging-associated lamin-A mutant, 'progerin'. Using a novel mass spectrometry-based workflow, we find that progerin phosphorylation in patient iPS-derived cells is lower and less mechanosensitive compared to normal lamin-A and C, suggesting that a loss in the nucleus' ability to dynamically remodel in response to stress could contribute to genome instability and aging. Mechanosensing by lamin-A is thus critical not only in embryonic development, but also in disease and aging of mature tissues.

Degree Type
Dissertation

Degree Name
Doctor of Philosophy (PhD)

Graduate Group
Chemical and Biomolecular Engineering

First Advisor
Dennis E. Discher

Keywords
Development, DNA damage, ECM, Matrix, Mechanobiology, Nuclear lamina

MECHANOSENSING BY THE NUCLEAR LAMINA:

FROM EMBRYONIC DEVELOPMENT TO AGING

Sangkyun Cho

A DISSERTATION

in

Chemical and Biomolecular Engineering

Presented to the Faculties of the University of Pennsylvania

in

Partial Fulfillment of the Requirements for the

Degree of Doctor of Philosophy

2018

Supervisor of Dissertation

_____

Dennis E. Discher

Robert D. Bent Professor of Chemical and Biomolecular Engineering

Graduate Group Chairperson

_____

John C. Crocker, Professor of Chemical and Biomolecular Engineering

Dissertation Committee

Daeyeon Lee, Professor of Chemical and Biomolecular Engineering

Ravi Radhakrishnan, Professor of Chemical and Biomolecular Engineering

Benjamin L. Prosser, Assistant Professor of Physiology

Jonathan A. Epstein, William Wikoff Smith Professor of Cardiovascular Research

Dedicated to

my family and friends

ACKNOWLEDGMENTS

The past five years have been a truly transformative journey. Early on I had been warned by many that ‘a PhD will turn you into a one-dimensional person’, but I have found my experience to be the opposite – it has been a time of immeasurable personal growth and exploration both into and well beyond my field of study.

To my advisor Dennis, who no one could ever outwork – it has been a great pleasure and opportunity to be able to pick your brain every day. On the first day we met, you told me that I am here to ‘learn how to learn’. I am grateful to have been able to learn with you, and I look forward to continue learning, wherever my path takes me.

I have been blessed with life-long friendships at every stage of my life, but the friendships I have built here at Penn will always have a special place in my heart. The memories we share are as valuable to me as the lessons learned in the lab. In particular, I would like to thank both previous and current members of the Discher lab cubicle line – I have enjoyed our daily lunch runs and our many conversations in between.

I would also like to acknowledge all of my collaborators at the Medical School and the Wistar Institute, as well as my thesis committee members for the many thought-provoking discussions and feedback that helped shape this thesis.

Most importantly, I am grateful for the loving support that my family (both ‘old’ and new members!) has given me over the years. Thank you for having faith in me in whatever I set out to achieve, and for always reminding me what is important in life.

ABSTRACT

MECHANOSENSING BY THE NUCLEAR LAMINA:

FROM EMBRYONIC DEVELOPMENT TO AGING

Sangkyun Cho

Dennis E. Discher

'Nuclear mechanosensing' encompasses a wide range of biophysical pathways that are emerging as key processes in the regulation of cell function and fate. Many of these mechanisms involve the main structural protein of the nucleus, lamin-A, which is abundant in stiff and mechanically stressed tissues such as striated muscle, but is comparatively low in soft tissues such as the brain. Lamin-A's increase with tissue stiffness correlates strongly with elevated levels of collagen-I fibers in the extracellular matrix (ECM), but mechanisms and functional consequences of any matrix-nucleus interplay remain unclear. Here, in the first set of studies, we show that lamin-A and collagen-I exhibit tightly coupled mechano-sensitivity in the first functional vertebrate organ, the beating embryonic heart, following a mechanism for tension-suppressed turnover that confers mechano-protection against DNA damage. Lamin-A and collagen-I increase together as the heart stiffens daily in embryogenesis, but their levels are found here to be modulated within 1-2 hours by rapid and reversible perturbations of actomyosin contractility or ECM mechanics. In both intact hearts and in isolated cardiomyocytes, suppression of lamin-A – combined with high contractile stress – results in i) increased nuclear envelope rupture, ii) cytoplasmic mis-localization of DNA repair factors, and iii) accumulation of DNA damage, which ultimately causes arrythmia. Embryonic cardiomyocytes on stiff collagen-coated gels show increased lamin-A levels compared to those on soft gels, suggesting a cell-intrinsic protective mechanism against DNA damage. Interphase phosphorylation of lamin-A emerges as a key posttranslational modification that gives rise to such mechano-sensitivity, as phosphorylation and subsequent degradation of lamin-A are suppressed with myosin-II-dependent cell spreading. This mechanism of tension-suppressed turnover is further examined in a second set of studies, which focuses on the aging-associated

lamin-A mutant, ‘progerin’. Using a novel mass spectrometry-based workflow, we find that progerin phosphorylation in patient iPS-derived cells is lower and less mechanosensitive compared to normal lamin-A and C, suggesting that a loss in the nucleus’ ability to dynamically remodel in response to stress could contribute to genome instability and aging. Mechanosensing by lamin-A is thus critical not only in embryonic development, but also in disease and aging of mature tissues.

TABLE OF CONTENTS

LIST OF TABLES

LIST OF FIGURES

GLOSSARY

Acronym	***Full term/name***
AGN	Antagonist to retinoic acid
BSA	Bovine serum albumin
CM	Cardiomyocyte
Col'ase	Collagenase
DCM	Dilated cardiomyopathy
ECM	Extracellular matrix
EM	Electron microscopy
ER	Endoplasmic reticulum
FCH	Familial cardiac hypertrophy
FEA-MS	Fine excision-alignment mass spectrometry
GFP	Green fluorescent protein
HCC	Hepatocellular Carcinoma
HCM	Hypertrophic cardiomyopathy
HGPS	Hutchinson-Gilford progeria syndrome
IF	Immunofluorescence
INM	Inner nuclear membrane
iPS	Induced pluripotent stem cell
LINC	Linker of nucleoskeleton and cytoskeleton
MMP	Matrix metalloprotease
MS (LC-MS/MS)	Mass spectrometry (liquid chromatography-tandem mass spectrometry)
MSC	Mesenchymal stem cell
ONM	Outer nuclear membrane
PBS	Phosphate buffered saline
pSer	Phosphorylated serine
PTM	Post-translational modification
RA	Retinoic acid
ROCK	Rho-associated protein kinase
SRF	Serum response factor
SUN1/2	SUN domain-containing protein 1/2
TGM	Transglutaminase
YAP/TAZ	Yes-associated protein / transcriptional coactivator with PDZ-binding motif

Table 1. Glossary of terms and abbreviations

CHAPTER 1
Mechanosensing by the nucleus: from pathways to scaling relationships

This chapter appears in *Journal of Cell Biology* 10.1083/jcb.201610042 (2017), and in *Annual Reviews of Biophysics* 46:295-315 (2017)

Dr. Jerome Irianto contributed to writing the last paragraph of Section 1.2.1

Abstract

The nucleus is linked mechanically to the extracellular matrix (ECM) via multiple polymers that transmit forces to the nuclear envelope and into the nuclear interior. Here, we review some of the emerging mechanisms of nuclear mechanosensing, which range from changes in protein conformation and transcription factor localization to chromosome reorganization and membrane dilation up to rupture. Nuclear mechanosensing encompasses biophysically complex pathways that often converge on the main structural proteins of the nucleus, the lamins. We also perform meta-analyses of public transcriptomics and proteomics data, which indicate that some of the mechanosensing pathways relaying signals from the collagen matrix to the nucleus apply to a broad range of species, tissues, and diseases.

1.1 Introduction

The physical properties of tissues depend on the cells that comprise them and seem to be affected by tissue use. For example, muscle, cartilage, and bone when suitably exercised generate or resist mechanical forces that can be many times their own weights, and so it is understandable that these tissues and their cells require some stiffness or rigidity to maintain their form under high stress. Brain and marrow, in contrast, are protected from external stress by bone, and so perhaps one reason they are soft is that they simply do not need to be stiff to resist stress. It is now reasonably well-established that cells have the ability to sense and respond to mechanical forces of varying magnitude, direction, and frequency (Ingber, 2006). Since the largest organelle of a cell is its nucleus, it is also plausible that the nucleus has a similar ability to 'mechanosense' the tissue microenvironment. Forces and resistance external to nuclei are increasingly understood to affect processes ranging from protein conformation and assembly, to localization of transcription factors, chromosome organization, and nuclear envelope dilation up to rupture – all of which might affect gene expression (**Figure 1.1**).

Tissue stiffness is molecularly determined by the most abundant proteins in vertebrates, the helical fibrillar collagens of the extracellular matrix (ECM). Cells interact physically with the ECM as the cytoskeleton exerts stress on the ECM via adhesions, and this stress is sufficient to alter the morphologies of cells (Discher et al., 2005; Marganski et al., 2003) and their nuclei (Dahl et al., 2008; Khatau et al., 2009; Kim et al., 2014a; Kim et al., 2015; Versaevel et al., 2012). With soft ECM, most normal cell types downregulate their actin-myosin contractile machinery and exert much less tension than with stiff ECM. Importantly, cytoskeleton-induced stresses on matrix *outside* of the cell puts an equal-but-opposite cytoskeletal stress on the nucleus *inside* (Alam et al., 2015; Chancellor et al., 2010; Lovett et al., 2013) – as if the nucleus is just a spheroidal inclusion of ECM anchored within the cell by factors and assemblies that are functionally analogous to focal adhesions (which are well-known to be mechanosensitive). Indeed, much like the plasma membrane and cortex at the cell-ECM boundary, the nuclear envelope is a dynamic, force-sensitive interface between the cytoplasm and the chromatin. The nuclear envelope's main structural 'cortex' is the lamina, composed of the helix-rich fibrillar lamin proteins (Goldman et al.,

2002) that assemble just below the inner nuclear membrane (INM) (Gruenbaum et al., 2005). A-type (lamin-A & C) and B-type (lamin-B1 & B2) lamins tether the nucleus to the cytoskeleton via the LINC (Linker of Nucleoskeleton and Cytoskeleton) complex (Crisp et al., 2006). The nuclear envelope harbors many other proteins (Korfali et al., 2012; Schirmer et al., 2003), and some such as those of the LEM family (LAP2α, emerin, and MAN1) specifically associate with the lamins. Heterochromatin at the nuclear periphery (Paddy et al., 1990; Solovei et al., 2013) and a wide range of transcription factors (Lloyd et al., 2002; Margalit et al., 2005; Rodriguez et al., 2010; Wilson and Foisner, 2010) also interact with the lamina. The nuclear envelope and its lamina are thus well-positioned within the cell to serve as a multiplexing interface that can mechanotransduce in its regulation of the cell's genome.

Recently, new approaches that range from biophysical methods for probing nuclear mechanics to mass spectrometry (MS)-based characterization of protein modifications have expanded our understanding of nuclear mechanosensing. We start the review by discussing the recent insights these new technological advances have provided, in particular in the assessment of the direct physical effects that external force has on nuclear protein conformation and phosphorylation states. This is followed by summaries of stress-induced changes in localization of transcription factors, chromosome conformation and organization, nuclear envelope dilation, and finally, rupture. Links to embryonic development, disease, and aging are discussed, particularly in the context of the many 'nuclear envelopathies' that result from mutations in structural components of the nucleus. Lastly, a 'big picture' analysis of public transcriptome and proteome data for diverse tissues helps to establish stiffness-dependent scaling of key mechanosensory proteins as a broad, polymer physics foundation for nucleus mechanosensing.

1.2 Mechanosensing mechanisms and pathways

1.2.1 Force-induced changes in protein conformation and phosphorylation states

Mechanical stress exerted on or by the cell can deform proteins, and in some cases the stress-induced conformational changes regulates the activity of enzymes acting on the protein. In the ECM, tension stabilizes collagen-I fibrils against enzymatic degradation by matrix metalloproteinase (Flynn et al., 2010). Given the primary role of collagen in maintaining the mechanical integrity of tissue, such resistance with stress seems reasonable. In the cytoskeleton, the Cas substrate domain protein p130Cas unfolds upon mechanical stretching, exposing cryptic tyrosine residues for subsequent phosphorylation by Src-family kinases (Sawada et al., 2006). In isolated nuclei, at least one domain of lamin-A/C unfolds when nuclei are sheared, as evidenced by increased reactivity of a cryptic cysteine residue (Cys^{522}) (Swift et al., 2013). MS analyses further reveal that, in intact cells cultured on soft collagen-coated gels versus stiff gels, lamin-A/C phosphorylation increases at all of four different sites in either the head domain (Ser22) or tail domain (Ser390, Ser404, Thr424) (Swift et al., 2013). Importantly, culturing cells on soft gels results in rounded cells with wrinkled nuclei – as if there is excess membrane compared to cells grown on stiff gels that promote cell spreading and nuclear flattening. Total lamin-A/C levels ultimately reach lower steady-state levels (by about 50% or more) in cells cultured on soft gels (without affecting lamin-B1/B2), suggesting that low tension in the cell and nucleus destabilizes the lamin-A/C coiled-coil dimers, favoring phosphorylation by constitutive kinase(s) and promoting subsequent degradation (**Figure 1.1A**). Increased turnover is evident in highly phosphorylated, low molecular weight bands in immunoblots (Buxboim et al., 2014). 'Stress-strengthening' thus seems to apply to lamin-A/C as well as collagen-I, which are both fibrous assemblies of helical multimers.

Interphase phosphorylation of nuclear lamins – as with cytoskeletal intermediate filament (IF) proteins (Chang and Goldman, 2004) – is thought to be a major mechanism responsible for regulating filament assembly and localization. Another recent study identified 20 phospho-sites within the lamin-A/C protein, eight of which were high phosphate-turnover sites located within

three ‘hot spot’ regions (Kochin et al., 2014). Imaging of phospho-mimetic mutants in interphase cells revealed that Ser22 and Ser392 (and to a lesser degree Ser390, Ser404, and Ser407) dominated the regulation of lamin assembly and dynamics. Phosphorylation favors dissociation from the lamina into the nucleoplasm and enhances nucleoplasmic mobility (Kochin et al., 2014) – although degraded forms of these constructs should be considered (Buxboim et al., 2014). Even the precursor prelamin-A degrades more upon Akt-mediated phosphorylation at Ser404 (**Figure 1.1A**) (Bertacchini et al., 2013). Mitotic phosphorylation of lamins is a key driver of nuclear envelope disassembly in cells rounded for division (Gerace and Blobel, 1980; Heald and McKeon, 1990) and is 10-20 fold higher than during interphase (Buxboim et al., 2014). The higher phosphorylation of lamin-A/C (and lower total lamin-A/C levels) observed in cells cultured on soft gels is consistent with such cells being more rounded under low stress, although key kinases that are upregulated in mitosis (eg. CDK1) are unlikely to have a role in interphase (Buxboim et al., 2014). These results collectively suggest that matrix stiffness-derived cell and nuclear tension induces conformational changes in lamin coiled-coil dimers (analogous to a rope being stretched from either side) (Fig. 1A & a), which sterically hinders access of kinases including Cdks, PKC, and Akt (Buxboim et al., 2014). This mechanism of tension-inhibited phosphorylation provides the biophysical basis for a ‘lose it or use it’ model (Dingal and Discher, 2014), whereby lamin-A/C is degraded under low-stress conditions but stabilized under high-stress conditions.

Tensile forces can also alter phosphorylation states of emerin (Guilluy et al., 2014), another nuclear envelope protein that mediates the mechanical communication between the nucleus and the cytoplasm (**Figure 1.1B&b**). With isolated nuclei, application of sequential mechanical tension using magnetic tweezers on nesprin-1 antibody-coated beads led to stress-stiffening and an increase in phosphorylation of emerin at Tyr74 and 95 by Src kinase. Mutation of these residues abolished the stiffening effect, indicating the importance of these phospho-sites for emerin mechanosensitivity. Intact cells on stiff substrates showed high emerin phosphorylation that was reduced with myosin-II inhibition by blebbistatin treatment. These results confirm nuclear regulation of signaling by intracellular tension. However, contrary to lamin-A/C, lower expression of emerin stiffens the nucleus, and stress application increases emerin phosphorylation. Indeed,

non-phosphorylatable mutants of Tyr74 and Tyr95 in intact cells led to fewer stress fibers, reduced migration, decreased nuclear localization of the transcription co-activators YAP/TAZ, and decreased transcription by the transcription factor serum response factor (SRF) that is a master regulator of numerous actin cytoskeletal proteins. Detailed mechanisms of how emerin phosphorylation initiates these downstream changes remain unclear, but these findings confirm the crucial role of nuclear envelope proteins not only in sensing mechanical stress but also in regulating cell behavior and phenotype.

1.2.2 Nuclear localization of mechanosensitive transcription factors

Cell tension modulates nuclear translocation of mobile regulators (e.g. transcription factors), at least in cellular mechanotransduction, if not direct mechanosensing by the nucleus (**Figure 1.1C**&**c**) (Halder et al., 2012; Ho et al., 2013). Perhaps the best characterized mechanotransducing transcriptional regulators are YAP/TAZ, which influence growth in the canonical Hippo pathway and tend to localize to the nucleus in high-tension cells cultured on stiff substrates (Dupont et al., 2011). Although there have been many reports of exceptions and complexity in YAP/TAZ responses (Chopra et al., 2014; Swift et al., 2013), nuclear entry of YAP/TAZ can induce a wide range of downstream signaling cascades mediating complex cellular processes including differentiation (Dupont et al., 2011; Sun et al., 2014) and even contribute to storage of mechanical 'memory' of past ECM interactions (Yang et al., 2014a). Conversely, at least one transcription factor, NKX-2.5, enters the nucleus in response to *low* tension, and in the nucleus it functions as a 'mechano-repressor' to repress expression of genes contributing to high tension states (e.g. α-smooth muscle actin, *ACTA2*) (Dingal et al., 2015). Translocation in and out of the nucleus can be regulated by a variety of mechanisms including phosphorylation (of YAP1 (Murphy et al., 2014)), but whether YAP/TAZ or NKX-2.5 interact directly or even indirectly with mechanosensitive factors in the nucleus or at the nuclear envelope remains unclear.

Translocation into the nucleus can indeed result from stresses affecting specific interactions with nuclear envelope proteins (Ho et al., 2013; Swift et al., 2013). Stiff substrates drive translocation of the transcription factor RARγ (retinoic acid receptor gamma) into the

nucleus, a nuclear receptor modulated by retinoic acid agonists and antagonists, and entry drives lamin-A/C transcription (**Figure 1.1D&d**) (Swift et al., 2013). Immunoprecipitation followed by MS (IP-MS) identified several binding partners of RARγ including SUN2, which shuttles between the ER (endoplasmic reticulum) and the INM (inner nuclear membrane) (Figure 1.1A). Overexpression of SUN2 floods the ER with protein and results in rounded nuclei with decreased lamin-A/C levels and increased cytoplasmic RARγ. Conversely, high lamin-A/C effectively stabilizes nuclear retention of SUN2 and RARγ so that lamin-A/C ultimately regulates its own transcription. This feedback mechanism between the level of a protein, as regulated by tension on the nucleus, and the level of its transcript is illustrative of a 'mechanobiological gene circuit' (Swift et al., 2013). Additionally, lamin-A/C as well as emerin modulate nuclear actin polymerization, which controls nuclear localization and transcriptional activity of MKL1 as a co-factor for the transcription factor SRF (Ho et al., 2013; Vartiainen et al., 2007). Perinuclear actin polymerization increases with stress (Shao et al., 2015), which could influence the state of nuclear actin and SRF regulation. High SRF drives expression of the actin-myosin cytoskeleton, which stresses ECM only up to a roughly constant strain in the matrix (Discher et al., 2005; Marganski et al., 2003), with excess actin-myosin turning over and thereby limiting SRF as well as nuclear tension, lamin-A/C, and nuclear RARγ. This current understanding suggests a tight coupling between a mechanobiological gene circuit for lamin-A/C and another for the actin-myosin cytoskeleton – at least above a baseline level of cytoskeleton expression and tension that is independent of lamin-A/C (Buxboim et al., 2014).

1.2.3 Stress-induced changes in chromatin organization and conformation

Although considerable force (e.g. in the nanoNewton (nN) range) is typically required to significantly deform the nucleus in adherent mammalian cells (Neelam et al., 2015), recent reports show that even weak forces in the picoNewton range can affect histone acetylation states (Li et al., 2011), chromatin dynamics (Hampoelz et al., 2011), and protein-protein interactions (e.g. coilin-SMN complexes) in the nucleus (Poh et al., 2012). Physical stress could also cause global or local rearrangement of chromosomes (**Figure 1.1E&e**), affecting the distinct 'territories'

that chromosomes occupy (Cremer and Cremer, 2001). Transcriptionally active euchromatin largely resides in the center (and near nuclear pores) and transcriptionally repressed heterochromatin typically anchors to the lamina at the nuclear periphery, but also around nucleoli (Solovei et al., 2013). The organization of such domains is believed to influence differentiation; embryonic stem cells (ESCs) have no heterochromatin and exhibit more random and hyperdynamic arrangement of chromosome territories compared to differentiated cells (Maharana et al., 2016). Key chromatin proteins such as histones immobilize with differentiation (Meshorer et al., 2006), supporting the notion that chromosome arrangement becomes increasingly stabilized as cells commit to a lineage-specific fate. However, stresses that distort the nuclear envelope can directly re-organize chromosome domains, affecting transcriptional activity without any biochemical intermediates: in cell/nuclear flattening, for example, chromosome territories are seen to intermingle and overlap (Maharana et al., 2016). One possible explanation is that heterochromatin is tethered to nuclear envelope components which undergo structural remodeling in response to stress. Epitope masking in immunostaining of nuclear envelope components has long been a concern (Tunnah et al., 2005), and confocal imaging of cells in culture show that cell/nuclear compression induces basal-to-apical polarization of immunostained lamin-A/C (but not B-type lamins) (Ihalainen et al., 2015; Kim and Wirtz, 2015). This polarization could have its origins in the higher mobility of lamin-A/C relative to B-type lamins (Dahl et al., 2006) combined perhaps with a stress-driven increase in lamin-A/C multimerization at the basal nuclear envelope (Ihalainen et al., 2015). Extrinsic mechanical strain has also been shown to enrich emerin and non-muscle myosin-IIa at the outer nuclear membrane (Le et al., 2016). Corresponding loss of emerin at the INM associates with altered global histone modification states, coupled to defective heterochromatin anchorage to the lamina.

Single cell studies in culture have elegantly probed strain propagation into engineered chromatin from the cell surface (using magnetic beads) using a large GFP-tagged transgene. The transgene has been seen to stretch when the bead is pulled, which upregulates transcriptional activity (Figure 1.1E&e) (Tajik et al., 2016). Stress-induced extension of chromatin depended on the direction of the applied stress as well as acto-myosin contractility and the

presence of nuclear envelope proteins (e.g. lamins and LINC components). In addition, 2 min of 17.5 Pa stress at the cell surface increased transgene expression 20%, whereas knockdown of lamins, SUNs, or emerin only gave 5% more expression or less (LBR knockdown had no effect in these cells), and basal expression of the transgene depended on acto-myosin contractility. Physical forces propagating to the nuclear envelope can thus cause global and local rearrangements of chromosome to affect transcriptional activity of genes. Similar results for some native loci within cells in native tissues – perhaps exploiting CRISP methods – could be extremely interesting.

1.2.4 Nuclear envelope dilation and rupture

Large changes in nuclear shape or increases in nuclear volume are expected to increase tension in the nuclear envelope. In zebrafish, tissue damage induces osmotic nuclear swelling, which causes dilation of the nuclear membrane and accumulation of cytosolic phospholipase A2 (cPLA2) from the nucleoplasm to the INM (Enyedi et al., 2016). Activation of cPLA2 initiates lipid signaling, which results in the release of proinflammatory eicosanoids that play important roles in tissue damage repair. Perinuclear F-actin and the nuclear lamina help mediate this process, suggesting cPLA2 translocation and activation indeed depend on mechanical tension at the nuclear envelope.

If lamin-A/C is compromised through knockdown or mutation, cells on stiff 2D substrates can apply sufficient tension to strain and even rupture the nuclear envelope transiently during interphase (**Figure 1.1F**) (De Vos et al., 2011; Tamiello et al., 2013; Vargas et al., 2012). Rupture has been seen to regulate localization of transcription factors (e.g. RELA, and OCT1) as well as constructs of GFP-NLS (nuclear localization sequence). Importantly, rupture is suppressed by culturing cells on soft gels (Tamiello et al., 2013) where cell tension is low (Discher et al., 2005; Marganski et al., 2003). Cell migration in 3D through narrow, rigid pores (~3 μm in diameter) can likewise stress the nucleus sufficiently to disrupt the lamina (Harada et al., 2014) and to increase DNA damage throughout the nucleus based on quantitation of repair foci of gH2AX and phosphorylated ATM kinase as well as single cell electrophoreses (comet assays) (Irianto et al.,

2016c). Transient rupture of GFP-NLS into the cytoplasm and local accumulations of the DNA repair factor GFP-53BP1 in the nucleus (Denais et al., 2016; Raab et al., 2016) has led to speculation that constitutive nucleases leak into the nucleus to cleave DNA during envelope rupture events. Alternatively, repair factors have been seen to leak into the cytoplasm after constricted migration (Irianto et al., 2016a; Irianto et al., 2016c), which is consistent with rupture-induced loss of nuclear factors from lamin-A defective cells cultured on rigid substrates. For the latter cells, at least some DNA repair factors exhibit low steady state levels attributable to their degradation, and the slow repair of DNA damage caused by ionizing radiation can be rescued by overexpression of 53BP1 (Gonzalo 2014). Migration-induced DNA damage could be similar but more transient and could also involve additional mechanisms. For example, the mobile DNA repair factors always segregate away from DNA which is squeezed and aligned in a pore (Irianto et al., 2016a). In addition, live-imaging of a chromatin locus in constricted nuclei demonstrated stretching by more than 10-fold (Irianto et al., 2016b), which could modulate repair of pre-existing breaks. Regardless of mechanism, constricted migration of cancer cell clones has been shown by genotype and phenotype analyses to cause heritable changes affecting cell shape (Irianto et al., 2016c).

Transient ruptures are not selective for entry/exit of specific proteins, but mechanosensitive factors that are already 'primed' to favor entry into the nucleus under high-stress conditions (e.g. YAP1, RARγ, SRF) might bind accessible loci and accumulate more readily upon rupture than other factors. Subsequent upregulation of major structural and cytoskeletal genes might thus better equip a cell for resisting large mechanical strains, as seen with RARγ nuclear entry driving up *LMNA* expression to produce a stiffer nucleus (Swift et al., 2013). Further kinetics-focused studies are required to assess whether such protective responses can indeed be observed in different contexts, especially with cells such as those of the immune system that undergo repetitive constrictive events throughout their lifetime.

1.3 Nuclear mechanosensing in development, disease, and aging

Early embryos are uniformly soft and compliant, with correspondingly low levels of collagenous ECM (Majkut et al., 2013). Nuclei of embryonic stem cells are likewise very soft with low lamin-A/C (Eckersley-Maslin et al., 2013; Pajerowski et al., 2007). However, from an initial embryonic disk stiffness of ~0.3 kiloPascal (kPa, which is 100-fold softer than a gummy bear), the embryonic chick heart stiffens every day by ~0.3 kPa/day largely because of accumulation of collagenous ECM made by cardiac fibroblasts (Majkut et al., 2013). The brain, on the other hand, remains throughout life as soft and as low in collagen as the embryo. Surprisingly, *Lmna*-knockout mice survive the tissue stiffening of embryogenesis and generate all tissues, but fail to grow after birth (small skeleton) and die within weeks due to chronic injury and dystrophy in cardiac and skeletal muscle among other stiff tissues (Jahn et al., 2012; Kubben et al., 2011; Sullivan et al., 1999). The lack of a strict need for a robust nucleus during the earliest stages of development is understandable for ultra-soft embryonic tissue that does not generate or bear large mechanical stresses while protected inside the womb. In normal development, however, lamin-A/C is expressed following tissue differentiation and the timing of initial expression varies depending on the tissue considered in both chick embryos (Lehner et al., 1987) and mouse embryos (Rober et al., 1989). Interestingly, the lamin-B receptor (LBR) tends to show an opposite expression pattern from lamin-A/C, with either one able to control chromatin tethering at the envelope (Solovei et al., 2013). One plausible model is that LBR is progressively displaced by lamin-A/C as tissue-specific stiffening in the embryo drives the expression of lamin-A/C. This mechano-regulation of lamin-A/C in the embryo is likely maintained throughout tissue maturation, until steady-state levels are reached in adulthood (Swift et al., 2013).

Defects in nuclear mechanosensory proteins are linked to a large number of post-natal progressive diseases. Nearly all of these diseases affect stiff tissues including heart and skeletal muscle, as well as cartilage and bone, which generate and/or sustain considerable mechanical stress, but fat can also be affected as it has intermediate levels of collagens, and this suggests it bears some stress (Swift et al., 2013). Cardiomyopathies are common (Narula et al., 2012), with

more than 120 different *LMNA* mutations linked to dilated cardiomyopathy (DCM), characterized by progressive thinning of the ventricular wall and weakened cardiac contractility. Mutant forms of other nuclear envelope proteins including emerin, nesprins-1/2, Lap2α, and LUMA (Bengtsson and Otto, 2008; Bione et al., 1994; Taylor et al., 2005) also cause DCM and various forms of Emery-Dreifuss muscular dystrophy (EDMD) (Bengtsson and Otto, 2008; Bione et al., 1994; Bonne et al., 1999; Isermann and Lammerding, 2013; Zhang et al., 2007). Impaired mechanotransduction (Lammerding et al., 2005) and nuclear envelope fragility (with low lamin-A/C levels (Narula et al., 2012)) are often considered to be part of the disease pathogenesis mechanism. The large number of different genetic diseases caused by mutations in nuclear envelope proteins (Worman, 2012) reflects the importance of nuclear mechanosensing in normal cell function.

An inability of the nucleus to respond dynamically to mechanical stress might also contribute to normal and accelerated aging. In HGPS (Hutchinson-Gilford Progeria Syndrome), a rare premature aging disorder, a farnesylated mutant product of the *LMNA* gene called progerin causes the nucleus to be more brittle and 'solid-like' (as opposed to a viscous or 'fluid-like' lamina) (Dahl et al., 2006). FRAP (fluorescence recovery after photobleaching) experiments confirm that progerin is immobile compared to lamin-A/C (Dahl et al., 2006), consistent with an inability to flow and remodel dynamically in response to mechanical stress. Phosphorylation of progerin might also be lower than that of normal lamin-A/C (Moiseeva et al., 2016), supporting the notion that farnesylated lamins (i.e. prelamin-A, progerin, and B-type lamins) are more tightly anchored to the membrane and less soluble. HGPS cells also exhibit elevated levels of DNA damage (Burtner and Kennedy, 2010; Gonzalez-Suarez et al., 2009a; Liu et al., 2005; Liu et al., 2006), which again suggests a mechanistic link between the mechanical properties of the nuclear envelope and the accumulation of DNA breaks. Indeed, other premature aging disorders that are also pan-tissue (e.g. Werner syndrome) result from mutations in DNA repair factors. Consistent with a shift from lamin-A/C to a more lamin-B-like progerin, the accelerated aging phenotype in HGPS patients and progeria mouse models is like that of lamin-A/C deficient mice in that they exhibit more pronounced effects on stiff tissues such as heart and skeletal muscle with

increasingly fibrotic, collagen-rich ECM and, for progeria mice, death in 3-8 months (Osorio et al., 2011). Extrinsic feedback with ECM stiffness is likely to be defective and could be key to disease. Indeed, a mosaic mouse model in which 50% of cells in all tissues express farnesylated prelamin-A is normal and long-lived which is surprising given that the homozygous mouse dies in weeks like other progeria and lamin-A null mice (de la Rosa et al., 2013b). Since culture studies further showed that ECM can rescue the proliferative defects of prelamin-A expressing fibroblasts (de la Rosa et al., 2013b), soft ECM could be suppressing nuclear stress, DNA damage, and the senescence that can result. Consistent with such outside-in signals, the same group also reported a mouse knockout for a collagenolytic protease (MMP14) that exhibits a progeria-like course of disease, including anomalous lamin-A/C, in which premature death was delayed by administration of retinoic acid (Gutierrez-Fernandez et al., 2015). Understanding the interplay of collagenous matrix stiffness and mechanosensitive lamin-A/C expression as modulated by retinoic acid is thus beginning to impact therapeutic approaches to aging-related diseases.

1.4 'Universal' stiffness-dependent scaling of lamin-A/C and other nuclear envelope proteins

1.4.1 Introduction

Tissue microelasticity or 'stiffness' E_t is measured in units of stress (kPa) and is largely determined by the concentration of collagens and other ECM components (Figure 1.1) (Brower et al., 2006). At the scale of a cell, the magnitude of E_t spans at least two logs from soft brain or marrow to the very stiff osteoid that osteoblasts calcify to bone (Discher et al., 2009). Identifying log-scale variations is crucial to recognizing any potential polymer physics-based trends (Gennes, 1979), and recent MS-based studies of adult mouse tissue proteomes (Swift et al., 2013) indeed indicate a power-law scaling relationship over several orders of magnitude between tissue stiffness (E_t; units of kPa) and the molar concentration of collagen-I:

$$E_t \sim [\text{Collagen-I}]^n \quad \text{with } n \approx 0.67 \qquad \text{(Eq.1)}$$

where n is the scaling exponent, i.e. the slope that results from a log-log plot of the two quantities. Of course, such scaling expressions leave out proportionality factors (in units of kPa/Molar^n) and ignore small offsets (e.g. critical concentrations to percolate a network), but they make clear that high levels of fibrillar collagen are found in stiffer tissues (e.g., cardiac/skeletal muscle or osteoid). Indeed, direct perturbation of collagens in intact tissue, either by enzymatic degradation or cross-linking, generally changes tissue stiffness even for a soft embryonic heart (Majkut et al., 2013). As the most abundant proteins in our bodies, comprising more than 30% of all proteins present and 90% of the ECM (Shoulders and Raines, 2009; van der Rest and Garrone, 1991), it should not be surprising that tissue stiffness exhibits power-law scaling with the concentration of this prominent structural biopolymer. Scaling is seen for the stiffness of gels made from purified collagen-I (Yang et al., 2009) and is generally found for the physical properties of polymer networks (Gennes, 1979).

In addition to collagenous ECM, MS-based proteomic profiling of ~100 of the most abundant structural proteins in adult mouse tissues (Swift et al., 2013) revealed that the molar concentration of A-type lamins scales over several orders of magnitude with tissue stiffness E_t:

$$[\text{Lamin-A}] \sim E_t{}^m \quad \text{with } m \approx 0.7 \qquad \text{(Eq.2)}$$

where m denotes the scaling exponent. This scaling expression quantifies upregulation of A-type lamins (by 30-fold from soft brain to rigid bone) in response to tissue stiffness, rather than indicating that nuclei contribute to tissue stiffness. B-type lamin levels remain relatively constant: for lamin-B1, $m \sim 0.2$, and for lamin-B2, $m \sim 0.0$. Thus, whereas collagens and other ECM proteins set the stiffness of the tissue, lamin-A/C at the nuclear envelope responds (as shown in Figure 1.1) to resist cell tension that is matrix-driven. Importantly, rearrangement of the equations above gives the following correlation between the concentrations of collagen and lamin-A:

$$[\text{Lamin-A}] \sim [\text{Collagen-I}]^{\alpha} \quad \text{with } \alpha_{\text{Lmna}} = m \times n \approx 0.45 \qquad \text{(Eq.3)}$$

where α_{Lmna} denotes the scaling exponent obtained by combining Eq. 1 and 2. Causality must be established of course by in-depth cell biological studies such as those reviewed and summarized schematically in Figure 1.1, but emerging trends might at least be sought in publicly available, standardized '-omics' datasets.

1.4.2 Meta-analysis of public –omics data

As an example of a broad meta-analysis in today's big data era (**Figure 1.2**), we focused on heart tissue. First, the heart offers the largest number of normal and diseased transcriptomic and/or proteomic datasets relevant to mechanosensation. Open-access datasets are available for normal development and aging, as well as fibrosis, myocardial injury, and hypertrophy. Second, datasets span a wide range of species, including mouse, human, rat, boar, dog, zebrafish (Barrett et al., 2013; Vizcaino et al., 2016). Once a dataset is selected, a first check on quality is provided by collagen-I's two stoichiometric subunits (**Figure 1.3**): if collagen alpha-1(I) increases or decreases in level then collagen alpha-2(I) should do the same in proportion. Changes in collagen alpha-1(I) between samples in a dataset could be due to normal variation, experimental perturbation, or even perhaps experimental noise in other components of analysis. However, provided one finds for a given dataset an exponent (α_{Col1a2}) close to 1 and a reasonable fit ($R^2 > 0.85$) of the form:

$$[\text{Collagen alpha-2(I)}] \sim [\text{Collagen alpha-1(I)}]^{\alpha} \quad \text{with} \quad \alpha_{\text{Col1a2}} = 1.0 \pm 0.2 \qquad \text{(Eq.4)}$$

then the dataset passes a first validation. Of course it should be noted here that, while collagen-I seems a reasonable surrogate for tissue stiffness, most tissues in the body exhibit some heterogeneity in their mechanical properties (Koser et al., 2016), and other ECM proteins could

add complexity to rheology measurements. Therefore, in order to take into account different sources of variation, a large number of datasets should be carefully analyzed for a diversity of tissue samples and disease models before we can begin developing broad hypotheses.

For illustration, transcript data for genes of interest from a mouse model of familial cardiac hypertrophy and fibrosis (Rajan et al., 2006) is plotted in log-log form versus *Col1a1* (**Figure 1.4A**). A statistically robust positive correlation between *Col1a2* and *Col1a1* (Pearson coefficient, $r = 0.93$), with a suitable slope ($\alpha_{Col1a2} \approx 1.0$) and goodness of fit ($R^2 = 0.87$), provides some validation for further analysis. In comparison, *Lmna* increases more weakly ($\alpha_{Lmna} \approx 0.22$; R^2=0.81), but this is factor-of-two consistent with the proteomics-based scaling above ($\alpha_{Lmna} \approx 0.45$) and thus supports the model wherein increased deposition of collagenous ECM results in correspondingly higher lamin-A/C levels. One might expect an increase in contractility (per Fig.1), and indeed non-muscle myosin-IIa (*Myh9*) and smooth muscle actin (*Acta2*) exhibit similar positive correlations. Not everything changes: *Lmnb1* and *Lmnb2*, showed little to no correlation with collagen-I ($r = 0.012$ and 0.21, respectively), which is consistent with constant B-type lamin levels quantified for adult mouse tissue proteomes (Swift et al., 2013).

Based on more than 20 datasets for heart, the scaling exponent for *Lmna* vs *Col1a1* converges to: $\alpha_{Lmna} = 0.3 \pm 0.04$ (**Figure 1.4B**). The majority of the highly diverse datasets (different species and perturbations) showed the expected collagen-I scaling of $\alpha_{Col1a2} \approx 1.0$, and were therefore included in the best estimate of α_{Lmna}. The implied stiffness-dependent scaling of lamin-A/C thus appears to be a highly conserved phenomenon, perhaps generalizable to a broader range of cell types and tissue/organ systems. Phylogenetic analyses have indeed indicated that lamins are the most ancient of the IF proteins (Dittmer and Misteli, 2011), and so it is sensible that, in animals, lamins have evolved and maintained a shared ability to mechanosense.

Other nuclear envelope proteins that interact closely with lamins do not show the same scaling relationships with collagen-I (**Figure 1.4C**). For example, *Sun1* and *Sun2* remain constant in most datasets, with average scaling exponents of $\alpha_{Sun1} = -0.05$ and $\alpha_{Sun2} = -0.007$. The results for *Sun2* message are consistent with past analyses that further showed the nuclear fraction of

Sun2 protein does scale with tissue stiffness (Swift et al., 2013); thus the mRNA understandably reflects the overall level of a factor in a cell, whereas proteins that partition between ER and nucleus (Sun's) or between cytoplasm and nucleus (perhaps DNA repair factors) can exhibit nuclear fractions that are more revealing of mechanosensitivity. Emerin (*Emd*) correlates inversely with collagen-I ($p < 0.05$). This seems consistent with lower emerin expression in a stiffer nucleus (Guilluy et al., 2014). However, transcripts of ECM crosslinkers (e.g. LOX) (**Figure 1.5)**, *Acta2* and *Myh9* (readouts for basal cytoskeletal contractility), as well as *Rarg* (transcriptional regulator of *Lmna*) and (most weakly) *Yap1* all scaled with collagenous ECM. Such positive scaling of transcripts does not prove causality – as emphasized above – but nonetheless supports the general model of mechanotransduction from ECM to nucleus, involving contractile strain as well as transcriptional activation (Figure 1.2C). The larger exponents in these datasets are likely to be the easiest to demonstrate as significant by cell biology methods. Conversely, if one discovers a relationship between transcripts *in vitro* that is not evident in such meta-analyses of real, 3D tissues, then many questions should be asked about the culture systems as well as the source(s) of the datasets.

Proteomics datasets are currently less standardized than transcriptomics datasets, but two proteomics datasets for diverse adult tissues were examined. Both show the expected linear scaling of collagen subunits over many logs and are therefore reasonable for further meta-analysis. For mouse (Swift et al., 2013), LMNA protein scales linearly with COL1A1 protein for softer tissue with low collagen, whereas for a larger range of higher collagen-I: $\alpha_{Lmna} \approx 0.3$ (Figure 1.4D). The unexpectedly low amount of lamin-A/C is most evident in brain, which is notable for having abundant miR-9 that represses lamin-A/C expression (Jung et al., 2012). However, the transition to weaker scaling suggests the miR-9 mechanism does not apply to stiffer tissues, although this requires deeper investigation. Additionally, because the weaker scaling in stiffer tissues applies to a larger range of data, an overall exponent of $\alpha_{Lmna} = m \times n \approx 0.45$ is close to the weighted average. For the one human dataset (Kim et al., 2014b), the lamin-A/C data is much noisier but yields a similar result: $\alpha_{LMNA} \approx 0.3$. These results are thus reasonably consistent with transcriptomics analyses of heart, and therefore suggest some universality and robustness to the

stiffness-dependent scaling of lamin-A/C protein and message levels. Of course, all of this analysis of protein and mRNA levels in tissues merely motivates molecularly detailed cell biological studies of nuclear mechanosensing by the lamins among other nuclear components.

1.5 Conclusions

Many recent studies now demonstrate that the nuclear envelope as well as chromatin itself can sense and respond to mechanical forces exerted on or by the cell's cytoskeleton. Nuclear mechanosensing is achieved via several pathways, including stress-induced changes in protein conformation (interaction with binding partners, e.g. enzymes), translocation of transcriptional regulators, chromosome conformation and organization, and membrane dilation and/or rupture. An -omics based meta-analysis suggests that at least some of these mechanosensitive processes, particularly those pertaining to the nuclear lamina, are applicable to a broad range of species, tissues, and diseases. Deeper insight into downstream effects will likely improve our basic understanding of how our cells and tissue are shaped by mechanical cues and might also potentiate novel approaches to therapy for the large number of disease linked to mutations of genes encoding part of the nuclear envelope.

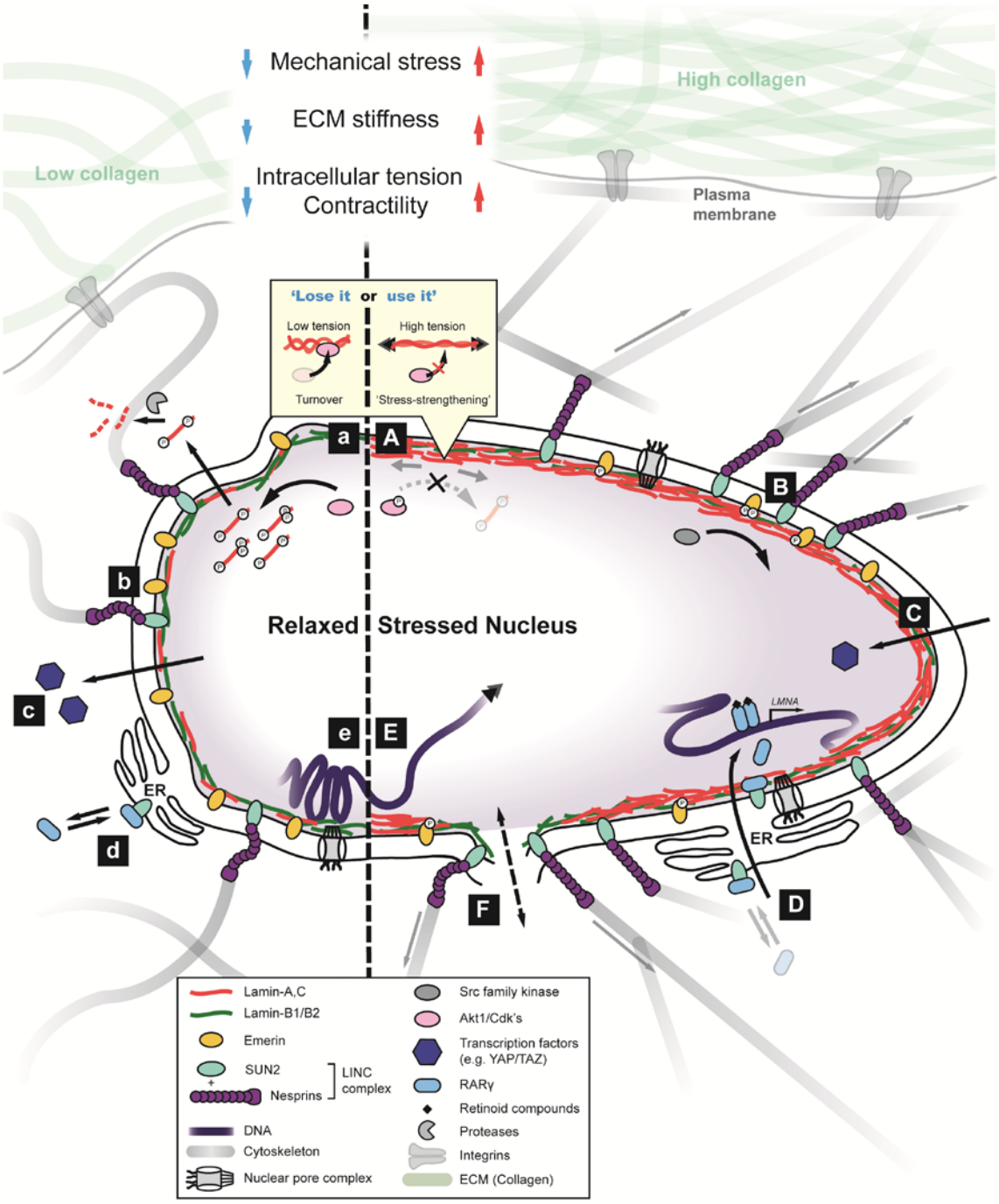

Figure 1.1. Nuclear mechanosensing.

Left and right sides indicate relaxed (soft) and mechanically stressed nuclei, respectively. (**A** & **a**) High nuclear tension may induce conformational changes in lamin coiled-coil dimers, leading to steric inhibition of access by kinases (Buxboim et al., 2014; Swift et al., 2013). In a relaxed nucleus, lamins are hyper-phosphorylated and solubilized into the nucleoplasm (as during cell division). Phospho-solubilized lamins may ultimately become degraded (Bertacchini et al., 2013). Tension-inhibited turnover of lamins is similar to that of collagen-I (Flynn et al., 2010), and is an example of structural proteins exhibiting 'stress-strengthening' properties. (**B** & **b**) Pulling on

nesprin-1 leads to phosphorylation of emerin by Src kinases (Guilluy et al., 2014), and results in stress-stiffening of the nucleus. Emerin phosphorylation is high in cells cultured on stiff substrates and regulates many downstream mechano-responses including formation of stress fibers, migration, localization of YAP/TAZ, and SRF transcription. (**C** & **c**) Mechanosensitive transcription factors such as YAP/TAZ translocate into the nucleus under stress to modulate gene expression (Dupont et al., 2011). (**D** & **d**) Mechanical stress leads to nuclear localization of RARγ, which directly regulates *LMNA* transcription. Nuclear translocation of RARγ is facilitated by its interactions with SUN2 as well as lamin-A/C, suggesting a feedback mechanism wherein the protein product lamin-A/C regulates its own transcription (Swift et al., 2013). (**E** & **e**) Application of mechanical force may lead to changes in chromatin conformation (e.g., local stretching of genes), thereby altering transcriptional activity (Tajik et al., 2016). Mechanical perturbation can also affect the global arrangement of chromosome 'territories' (Maharana et al., 2016). (**F**) High tension can induce membrane dilation and in extreme cases may lead to transient ruptures, allowing for the exchange (and possible mislocalization) of nucleoplasmic and cytoplasmic content.

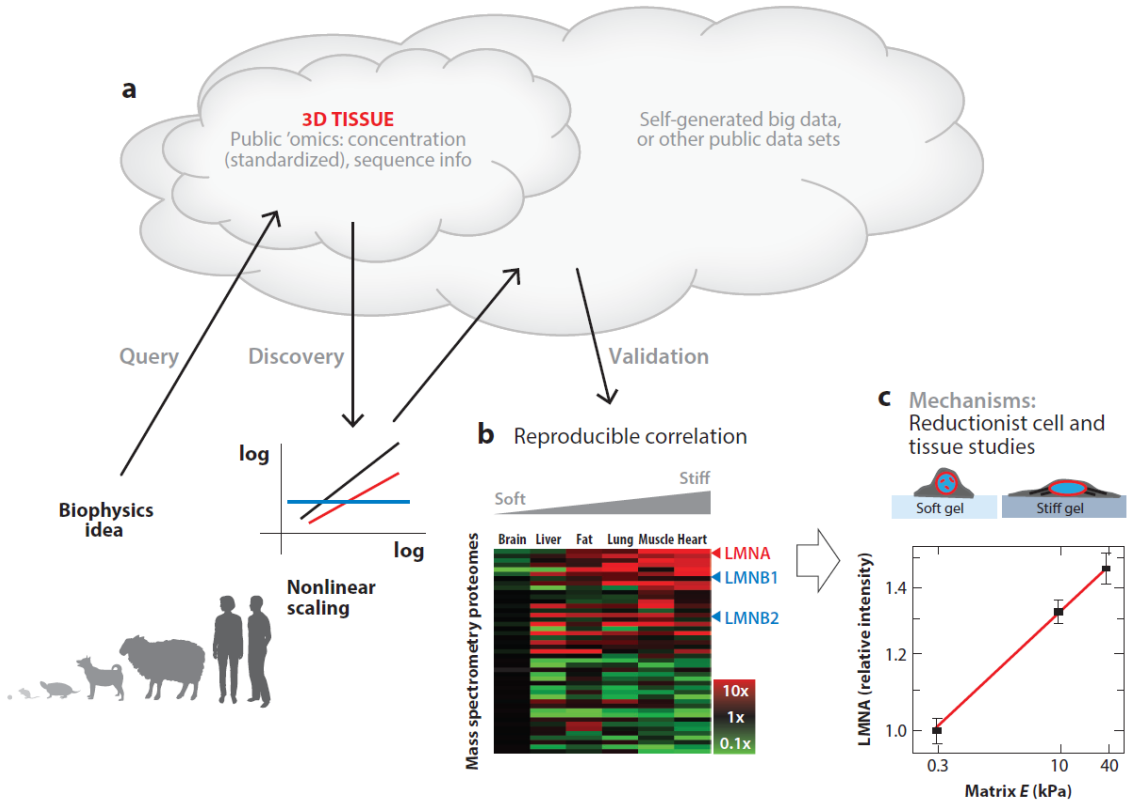

Figure 1.2. Tissue-based hypothesis development and testing in the Big Data Era.

(**A**) Beginning with an idea rooted in biophysics, such as tissue stiffness increasing with tissue levels of the abundant biopolymer collagen-I, one can query publicly available 'omics data sets for three-dimensional (3D) tissue and seek out other factors that correlate with collagen-I. Such data sets are standardized and provide relative concentrations or sequence information, or both. Scaling relations as power laws in log–log plots would be particularly sensible for relationships between polymers, given collagen as an implicit expression of stiffness. The sketched plot illustrates, for example, a gene expression data set in which two genes increase in relative level when plotted against the relative level of a third gene, whereas one gene remains relatively constant. Self-generated 'omics data or other public data sets, or both, can provide a test of the scaling relationship. (**B**) Reproducible correlations across 'omics analyses might agree, for example, with an increase in lamin-A (LMNA) from soft tissue (brain) to stiff tissue (heart), whereas the B-type lamins (LMNB1 and LMNB2) remain constant, as detected by quantitative mass spectrometry (Swift et al., 2013). (**C**) To understand molecular mechanisms for such relationships, reductionist approaches include low dimensionality and sparse cultures on 2D gels of controlled stiffness that are coated equally with collagen-I for cell adhesion.With such systems, studies of mesenchymal stem cells show that lamin-A increases (in relative intensity) from soft gels to stiff gels, with mechanisms involving cytoskeletal stress on the nucleus stabilizing lamin-A against phosphorylation and degradation (Buxboim et al., 2014).

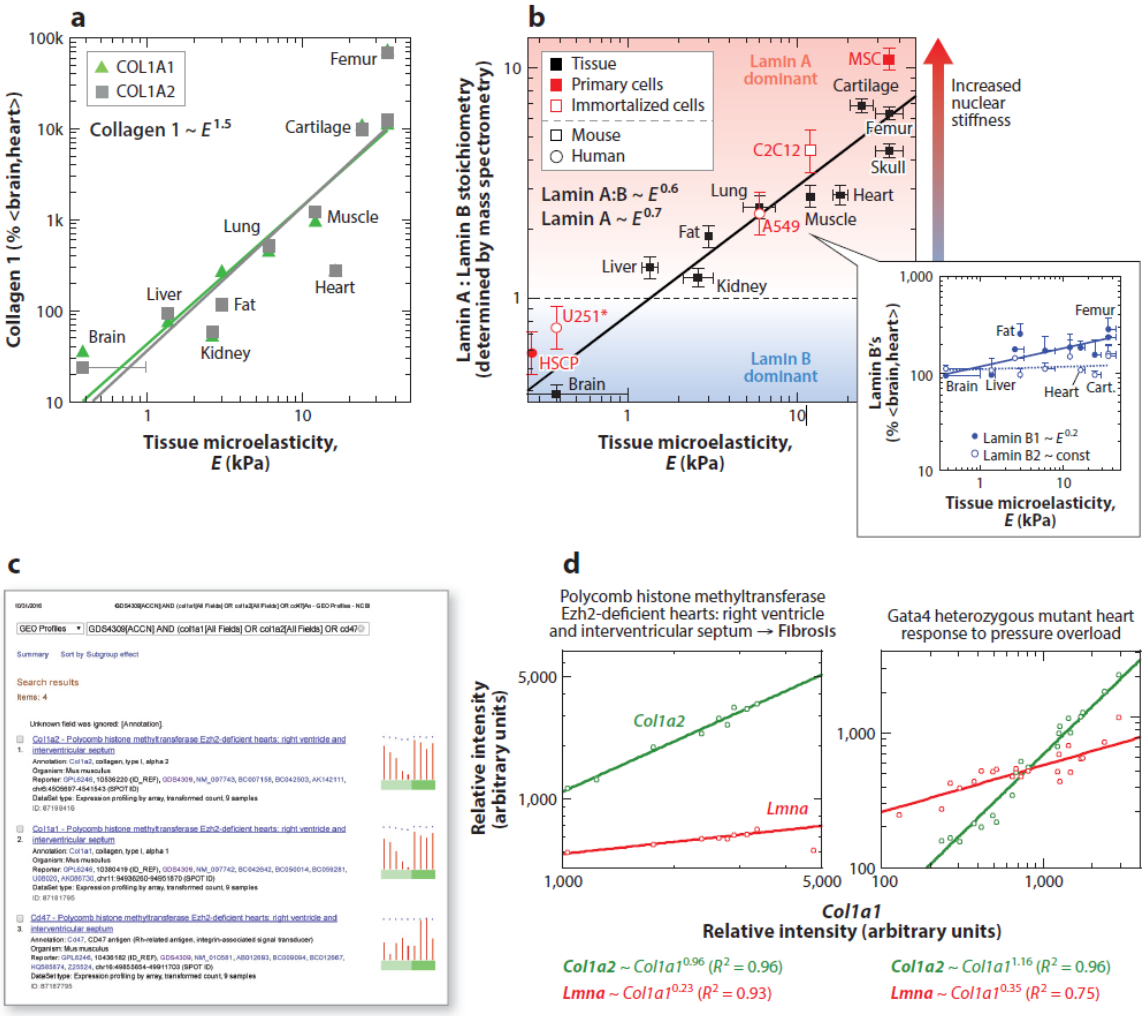

Figure 1.3. Scaling of collagen-I and lamin-A proteins with cell-scale tissue stiffness compared with transcriptome data mined for similar scaling relationships.

(**A,B**) As measured with a variety of microtools at the scale of cells, tissue microelasticity or stiffness increased by two orders of magnitude for various species tested (see references in (Swift et al., 2013)). For bones such as femur and skull, the stiffness of precalcified bone (called osteoid) is plotted. As a reference, a gummy bear is approximately 70 kPa. Quantitative mass spectrometry done on mouse tissue was used to determine the relative amounts of collagen-I subunits. The two subunits exhibited similar scaling on the log–log plot because they form a stoichiometric complex as they assemble into collagen-I fibers. The average level for heart and brain tissue was defined as 100%. For the lamins quantified in the same studies, lamin-A (LMNA) is normalized to the B-type lamins (LMNB1 and LMNB2) that remain relatively constant across tissues. Nuclear stiffness increases with lamin-A and, hence, with tissue stiffness. (**C**) A screen snapshot from the public transcriptome database GEO (Gene Expression Omnibus, accessible via the US National Institutes of Health at https://www.ncbi.nlm.nih.gov/geo/) shows the expression of *Col1a2* (top) in nine different mouse hearts and *Col1a1* (middle) in the same hearts. A similar pattern of expression is evident between these two, whereas *Cd47* (bottom) is a miscellaneous gene that exhibits a very different pattern of expression among samples. (**D**) Plots of *Col1a2* against *Col1a1* for such data sets reveal a linear scaling consistent with stoichiometric

association at the protein level. Lamin-A transcript (*Lmna*) also scales with *Col1a1*, but the scaling is much weaker with a log–log slope of approximately 0.3 across these two data sets from mouse hearts. Such weak scaling of mRNA is consistent with the weak scaling of protein, as can be deduced from panels A and B.

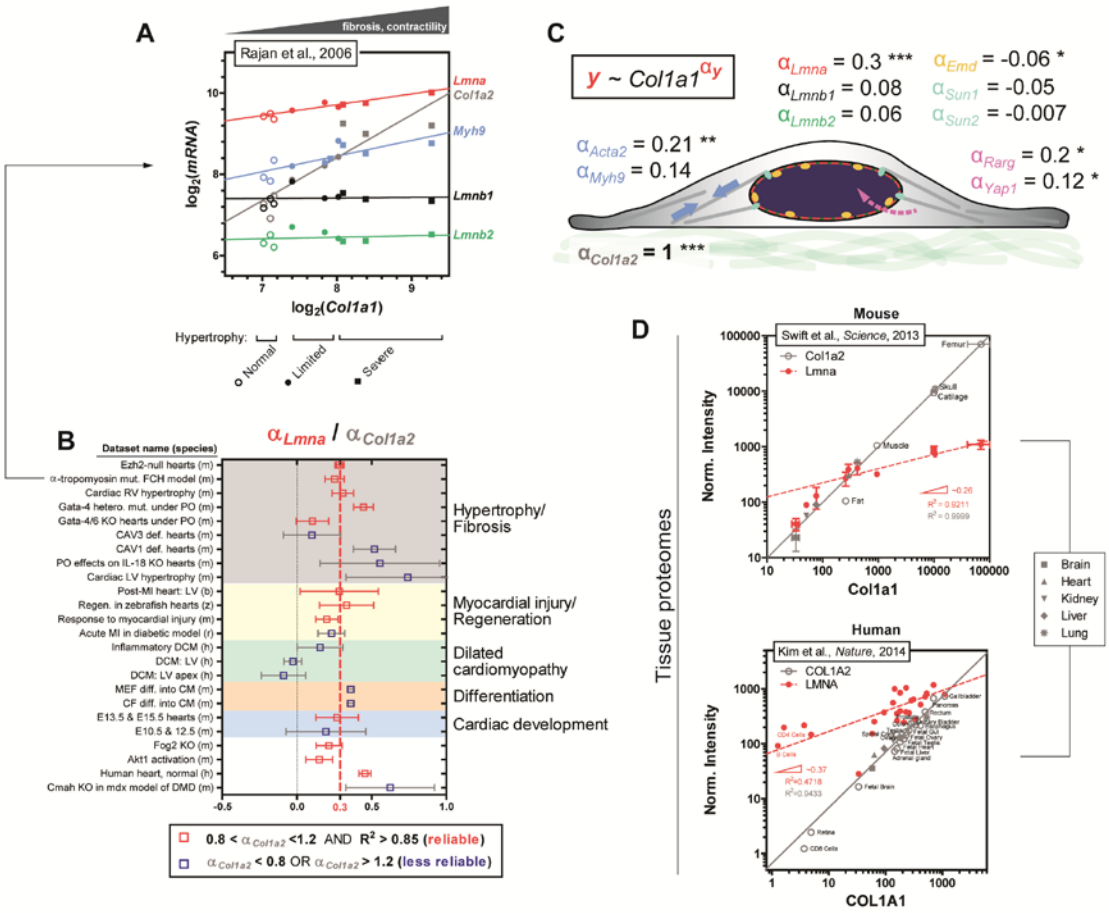

Figure 1.4. Meta-analysis of universal stiffness-dependent scaling of lamin-A/C and other nuclear envelope proteins.

Published –omics datasets of relevance were collected from various open-access databases (Barrett et al., 2013; Vizcaino et al., 2016), and as a first simple check for quantitative reliability, log-log plots of *Col1a1* vs *Col1a2* were generated for each dataset, since the two should in principle correlate well with each other as components of collagen's stoichiometric structure. Only those datasets which gave *Col1a2* scaling exponents (=slopes on a log-log plot) of $\alpha_{Col1a2} = 1 \pm 0.2$, with high R^2 >0.85 were selected for analysis, with the assumption that a robust correlation between *Col1a1* and *Col1a2* indicates minimal error arising from sample preparation and/or normalization. Such pre-processing of data provides an added advantage in that type I collagen content becomes a proxy for tissue stiffness (Swift et al., 2013). Once reliable datasets were identified, other proteins of interest (e.g. nuclear lamins) were plotted against *Col1a1* to determine scaling exponents relative to that of *Col1a2*. (**A**) Representative transcriptomics dataset for mouse model of familial cardiac hypertrophy (FCH) (Rajan et al., 2006) illustrating robust scaling between *Col1a1* and *Col1a2* (α_{Col1a2} = 0.95). *Lmna* and *Myh9*, among many other key mechanosensory proteins/genes also correlate with *Col1a1*, while *Lmnb1* and *Lmnb2* remain constant. Samples were parsed into three groups: "normal", "limited", and "severe" hypertrophy. (**B**) The average scaling exponent for *Lmna* (α_{Lmna}) normalized to that for *Col1a2* (α_{Col1a2}) obtained from ~25 transcriptomics datasets is equal to $\langle\alpha_{Lmna}\rangle$ = 0.3. Datasets span embryonic, fetal, and adult cardiac tissue samples from six different species (human (h), mouse (m), rat (r),

zebrafish (z), boar (b), dog (d)) and at least five different disease models including DCM, hypertrophy, fibrosis, and myocardial injury. Datasets which are deemed most quantitatively reliable with $0.8 < \alpha_{Col1a2} < 1.2$ & $R^2 > 0.85$ are in red. (**C**) Average scaling exponents (α_y) of several key proteins involved in nucleus mechanosensing. *Col1a2*, *Lmna*, *Emd*, *Acta2*, *Myh9*, *Rarg,* and *Yap1* have statistically non-zero exponents. (***p<0.0001, **p<0.01, *p<0.05). (**D**) Mass-spectrometry based profiling of mouse (upper panel) and human (lower panel) tissue proteomes show comparable scaling of LMNA with collagen-I over several orders of magnitude ($\alpha_{LMNA} \sim 0.3$), consistent with α_{Lmna} determined for heart transcriptomes above.

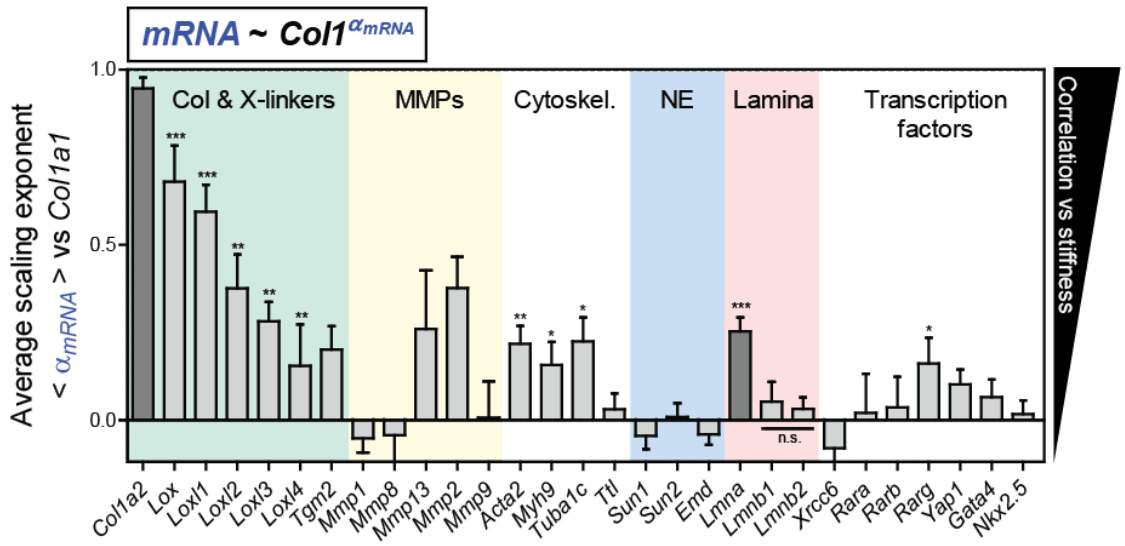

Figure 1.5. Average scaling exponents (vs *Col1a1*) of ECM crosslinkers, MMPs, cytoskeleton, nuclear envelope proteins, and transcription factors

Col1a2 scales most strongly with *Col1a1* ($\alpha_{Col1a2} \sim 1$), as expected for an obligate heterotrimer triple helix. Matrix crosslinkers including various *Lox* isoforms also scale with Type-I collagens. Cytoskeletal components such as *Acta2* and *Myh9* generally follow slightly weaker scaling, as does *Lmna* ($\alpha_{Lmna} \sim 0.3$).

CHAPTER 2
Mechanosensing to protect the genome during development

The work presented in this Chapter is currently in preparation for submission.

Preliminary imaging of nuclear deformation was performed by Dr. Stephanie Majkut.
Confocal imaging of hearts was done by Dr. Jerome Irianto and Dr. Ben Prosser.
Embryonic heart / CM isolation and culture were performed by Amal Abbas, Kenneth Vogel, and Manasvita Vashisth.
A549 phsphomimetic mutant work was performed by Manasvita Vashisth.

Abstract

Stiff adult tissues such as striated muscle bear high mechanical stress and have an abundance of collagen-I fibers in the extracellular matrix (ECM) and lamin-A filaments in the nucleus, but mechanisms and functional consequences of any matrix-nucleus interplay remain obscure. Here, lamin-A and collagen-I exhibit tightly coupled mechano-sensitivity in the first vertebrate organ, the heart, with a 'use it or lose it' mechanism for tension-suppressed turnover that confers mechano-protection against DNA damage. Lamin-A and collagen-I levels increase in parallel as the heart stiffens progressively in embryonic development, but their levels adapt within hours to rapid and reversible perturbations of actomyosin contractility or ECM mechanics. In both intact hearts and in human iPS-derived cardiomyocyte cultures, low lamin-A nuclei rupture with high contractile stress, with cytoplasmic mis-localization of DNA repair factors and accumulation of DNA damage – which causes aberrant beating. Embryonic cardiomyocyte cultures show interphase phosphorylation and subsequent turnover of lamin-A are suppressed with myosin-II-dependent cell/nuclear spreading on stiff collagen-I-coated gels, compared to those cultured on soft gels. Inhibition of actomyosin stress conversely results in increased phosphorylation of lamin-A, favoring its nucleoplasmic solubilization and degradation by intracellular matrix-metalloproteinase-2 (MMP2). Nuclear stress-sensing by lamin-A thus mechano-protects the genome.

2.1 Introduction

In culture, matrix elasticity (or 'stiffness', in units of kPa) regulates cell spreading and actomyosin forces within a few hours of cell attachment and eventually affects a variety of nucleus-dependent processes (Choquet et al., 1997; Engler et al., 2006; Paszek et al., 2005; Pelham and Wang, 1997; Trichet et al., 2012; Wang and Ingber, 1994). Mechano-sensitive proteins drive many of such responses, exhibiting dynamic changes in conformation (Sawada et al., 2006; Swift et al., 2013), post-translational modification (PTM) states (Buxboim et al., 2014; Guilluy et al., 2014), subcellular localization (Dingal et al., 2015; Dupont et al., 2011; Elosegui-Artola et al., 2017; Ho et al., 2013), and even protease-driven turnover (Dingal and Discher, 2014; Flynn et al., 2010) with increased or decreased mechanical load. *Within native tissues*, however, whether and how ECM, cells, and nuclei respond to microenvironment mechanics remains poorly studied, in part due to a lack of model organ systems with readily tunable mechanical phenotypes.

Early chick hearts beat spontaneously for days after isolation from embryos without any external pacemaking (**Figure 2.1A**), and the contractile beating of these hearts has long been known to be sensitive to pressure (Rajala et al., 1976), as well as to matrix stiffening (crosslinking by transglutaminase) or softening (by collagenase) (Majkut et al., 2013). Sparse cultures of cardiomyocytes (CMs) on collagen-coated gels confirm an optimal stiffness for contractile beating on collagen-coated gels that match native heart stiffness (Engler et al., 2008; Jacot et al., 2008; Majkut et al., 2013), revealing a cell-intrinsic mechanosensitivity consistent with the mathematics of force-driven sarcomere registration (Dasbiswas et al., 2015; Friedrich et al., 2011). Substrate stiffness further regulates CM differentiation and maturation *in vitro* (Przybyla et al., 2016; Tzatzalos et al., 2016; Yang et al., 2010); however, perturbations to tissue mechanics have no known effects on protein levels or states in the intact heart. With the contractile cytoskeleton surrounding the nucleus as it does in many cell types (Figure 2.1A), actomyosin forces could impact nuclear structure(s) or even DNA, but such effects remain unknown in development.

Lamin-A filaments in the nuclear lamina surround chromatin (Gruenbaum et al., 2005; Shimi et al., 2015; Turgay et al., 2017) and have long been known to be developmentally regulated in expression level. While B-type lamins are constitutively expressed across tissues,

lamin-A is ‘absent’ in early chick and mouse embryos and increases in a tissue-dependent manner (Lehner et al., 1987; Solovei et al., 2013; Stewart and Burke, 1987), with many *LMNA* mutations or deletions resulting in evident ‘laminopathies’ shortly after birth (Hennekam, 2006; Worman and Bonne, 2007). In normal adults, lamin-A is most abundant in stiff and mechanically stressed tissues such as bone and heart, compared to soft tissues such as brain (Swift et al., 2013). In culture, lamin-A is likewise higher in cells on stiff collagen-coated gels relative to soft gels, as lamin-A filaments become stabilized against degradation under high myosin-II tension (Buxboim, et al., 2014). Degradation of lamin-A during interphase depends on its phosphorylation and nucleoplasmic solubilization by a CDK1-like kinase among other kinases (Bertacchini et al., 2013; Buxboim et al., 2014; Kochin et al., 2014; Naeem et al., 2015; Swift et al., 2013; Torvaldson et al., 2015), and phosphorylation of lamin-A has been shown to be mediated by mechanical stress on the nucleus (Buxboim et al., 2014; Swift et al., 2013). Since the earliest embryo is very soft and the embryonic heart stiffens daily with increasing deposition of collagenous ECM (Majkut et al., 2013), large increases in lamin-A in development would be consistent with mechanosensing in adult cells and should give rise to a stiffer nucleus that better resists stress (Dahl et al., 2008; Lammerding et al., 2006; Osmanagic-Myers et al., 2015; Pajerowski et al., 2007). Early heart and muscle defects in *Lmna*-knockout neonatal mice (Kubben et al., 2011; Sullivan et al., 1999) might indeed be explained by an inability to ‘mechano-protect’ chromatin from increasing mechanical load during development – but lamin-A’s primary function in embryogenesis remains debated (Burke and Stewart, 2013; Constantinescu et al., 2006), perhaps because compensatory processes obscure molecular mechanisms that are best studied *on short time scales*.

DNA damage is generally implicated in heart failure (Higo et al., 2017) and while damage can in principle be repaired over hours by DNA repair factors that are well-characterized in cancer (Burma et al., 2001; Soubeyrand et al., 2010), excess accumulation of DNA breaks in early embryonic development can result in chromosome instabilities (Vanneste et al., 2009), *de novo* mutations (Peters et al., 2015), as well as tissue malformation (Hales, 2005). DNA damage in post-natal hearts also triggers a switch from proliferative regeneration toward senescence

(Puente et al., 2014) and is clearly increased in many laminopathies (di Masi et al., 2008; Liu et al., 2005) in which cells expressing defective lamin-A likewise undergo premature senescence/apoptosis. The effects are surprisingly rescued upon culture on almost any type of ECM (de La Rosa et al., 2013a; Hernandez et al., 2010) and by inhibition of cytoskeletal stress (Larrieu et al., 2014). Mechanical stress exerted on nuclei reportedly regulates the activity of key DNA repair factors (e.g. ATR (Kumar et al., 2014)) – but matrix stiffness, cytoskeletal contractility, and lamin-A-based mechanosensing have yet to be considered in relation to DNA damage. Here, mechanobiological studies of embryonic hearts reveals lamin-A's accumulation not only begins far earlier in development than previously recognized, but also proves to be mechano-protective against DNA damage. Rapid perturbations to beating hearts as well as isolated CMs show lamin-A protein levels adjust dynamically to myosin-II tension and matrix mechanics, with a surprising intracellular role for matrix metalloprotease-2 (MMP2).

2.2 Results

2.2.1 Lamin-A effectively stiffens nuclei during development and increases with collagen-I

To first assess within a developing heart what physically happens to the nuclei of CMs, nuclear deformations were imaged in beating hearts after isolation at embryonic day-4 (E4, or Hamburger-Hamilton stage 23-24 (HH23-24) (Martinsen, 2005)). Transfection of hearts with GFP-LMNA or mCherry-Histone-H2B facilitated the imaging as each ~1 Hz contraction of heart tissue was seen to strain individual CM nuclei by ~5-8% (**Figure 2.1B-*i*,*ii***). However, GFP-LMNA nuclei deformed 2~3-fold less than control (**Figure 2.1B-*iii***), consistent with many *in vitro* studies showing that lamin-A stiffens the nucleus as it confers resistance to nuclear stress (Lammerding et al., 2006; Pajerowski et al., 2007). Given that the heart stiffens rapidly during development while beating strains remain relatively constant (Majkut et al., 2013), the average stress in CMs

and their nuclei likely increases over time, and any accumulation of endogenous lamin-A – if expressed at all – would confer greater resistance to nuclear stress.

To determine rigorously whether endogenous lamin-A is expressed in the developing heart, lysates from various developmental stages (E4, E6, and E10) were separated based on molecular weight (MW) by SDS-PAGE, and the MW range spanning lamins (73 ± 10 kDa) was analyzed by mass spectrometry (LC-MS/MS; 'MS' hereafter). Detection of 29 unique peptides across the entire length of lamin-A in E4 hearts removed any doubt of its early expression (**Figure 2.1C**). Many more proteins were detected by MS in the E4, E6, E10 lysates (**Figure 2.1D**, **Figure A.1A**), and when ranked based on fold change relative to mean expression, collagen-I (α-1,2) ranked at the top with a >10-fold increase from E4 to E10. MS measurements of collagen-I were calibrated with spike-ins of known amounts of purified collagen-I to estimate absolute abundance (μg per heart, **Figure A.1B**). Collagen-I is of course the most abundant protein in animals and is a major determinant of tissue stiffness (Shoulders and Raines, 2009), so its increase together with a dozen other structural proteins of the ECM (Fig.S1A,B) is consistent with heart stiffening in development (**Figure A.1C**) (Butcher et al., 2007; Lahmers et al., 2004; Majkut et al., 2013). Similarly upregulated were mechanosensitive proteins at the interface between adhesions and actomyosin cytoskeleton (e.g. paxillin (Zaidel-Bar et al., 2007), vinculin (del Rio et al., 2009; Huang et al., 2017; Pasapera et al., 2010), etc.) (Fig.1D, S1A), which suggests increased adhesion and contractile stress (Geiger et al., 2009).

Lamin-A likewise ranked in the top 10% of upregulated proteins while B-type lamins remained relatively constant, consistent with lamin-A-specific mechanosensitivity in adult cells (**Figure A.1D, E**) (Swift et al., 2013). The increase in Lamin-A:B ratio from E4 to E10, when plotted against MS-calibrated measurements of collagen-I (**Figure 2.1E**), fit a power-law that also goes through E18 data obtained from other studies (Vizcaino et al., 2016), and the best-fit exponent α = 0.3 over several orders of magnitude agrees with a similar analysis of diverse tissue proteomes (α ~ 0.4) (Cho et al., 2017). Such trends in lamin-A:B were validated by confocal immunofluorescence of embryonic heart tissue (Fig.1E, top inset) as well as by immunoblot (**Figure 2.1F**, upper inset; **Figure A.1F**). Lamin-A:B plotted versus stiffness E_t of embryonic

hearts measured by micropipette aspiration (**Figure 2.1F**, lower inset) likewise fit a power-law, and the scaling exponent α ~ 0.7 was again consistent with that for adult tissues (α ~ 0.6 (Swift et al., 2013)). Measurements of lamin-A:B and stiffness for E10 brain (very soft) and E10 liver (moderately stiff) also fit the trends per immunoblot (Figure 2.1F & **Figure A.1G**). Importantly, addition of collagenase to E4 hearts for 45 min softened tissue (by ~40%) and resulted in correspondingly lower lamin-A levels, providing the first indication that collagens and lamin-A might be causally coupled.

2.2.2 'Use it or lose it' scaling of lamin-A with collagen-I and perturbations to scaling

Equations for a 'use it or lose it' mechanism of protein turnover, in which tension suppresses the degradation of filamentous proteins, have recently provided working models that fit the time-dependent increases in myosin-II and collagen-I in chick heart development (Dingal and Discher, 2014), as well as the steady-state scaling of lamin-A in adult tissues with actomyosin tension and tissue stiffness (α ~ 0.7) (Swift et al., 2013). The scaling of lamin-A with collagen-I in developing hearts (α = 0.3, Fig.1E) was therefore also reasonably well-fit using the same working model (**Figure 2.2E, Figure A.2**). Various terms in these equations further suggested moderate decreases in lamin-A and/or collagen levels upon inhibition of myosin-II tension (e.g. by blebbistatin) and with modulation (or not) by drugs affecting collagen matrix, transcription/translation, matrix degradation (e.g. by proteases), or lamin-A phosphorylation.

To assess some of the expected changes in protein levels, broader profiling by MS was performed on E4 hearts treated with collagenase (45 min) or blebbistatin (1 h) in combination or not with multiple drugs (**Figure 2.3A**). Heatmaps for a subset of ECM, cytoskeletal, and nuclear proteins illustrate responses to collagenase, blebbistatin, and collagenase + blebbistatin that are all very similar, with rapid and large decreases in collagen-I subunits, vinculin, and lamin-A (30-40% as confirmed by immunoblot, **Figure 2.3B**). Little to no change was observed in most of the other detected proteins across the proteome, including matrix-metalloproteinase MMP2, cytoskeletal proteins (cardiac myosin-II, MYH7B; vimentin, VIM), B-type lamins, and the DNA

repair factor KU70 (XRCC6). Importantly, similar results were seen even with addition of a protein translation inhibitor ('Trx-i': cycloheximide), except for decreases in a few abundant cytoskeletal proteins (suggesting these are rapidly regulated by transcription/translation, as reported for β-actin (Katz et al., 2012)). Decreased collagen-I and lamin-A with blebbistatin and/or collagenase were nonetheless robust and strictly a matter of protein dynamics.

Combining blebbistatin with a broad inhibitor of matrix-metalloproteinases ('MMP-i': GM6001) prevented degradation of collagen-I (per MS of Figure 2.3A), whereas blebbistatin plus a CDK inhibitor ('CDK-i': RO3306 at >3.5 μM doses to inhibit many CDKs) that limits interphase phosphorylation of lamin-A (e.g. phosphorylation at serine 22 normalized to total lamin-A: 'pSer22/lamin-A' in Figure 2.3B) rescued the blebbistatin-induced decrease in lamin-A levels. Vinculin's decrease remained consistent with inhibition of actomyosin tension regardless of MMP-i (Figure 2.3A). Surprisingly, MMP-i treatment also rescued the blebbistatin-induced decrease in lamin-A with effects similar to CDK-i (Figure 2.3), suggesting lamin-A's mechanosensing mechanisms might be regulated by collagen-I independent of myosin-II, or by MMPs directly.

2.2.3 Contractility and collagen perturbations rapidly impact beating, lamin-A, and DNA breaks

Before addressing how MMPs might modulate lamin-A levels, we first sought to clarify the functional consequences as well as the kinetics of lamin-A mechanosensing. Intact E4 hearts were therefore treated with blebbistatin for varying durations of time. Blebbistatin caused hearts to stop beating within minutes (**Figure 2.4A, Figure A.3A**), consistent with rapid inhibition of myosin-II contractility. The effects were reversible, however, as beating recovered within minutes after washout of drug (Figure 2.4A right inset & Figure A.3A) or upon addition of the cardiac myosin-II activator omecamtiv mecarbil ('OM'; which is in Phase-III clinical trials for treating chronic heart failure: #NCT02929329 in clinicaltrials.gov). Lamin-A immunoblots revealed a decay constant of ~45 min (**Figure 2.4B & C-*i***) which was consistent with MS quantitation (Figure 2.3A) as well as with results for an inhibitor specific for cardiac myosin-II, 'MYK' (which is in Phase-II clinical trials to treat non-obstructive hypertrophic cardiomyopathy: #NCT02842242 in

clinicaltrials.gov). Treated hearts were viable for the full duration of blebbistatin treatment (4.5 h), with rapid recovery of beating upon washout of drug (Figure 2.4A). However, recovery of lamin-A levels was relatively slow, at >3h with or without OM, suggesting slow synthesis of new lamin-A protein.

Since lamin-A loss and mutation had been associated with increases in DNA damage in post-natal development of stiff tissues (Liu et al., 2005), we hypothesized that the rapid decrease in lamin-A in blebbistatin-treated E4 hearts would also associate closely with DNA damage. A primary marker for DNA breaks, phospho-histone H2AX (γH2AX) indeed changed in level about as rapidly as lamin-A (**Figure 2.4C-*i*,*ii***), but the *decrease* in DNA damage which we confirmed by electrophoretic comet assays (**Figure 2.4D, Figure A.3B**) was opposite in trend compared to past studies (Gonzalez-Suarez et al., 2009b; Redwood et al., 2011; Singh et al., 2013). We hypothesized therefore that an increase in DNA damage requires both high actomyosin tension *and* low lamin-A levels. Since washout of blebbistatin led to rapid recovery of beating (Figure 2.4A, right inset) but slow recovery of lamin-A (+5% at 1h; Figure 2.4C-*i*), DNA breaks were assayed shortly after washout, and were seen to increase sharply (+50% at 1h; Figure 2.4C-*ii*, right inset). Eventual recovery of lamin-A levels to match the steady-state stress levels appeared to suppress the excess in DNA damage, but the transient spike in DNA damage immediately after washout reveals the potentially disruptive effects of actomyosin stress on genome integrity.

Actomyosin contractility has been demonstrated in many contexts to be downstream of matrix stiffness (Mih et al., 2012; Ulrich et al., 2009), and so the results above suggested DNA damage would likewise respond to acute perturbations of collagen matrix. E4 hearts treated with collagenase for 45 min resulted in a sharp decrease in DNA damage as well as lamin-A in a dose-dependent manner (**Figure 2.5E**), consistent with rapid softening of the hearts (Figure 2.1F). Treatment with tissue transglutaminase (TGM), a cross-linker of ECM which stiffens heart tissue (>2-fold within 2h (Majkut et al., 2013)), resulted in a slight increase in lamin-A and γH2AX after 3h, both of which could be reversed by collagenase (Figure 2.5E). Taken together with the myosin-II perturbation experiments (Figure 2.4A-D), these findings indicate that lamin-A decreases quickly or increases slowly in response to matrix stiffness and actomyosin tension in

order to somehow limit DNA damage. Providing resistance against nuclear envelope rupture and accumulation of DNA breaks (e.g. as in constricted 3D migration (Denais et al., 2016; Harada et al., 2014; Irianto et al., 2017; Raab et al., 2016)) suggested one possible mechanism by which lamin-A in the heart might mechano-protect the genome (**Figure 2.5B**) – but the functional impact of DNA damage on early embryonic hearts remained unclear.

2.2.4 Excess DNA damage causes aberrant beating

To test the effects of DNA damage on the beating of E4 hearts, we added etoposide, which causes DNA double-strand breaks during replication or transcription (Tammaro et al., 2013), or H_2O_2, which oxidatively stresses multiple processes. Within 1h, etoposide caused a sharp increase in γH2AX by >4-fold, and washout of drug eventually reversed the DNA damage (**Figure 2.6A**). Kinetics in cultured cancer cells are similar (Irianto et al., 2017; Muslimovic et al., 2009), and the results here likewise indicate mechanisms of DNA repair in early cardiogenesis. Importantly, 1h etoposide treatment also resulted in many hearts exhibiting aberrant arrhythmic beating that could be suppressed by washout (**Figure 2.6B-*i,ii***), while aberrant beating was absent for DMSO control and H_2O_2 treated hearts. Prolonged etoposide treatment progressively increased the fraction of arrhythmic hearts (50% of hearts by 12h) and, like H_2O_2, eventually suppressed heart rate and the %-beating hearts (by 60h) (**Figure 2.6B-*iii,iv***). Acute DNA damage during early cardiac development can thus impair tissue-level function.

2.2.5 Lamin-A suppression in intact hearts and in human iPS-CMs: nuclear rupture & loss of DNA repair factors

To clarify how increased nuclear stress might cause DNA damage, the integrity of the nuclear envelope was first examined in intact embryonic hearts doubly transfected with the DNA repair protein, GFP-KU80 ('XRCC5'), and a cytoplasmic protein that binds DNA, mCherry-cGAS (cyclic GMP–AMP synthase) (**Figure 2.7A-*i***). Transfected hearts were treated with blebbistatin, then washed with culture medium to perturb actomyosin contractility and lamin-A levels, per Fig.2A-D. Blebbistatin treatment halted beating with partial disruption of z-band striation (**Figure 2.7A-*ii***,

upper inset) and resulted in a corresponding reduction in lamin-A immunofluorescence signal, consistent with immunoblots (Figure 2.4A, C-*i*). Upon drug washout, however, the rapid recovery in contractility (and slow recovery of lamin-A) resulted in an increase in the fraction of GFP^+ $mCherry^+$ (double positive) cells with cytoplasmic mis-localization of KU80 *and* concomitant formation of cGAS puncta at the nuclear periphery (Figure 2.7A-i, yellow arrow). Given that blebbistatin treatment and washout did not affect cell viability (determined by fraction of dead cells with fragmented DNA; **Figure A.4A**), simultaneous mis-localization of both KU80 and cGAS suggested the possibility of transient nuclear rupture under high stress, and proved consistent with the increase in DNA damage observed with blebbistatin washout (Figure 2.4C-*ii*, D).

To further assess the effects of lamin-A suppression on envelope rupture and DNA damage, nuclei were examined in human induced pluripotent stem cell-derived CMs (hiPS-CMs) cultured on collagen-coated soft or stiff gels. As with intact embryonic hearts, hiPS-CM nuclei were seen to 'beat' *in vitro* (**Figure A.4B**) and expressed lower lamin-A than a typical human cell line (e.g. A549 cells (Swift et al., 2013)), indicative of a soft nucleus, with cell morphologies and sarcomeric striations resembling those of an embryonic/fetal CM-like phenotype (Burridge et al., 2012; Yang et al., 2014b). On very stiff gels of 40 kPa, a small fraction of hiPS-CMs again exhibited cytoplasmic mis-localization of KU80 (**Figure 2.7B**), consistent with envelope rupture under high nuclear stress (Figure 2.7A). Nuclear blebs, which are typical of ruptured nuclei *in vitro* (Irianto et al., 2017), formed at points of high curvature (along major axis) in such cells, and were rich in lamin-A but depleted of lamin-B's (Figure 2.7BB). Stress-induced nuclear envelope rupture was also evident in the rapid and stable accumulation of mCherry-cGAS upon nuclear probing with a pointed Atomic Force Microscopy (AFM) tip (<1μm), at forces comparable to those exerted by the cell's own cytoskeleton (~7 nN) (**Figure A.4C**). Importantly, culturing hiPS-CMs on gels as soft as embryos (0.3 kPa) prevented rupture-induced mis-localization of KU80 (**Figure 2.8A-*i***, right), suggesting that a soft matrix limits actomyosin stress, and thereby preserves nuclear integrity, even with low lamin-A levels.

To assess whether nuclear rupture would be favored by suppression of lamin-A in hiPS-CMs on rigid collagen-coated plastic, siLMNA was used to knockdown lamin-A. Knockdown of

lamin-A resulted in a 2-fold increase in the fraction of cells with cytoplasmic leakage of KU80 (**Figure 2.8A-*i***, **Figure A.4D-*i***) as well as an increase in γH2AX foci per nucleus (**Figure 2.8A-*ii*** *&* **Figure A.4D-*ii***), indicating that DNA breaks accumulate when repair becomes limiting. Although lamin-A levels in hiPS-CMs exhibited similar sensitivity to stiffness as that in intact embryonic hearts, blebbistatin treatment in siLMNA-treated cells did not further lower lamin-A levels (~40% KD; **Figure 2.8A-*iii***). Blebbistatin did, however, cause nuclei to round up (**Figure 2.8A-*iv***) and rescued envelope rupture to basal levels (Figure 2.8-*i*). Relaxation of rigidity-driven actomyosin stress could thus limit rupture of the nuclear envelope.

KU80 is one repair factor for which immunofluorescence works well in human cells (but not chick), and at least two other major repair factors, 53BP1 and RPA2, also simultaneously mis-localized to the cytoplasm upon lamin-A knockdown (**Figure 2.8B**). Loss of such repair factors from the nucleus was seen to continue for >1 hr in culture, as shown by time-lapse images of GFP-53BP1 transduced cells upon siLMNA knockdown (**Figure A.4C**). Since total KU80 abundance did not vary across the treatments (**Figure A.4F**) nor did the abundance of its binding partner KU70 ('XRCC6') in our MS profiling of drug-perturbed embryonic hearts (Figure 2.5E), various repair factors were partially knocked down in hiPS-CMs by treating with siKU80, siRPA1, siBRCA1 as well as the combination of the three ('si-3'). BRCA1 was selected because it is implicated in myocardial infarction and ischemia (Shukla et al., 2011), and RPA1 appeared abundant and constant in level in our MS profiling (**Figure A.4G**). DNA damage increased in all four repair factor knockdowns and their combined effect seemed additive (**Figure 2.8C** *&* **Figure A.4H**). Over-expression of relevant DNA repair factors (with GFP-KU70, KU80, BRCA1) rescued only the excess DNA damage in ruptured siLMNA cells compared to non-ruptured cells (**Figure 2.8D**). A baseline level of damage in the latter cells was not affected, likely because repair factors become limiting only upon rupture or depletion. Some combinations ('GFP3') rescued the excess damage – but at least one repair factor was clearly ineffective on its own.

To assess any functional relevance of DNA damage to hiPS-CMs, beating of cultured 'organoids' was challenged with blebbistatin and the DNA damaging drug, etoposide. As shown with intact embryonic hearts (Figure 2.4A-D), the coordinated beating of hiPS-CM organoids was

reversibly inhibited by blebbistatin (**Figure 2.9A**). Furthermore, etoposide again caused irregular beating within 1h (**Figure 2.9B**), consistent with DNA damage-induced arrhythmia seen with embryonic hearts (Figure 2.6A,B). Such acute, functional effects of DNA damage raised questions about the effects of physiological pathways that regulate lamin-A.

2.2.6 Transcriptional repression of LMNA by retinoic acid (RA) increases DNA damage

Retinoic acid (RA) is a vitamin-A derivative that is a major regulator in differentiation and embryonic development (Rhinn and Dolle, 2012), and it directly upregulates *LMNA* transcription (Okumura et al., 2000; Swift et al., 2013). Antagonist to retinoic acid (AGN) has the opposite effect in adult cells (Ivanovska et al., 2017). Beating E4 hearts incubated with RA and AGN at pharmacological doses (1 μM) affected lamin-A protein levels by 72h but not by 3h **(Figure 2.10A-*i*,*ii***), consistent with past reports of slow transcriptional modulation (Swift et al., 2013). Immunoblots for γH2AX also revealed that DNA damage levels correlate inversely with lamin-A, and in particular, RA-treated hearts with lower lamin-A had ~50% more γH2AX signal, while AGN-treated hearts with greater lamin-A had less γH2AX (Figure 2.10A-*i*,*ii*). Although retinoids regulate many genes, the contractility machinery remained seemingly unaffected, with all hearts beating normally for up to 3d – until blebbistatin was added to stop the heart (**Figure 2.10B**). Thus, when actomyosin contractility is maintained, transcriptional modulation of lamin-A in intact beating hearts results in anti-correlated changes in DNA breaks, consistent with lamin-A's mechano-protective role against nuclear envelope rupture.

2.2.7 In isolated embryonic CMs, lamin-A mechanosenses matrix and actomyosin stress

Given the importance of lamin-A's mechano-protection of the genome to tissue-level function, we next sought to clarify mechanisms of lamin-A's adaptive response to matrix stiffness and actomyosin. CM culture models using gels of controlled elasticity have demonstrated matrix stiffness influences CM size, shape, myofibril assembly, and contractility (Engler et al., 2008;

Jacot et al., 2008; Ribeiro et al., 2015). As the heart stiffens during development, CMs undergo similar hypertrophic growth (with sarcomere assembly) (**Figure 2.11A**, **Figure A.5A-*i***), cell/nuclear elongation (driven in part by stabilization of microtubules (Robison et al., 2016), **Figure A.5A-*ii*, S4B**), cell-cell alignment (**Figure A.5**C), and nuclear volume reduction (**Figure A.5D**) (Hirschy et al., 2006). To elucidate matrix-to-nucleus mechanosensing mechanisms at the single cell level (**Figure A.5E**), E4 chick CMs were isolated and cultured for 24h on polyacrylamide (PA) gels of controlled stiffness (0.3 - 40 kPa) coated with constant collagen-I density (**Figure 2.11B**). Blebbistatin was added for an additional 2h to some CM cultures. Myosin-II dependent cell spreading, striation, and elongation increased on stiff gels (10 kPa) relative to soft gels (0.3 kPa) (**Figure 2.11C**), consistent with *in vivo* morphodynamics (Figure 2.11A, Figure A.5A-*i*,*ii*). Gels that mimic the stiffness of E4 heart tissue (1-2 kPa) were optimal for cell and nuclear beating (**Figure A.6A**), as shown in past studies (Engler et al., 2008; Majkut et al., 2013). Nuclear 'beating strain' in the well-separated CMs (Figure A.6A-*i,* **B-*i***) was also similar in magnitude to that seen in tissue (5-8%, as measured by $\triangle AR/AR_{ref}$) (Figure 2.1B). Surprisingly, however, lamin-A:B intensity ratio did not show such an optimum: it instead increased monotonically with gel stiffness, in parallel with myosin-II-dependent cell and nuclear elongation (AR) and with cell spreading (Figure 2.11C, **4D-*i*,*ii***, **Figure A.6G-*ii***). Sensitivity to gel stiffness at the single-cell level could be further extrapolated to collagen-coated rigid plastic (~1 GPa), and the distinct trend from optimal beating on gels merely highlights the fact that very stiff and rigid substrates cannot physically contract but nonetheless allow for an isometric tension that increases with matrix stiffness as in other cell types (e.g. (Engler et al., 2006)). Importantly, myosin-II inhibition with blebbistatin or MYK eliminated all actomyosin contractility and caused nuclei to round up and lamin-A:B to decrease to basal levels (Figure 2.11D-*i* & **Figure A.6H**) as cells became dendritic with disrupted sarcomeres (Figure 2.11C).

Since the myosin-II dependent increase in lamin-A:B with gel stiffness for isolated E4 CMs (Figure 2.11D) aligned well with lamin-A:B's increase with heart stiffness during development (Figure 2.2B-D), we assessed the mechanosensitivity of lamin-A phosphorylation in CMs cultured on gels. Immunofluorescence of phosphorylated serines 22 ('pSer22') and 390

('pSer390', a highly mechano-sensitive site based on our previous MS studies) indeed proved consistent with the proposed pathway of tension-suppressed lamin-A phosphorylation and turnover: compared to CMs on stiff gels, cells on soft gels showed higher nucleoplasmic phospho-signal, as did cells on stiff gels treated with blebbistatin (**Figure 2.11E-*i***). Phospho-signal normalized to total lamin-A ('pSer/LMNA') was also 2~3-fold higher in CMs on soft gels compared to stiff gels (**Figure 2.11E-*ii***). Blebbistatin-treated cells on stiff gels again showed increased pSer/LMNA for both phospho-sites (**Figure 2.11E-*iii***). Such changes in interphase cells were 10~20 fold lower than in the rare mitotic CMs (Fig.4E-*ii*, inset: yellow arrow). Reduction of nuclear stress by soft matrix or actomyosin inhibition thus favors lamin-A interphase phosphorylation, nucleoplasmic solubilization, and subsequent turnover – but the specific protease(s) involved in degradation of phospho-solubilized lamin-A remained unclear.

Given the surprising observation that the pan-MMP inhibitor MMP-i (GM6001) rescued lamin-A levels in blebbistatin-treated embryonic hearts (Figure 2.3A), we hypothesized that one or more MMPs could play a key role in degradation of nucleoplasmic lamin-A. Intracellular/nuclear localization and activity of at least one MMP isoform, MMP2, is well-documented for many cell types including CMs (Xie et al., 2017; Yang et al., 2010), and recent reports suggest lamin-A (but not B-type lamins) is a potential proteolytic target of MMP2, although proteolysis has not yet been demonstrated in intact cells or tissues (Baghirova et al., 2016). Isolated E4 CMs on rigid plastic were thus treated with the pan-MMP inhibitor MMP-i as well as an MMP2-specific inhibitor, 'MMP2-i' (ARP100) + blebbistatin. Indeed, inhibition of MMP2 by either MMP-i or MMP2-i rescued the blebbistatin-induced ~50% decrease in lamin-A:B (Figure 2.11D-*i*), despite no significant effect on striation, cell morphology, or gel stiffness. The findings confirm at the single cell level our MS profiling of embryonic hearts treated with MMP-i + blebbistatin (Figure 2.3A), and finally remove any confounding effect of collagen changes. Other MMP isoforms could have a similar role, including MMP9 which regulates myoblast proliferation (Zimowska et al., 2013), but the results here suggest MMP2 is a key isoform in CMs and in intact embryonic hearts.

2.2.8 Lamin-A is phospho-solubilized into the nucleoplasm and degraded by MMP2 under low nuclear stress

Given the surprising effects of MMP2 on lamin-A levels *in vitro*, we next sought to clarify mechanisms in the intact embryonic heart. Beating E4 hearts were treated with MMP-i or MMP2-i ± blebbistatin. Consistent with our gel culture results and with MS quantitation (Figure 2.3A), MMP2-i again rescued the blebbistatin-induced decrease in lamin-A, as did MMP-i (**Figure 2.12A-*i***). Immunoblots using a custom-made antibody for phosphorylated serine 390 ('pSer390') further revealed an increase in pSer390 on intact lamin-A (at ~73 kDa) upon blebbistatin treatment (**Figure 2.12A-*ii***, '$pSer390_{intact}/LMNA_{intact}$'). More dramatic was the suppression by MMP2-i and MMP-i (regardless of blebbistatin) of pSer390 signal on a ~42 kDa lamin-A fragment ('$pSer390_{fragm.}/pSer390_{intact}$') that matches the predicted degradation by MMP2 (Barrett, 2004; Song et al., 2012) (**Figure 2.12A-*iii***). This ~42 kDa fragment is likely a transient intermediate (**Figure 2.12B**), because similar perturbations *in vitro* produce many more low-MW degradation fragments that are highly phosphorylated (Buxboim et al., 2014). MS confirmed the trend for the 42 kDa fragment range (>6 detected LMNA peptides) in hearts treated with blebbistatin or collagenase (**Figure 2.12C**).

Importantly, blebbistatin treatment did not affect MMP2's overall abundance (as determined by MS; Fig.1H) or its catalytic activation ('cleaved/pro-MMP2' ratio as measured by immunoblots, **Figure 2.12D, Figure A.8A**). Immunofluorescence with anti-MMP2 (against both pro- and active forms) revealed that MMP2 is indeed present in the cytosol as well as the nucleus – mostly the nucleoplasm – of embryonic chick CMs, and that localization is unaffected by actomyosin inhibition (**Figure 2.12E**). Abundant nucleoplasmic signal suggested MMP2 is in the right place for degradation of phosphorylated, nucleoplasmic lamin-A (Kochin et al., 2014). MMP2 abundance and activity in CM nuclei thus appear independent of mechanical stress, while MMP2 degradation of lamin-A is downstream of lamin-A phosphorylation and suppressed by actomyosin tension (Figure 2.12B).

To further assess whether increased phosphorylation and solubilization of lamin-A indeed favors its degradation, cultured cells (human A549s) were transduced with phosphomimetic

mutants (GFP-S22A & GFP-S22E). Nucleus-specific GFP fluorescence of 'non-phosphorylatable' GFP-S22A was ~2x higher than 'phosphorylated' GFP-S22E (**Figure A.8B**), which suggests faster steady-state degradation of GFP-S22E relative to GFP-S22A. GFP-S22A was found to be clearly more lamina-associated than nucleoplasmic, but the opposite was true for GFP-S22E (**Figure A.8B-*i,ii***). Inhibition of protein synthesis by Trx-i did not affect localization (Figure A.9A-*i,ii*) but did decrease overall GFP intensities by <10% (**Figure A.8B-*i,iii***). Immunoblots against lamin-A and GFP also revealed multiple low-MW fragments for GFP-S22E (including ~40 kDa and many <30 kDa) but not for GFP-S22A (**Figure A.8C**, green arrows). MMP2-i treatment in GFP-S22E expressing cells resulted in an increase in intact lamin-A (as determined by GFP fluorescence signal (**Figure A.8D**)), consistent with inhibition of MMP2-degradation.

To assess the effects of MMPs on DNA damage, intact E4 hearts were treated with both MMP-i and blebbistatin. The combination maintained lamin-A at levels comparable to control (per Fig.1H, 6A) but had no effect on γH2AX relative to blebbistatin alone (**Figure 2.12F**). Treatment with a high dose of CDK-i (RO3306), on the other hand, reduced γH2AX by ~50% in addition to maintaining high lamin-A in blebbistatin-treated hearts. CDK-i inhibits phospho-solubilization of lamin-A (Figure 2.3B), similar to the S22A construct, and thereby stiffens and stabilizes the nucleus based on micropipette aspiration of nuclei in cultured cells (Buxboim et al., 2014). Thus, low actomyosin stress – combined with high non-phosphorylated lamin-A maintained at the nuclear periphery – minimizes DNA damage in the intact embryonic heart.

2.3 Discussion

The 'use it or lose it' model in which tension stabilizes filaments against turnover has been shown to apply rigorously to purified collagen gels with added MMP (Flynn et al., 2010) and, based on studies of cell cultures, has been inferred to also apply to phosphorylated lamin-A (Dingal and Discher, 2014) and phosphorylated myosin-II (Shin et al., 2014). Accumulation of such proteins is thus favored by a given mechanical stress, with any synthetic excess soon degraded. While early embryos are soft and have minimal collagen (Rozario and DeSimone, 2010), as the heart forms and pumps to perfuse the growing embryo, the increasing pressure favors accumulation of

collagen-I and stiffening of the developing heart. The increasing stiffness and stress necessitate an adaptive mechanism to protect against nuclear stress, and lamin-A mechanosensing fulfills this role by also accumulating (Figure 2.2) – unless actomyosin stress is inhibited (Figure 2.3A). Lamin-A thus maintains nuclear integrity and helps retain DNA repair factors in the nucleus (10A-C), and thereby prevents excessive accumulation of DNA damage in stiff microenvironments and/or under conditions of high actomyosin contractility (**Figure 2.13**). Remarkably, MMPs that degrade and remodel collagen-I matrix within hours or less also directly regulate lamin-A of the nuclear matrix (Figure 2.3A, Figure 2.13), which suggests a surprising inside-outside symmetry to the 'use it or lose it' mechanism. While nuclear MMPs are not new (Xie et al., 2017), tension regulation of the substrates for these enzymes seems unprecedented.

Lamin-A is found here to be expressed in the heart far earlier than previously reported (Stewart and Burke, 1987), but early expression is consistent with the progressive stiffening of the heart and tight coupling in levels to what eventually becomes the most abundant protein in adult animals, collagen-I. Calibrated measurements of collagen amounts (Figure 2.2C) agree with past reports for soluble collagen content in developing chick hearts (Woessner et al., 1967), but dividing by reported myocardium volumes (Kim et al., 2011) gives collagen-I densities far lower than those used in studies of collagen-I gels (Yang et al., 2009), suggesting lower densities are needed for a stiffness in the kPa range as measured for heart (Figure 2.2D). Nonetheless, collagen-I digestion resulted in softer tissue and decreased lamin-A consistent with scaling trends (Figure 2.2F), which indicates the physical insight gained from a scaling approach with concentration. Surprisingly, the scaling exponent of $\alpha = 0.3$ (in lamin-A ~ collagen-I$^{\alpha}$; Figure 2.2C,E) in embryonic development matches that obtained from meta-analyses of 25 transcriptomics datasets analyzed for a wide range of normal and diseased hearts spanning five species (**Figure A.9A**), which indicates potential feedback to gene expression (Figure A.2), as suggested by past studies (Swift et al., 2013). The scaling is also reasonably consistent with that across proteomes of diverse chick embryonic tissues at E18 (**Figure A.9B**) as well as adult mouse tissues ($\alpha = 0.4$) (Cho et al., 2017), and underscores the potential universality of the mechanism. Indeed, the tissue-dependent timing of detectable lamin-A expression (Lehner et al.,

1987; Rober et al., 1989; Solovei et al., 2013) correlates well with the stiffness that a given tissue eventually achieves in adult (**Figure A.9C**; adapted from (Rober et al., 1989; Swift et al., 2013)).

The findings might help explain why defects in lamin-A cause disease through cell-extrinsic mechanisms (de La Rosa et al., 2013a). Indeed, mosaic mice in which 50% of the cells express defective lamin-A maintain a normal lifespan, whereas mice with 100% defective cells die within weeks of birth. The same cells (and similar cell types (Hernandez et al., 2010) cultured on rigid plastic undergo premature senescence/apoptosis, as is common with excess DNA damage, but the defects are surprisingly rescued upon culture on almost any type of ECM. Soft matrix certainly reduces cytoskeletal stress and suppresses nuclear rupture and DNA damage in CMs with low lamin-A (Figure 2.8A). The effects are further consistent with the observation that laminopathies largely affect stiff and mechanically stressed adult tissues such as muscle or bone while sparing soft tissues such as brain, independent of lineage or developmental origin (Cho et al., 2018; Worman, 2012).

The progressive stiffening of embryonic tissues during development is further accompanied by frequent constricted migration events and dynamic contractile pulses that drive morphogenesis (Bone and Starr, 2016; Gjorevski et al., 2015; Krieg et al., 2008; Munjal et al., 2015; Wang et al., 2017; Wozniak and Chen, 2009) which could, in principle, undermine genome stability in cells with low or defective lamin-A. In the beating embryonic heart, normal lamin-A is found here to adjust dynamically in response to perturbations of actomyosin stress (Figure 2.4A-D). Importantly, such mechanosensing by lamin-A occurs in interphase nuclei (Figure 2.11E) independent of cell cycle changes (which may result from actomyosin or matrix perturbations in neonatal/larval myocytes (Wang et al., 2018; Yahalom-Ronen et al., 2015)). Our studies of isolated CMs on soft/stiff gels further demonstrate that steady-state lamin-A levels are determined primarily by a basal tone related to average morphologies of cells and nuclei, as opposed to dynamic contractions that intermittently strain the nucleus (Figure 2.11D, Figure A.6B). Studies using 3D cardiac microtissue constructs indeed demonstrate that a stiffer matrix with higher collagen density results in a significant increase in ‘static’ isometric tension, but not necessarily higher ‘dynamic’ stress (Boudou et al., 2012). On the other hand, both basal and dynamic strain

might contribute to a ‘tension-time integral’ model (based on cumulative time spent under high tension) that also predicts hypertrophic versus dilated cardiomyopathy disease fates (Davis et al., 2016).

Suppression of lamin-A by siRNA knockdown (Figure 2.8) or by treatment with RA (Figure 2.10A) resulted in increased DNA damage, suggesting that lack of protection by lamin-A compromises genome integrity when actomyosin stress is kept high. Conversely, inhibition of contractile stress and lamin-A phosphorylation (by blebbistatin & CDK-i co-treatment; Figure 2.12F), or transcriptional upregulation of lamin-A by AGN (Figure 2.10A), led to a reduction in DNA damage, consistent with enhanced mechano-protection of the genome. These results, however, raise a fundamental question as to why cells do not simply maintain high lamin-A levels at all times. Although lamin-A does exhibit stress-stiffening behavior with large nuclear strains over short time-scales (Stephens et al., 2017), one possible explanation for why its levels need to be optimally regulated could be that an overly rigid ‘nucleoskeletal matrix’ with excess lamin-A disrupts sarcomere assembly and/or contractility, analogous to defects seen with rigid fibrotic ECM. Lamin-A further regulates a wide range of cytoskeletal genes (e.g. ACTA2) via the MKL1/SRF pathway (**Table 2**,

Figure A.10) (Buxboim et al., 2014; Ho et al., 2013), contributes to chromatin organization (Guelen et al., 2008; Harr et al., 2015; Poleshko et al., 2017; Uhler and Shivashankar, 2017), and interacts with various regulatory factors at the nuclear periphery (e.g. lamin-B receptor, LBR ((Buxboim et al., 2017), lamina-associated polypeptide 2alpha, LAP2α (Gotic et al., 2010)) (Serebryannyy and Misteli, 2017). Thus, constitutively high lamin-A levels to protect the genome may compromise lamin-A’s fine-tuning of downstream processes in differentiation and maturation. A tension-mediated ‘use it or lose it’ mechanism would help prevent such excessive accumulation by ensuring optimal lamin-A levels are achieved in close coordination with the changing mechanical environment.

Failure to appropriately protect against the increasing mechanical loads of the stiffening heart appears to have severe consequences on cardiac function and survival. Mutations in *LMNA* or other nuclear proteins that cause defective post-translational processing (Bergo et al., 2004) or

aberrant assembly of lamin-A to the nuclear periphery (as with nucleoplasmic aggregates seen in some DCM phenotypes (West et al., 2016)) could therefore result in increased DNA damage, in turn affecting transcription (Shanbhag et al., 2010) and tissue-level function. Recent iPS-CM models of *LMNA* cardiomyopathies (e.g. R225X which causes DCM) indeed report significant nuclear blebbing (Lee et al., 2017), focal loss of nuclear membrane (perhaps indicative of rupture) (Siu et al., 2012), cytoskeletal defects (Bollen et al., 2017), and fibrosis (Captur et al., 2018), all of which increase with electrical stimulation and enhanced contractility. Furthermore, arrhythmias and broader conduction defects that are common for many cardiac laminopathies (Fatkin et al., 1999; Muchir et al., 2000) provide additional evidence of a potential causal link between DNA damage and the coordinated contractions of CMs (Figure 2.6). Thus, mechanosensing by lamin-A to protect the genome is not only critical during embryonic development, but also has potential clinical implications for a broad range of adult musculoskeletal diseases.

2.4 Materials and Methods

2.4.1 Embryonic chick heart isolation

White Leghorn chicken eggs (Charles River Laboratories; SPF Fertilized eggs, premium) were incubated at 37˚C with 5% CO_2 and rotated once per day until the desired developmental stage. Embryos were extracted at room temperature (RT) by windowing eggs, carefully removing extra-embryonic membranes with sterile forceps, and cutting major blood vessels to the embryonic disc tissue to free the embryo. The extracted embryo was then placed in a dish containing pre-warmed PBS and quickly decapitated. For early E2-E5 embryos, whole heart tubes were extracted by severing the conotruncus and sino venosus. For older (>E5) embryos, embryonic discs were extracted by windowing the egg, cutting out the embryo with the overlying vitelline membrane intact, lifting out the embryo adherent to the vitelline membrane and placing in a dish of pre-warmed PBS. Extra-embryonic tissue was carefully cut away using dissection scissors and the embryo was teased away from the vitelline membrane using forceps. Whole hearts (>E5) were extracted by severing the aortic and pulmonary vessels. The pericardium was

carefully sliced and teased away from the ventricle using extra-fine forceps. E10 brain and liver tissue were collected from the presumptive midbrain and hepatic diverticulum, respectively. All tissues were incubated at 37˚C in pre-warmed chick heart media (α-MEM supplemented with 10 % FBS and 1% penn-strep, Gibco, #12571-063) until ready for use.

2.4.2 Whole heart tube transfection

Lipofectamine/plasmid complexes were prepared as described by the manufacturers (Lipofectamine 2000, Invitrogen). In particular, 3-4 μg of plasmid (mCherry-Histone H2B or GFP-LMNA) and 10 μL Lipofectamine were each diluted to total volumes of 50 μL in Opti-MEM (Gibco, 31985-070) and incubated at RT for ~15 min. Both solutions were combined to make the 1 mL final transfection solution which was incubated for an additional 25 min. Heart tubes were pre-incubated in 0.9 ml pre-warmed chick heart media during lipofectamine/plasmid complex formation. The lipofectamine/plasmid complex was then added to the heart tubes in heart media and the heart tubes were incubated at 37˚C and 5% CO_2 for 8-12 hours. Transfection media was replaced with pre-warmed chick heart media and the hearts were incubated until use in subsequent imaging.

2.4.3 Quantification of beating strain

Transfected E4 chick hearts were video-imaged using an Olympus I81 at 4x magnification, with a CCD camera. Procedures described by Taber et al. (Taber et al., 1994) were followed to calculate 2D tissue beating strain. Briefly, ≥3 groups of 3 cells located within 20 microns of each other were selected as fiduciary markers along the outer walls of ventricular tissue. A custom Matlab program was written to track their displacements and compute trace of the tissue strain tensor (Taber et al., 1994). Alternatively, for higher throughput quantification of contractility changes (n>10 hearts per sample, e.g. following blebbistatin treatment), morphological measurements (projected 2D area, aspect ratio (AR), circularity, perimeter, etc.) of beating whole-hearts were traced with time. Morphology measurements were normalized to baseline reference

values, and peak-to-valley 'amplitudes' were averaged over >5 beats to quantify beating strain (e.g. $\triangle AR/AR_{ref}$). Similar methods were used to quantify nuclear deformations: the projected 2D area and aspect ratio (AR) of transfected nuclei (e.g. expressing GFP-LMNA, see *Whole heart tube transfection* section above) were traced with time, and the normalized amplitudes were measured and compared across experimental conditions to quantify differences in beating strain on the nucleus.

2.4.4 Isolation of embryonic CMs

To isolate embryonic CMs from tissue, whole hearts were diced to sub-millimeter size and digested with Trypsin/EDTA (Gibco, 25200-072). Approximately 1 ml of Trypsin per E4 heart was added and incubated for 13 min at 37˚C with gentle shaking, then placed upright for 2 min to let large tissue pieces settle to the bottom. The supernatant was carefully removed and replaced with an equal volume of fresh Trypsin for a second round of 15 min incubation at 37˚C. Digestion was blocked by adding an equal volume (1:1) of chick heart media. Isolated cells were plated onto collagen-I-coated polyacrylamide (PA) gels (see *Synthesis of soft and stiff polyacrylamide (PA) gels for cell culture*) and were allowed to adhere for >4h. Spontaneously beating CMs were imaged using an Olympus I81 microscope with a 40x air objective configured for phase contrast after 24 hrs in culture. As with intact hearts, a custom Matlab program was used to segment CMs and track cell area and AR. For each cell, normalized amplitudes were averaged over >5 beats to quantify beating strain (e.g. $\triangle AR/AR_{ref}$), and results for >10 cells were pooled for each experimental condition.

2.4.5 Mass spectrometry (LC-MS/MS) of whole heart lysates

Mass spectrometry (MS) samples were prepared using the same procedures outlined in Swift et al. (Swift et al., 2013). Briefly, ~1 mm^3 gel sections were excised from SDS–PAGE gels and were washed in 50% 0.2 M ammonium bicarbonate (AB), 50% acetonitrile (ACN) solution for 30 min at 37°C. The washed slices were lyophilized, incubated with a reducing agent (20 mM TCEP in 25

mM AB solution), and alkylated (40 mM iodoacetamide (IAM) in 25 mM AB solution). The gel sections were lyophilized again before in-gel trypsinization (20 mg/mL sequencing grade modified trypsin, Promega) overnight at 37°C with gentle shaking. The resulting tryptic peptides were extracted by adding 50% digest dilution buffer (60 mM AB solution with 3% formic acid) and injected into a high-pressure liquid chromatography (HPLC) system coupled to a hybrid LTQ-Orbitrap XL mass spectrometer (Thermo Fisher Scientific) via a nano-electrospray ion source.

Raw data from each MS sample was processed using MaxQuant (version 1.5.3.8, Max Planck Institute of Biochemistry). MaxQuant's built-in Label-Free Quantification (LFQ) algorithm was employed with full tryptic digestion and up to 2 missed cleavage sites. Peptides were searched against a FASTA database compiled from UniRef100 gallus gallus (chicken; downloaded from UniProt), plus contaminants and a reverse decoy database. The software's decoy search mode was set as 'revert' and a MS/MS tolerance limit of 20 ppm was used, along with a false discovery rate (FDR) of 1%. The minimum number of amino acid residues per tryptic peptide was set to 7, and MaxQuant's 'match between runs' feature was used for transfer of peak identifications across samples. All other parameters were run under default settings. The MaxQuant output tables were then fed into its custom bioinformatics suite, Perseus (version 1.5.2.4), for protein annotation and sorting.

2.4.6 Mechanobiological gene circuit model for tension-suppressed turnover

Protein (lower case: l, m, c) and mRNA transcript (upper case: L, M, C) circuitry for lamin-A, myosin-II, and collagen-I is illustrated schematically in Fig.S1H. Expression kinetics are described by a system of coupled rate equations adapted from Dingal et al. (Dingal and Discher, 2014). For simplicity, RNA translation and degradation were assumed linear in transcript concentration. Lamin-A protein (l) is a weak regulator of serum response factor (SRF), which enhances myosin-II transcription (with rate constant $\tilde{\alpha}_3$). Our previous studies suggest mechanical regulation of protein phosphorylation and turnover, and so we describe l, m, c protein degradation with suitable Hill functions (with rate constants $\tilde{\delta}_1$, $\tilde{\delta}_2$, $\tilde{\delta}_3$, respectively) to incorporate the stabilizing effects of

tension (K). Specifically, lamin-A and collagen-I protein (l and c) turnover are dictated by $K_l \sim m^{x/n_l}$ and $K_c \sim m^{z/n_c}$, respectively, for some x and z that dictate sensitivity of degradation to myosin-generated tension. Myosin-II protein (m) turnover in turn depends on matrix elasticity E which correlates strongly with collagen-I (c), such that $K_m \sim c^{y/n_m}$ for some y that represents the affinity for myosin degradation. Collagen mRNA (C) production is assumed to be proportional to the population of cardiac fibroblasts, which is ultimately limited by tissue stiffness imparted by ECM density. The rate equations were solved numerically using a custom Matlab code.

2.4.7 Micropipette aspiration of tissue

Micropipettes were pulled from 1 mm glass capillaries (World Precision Instruments, Sarasota, FL) using a Flaming-Brown Micropipette Puller (Sutter Instrument, Novato, CA). Pulled pipettes were scored with the tapered base of another pulled pipette and broken such that the final inner diameters were 35-45 μm. Pipettes were then filled with PBS and attached to a manometer-double reservoir set-up. Tissue samples were aspirated at RT in PBS supplemented with 3% BSA, without Ca^{2+} to suppress beating. Prior to each aspiration experiment, pipette tips were incubated in PBS/BSA solution for ≥20 min to minimize tissue sticking to the inner walls of the pipette. During aspiration, ≥ 3 different pressures were applied from 0.5 – 1.4 kPa for brain tissue and 0.5-20 kPa for heart and liver tissue. Aspiration of samples was video-recorded using a Nikon TE300 microscope with a 20x air objective and CCD camera. The effective Young's modulus E_t of the tissue was obtained based on the linearity between the pressure differential (between inside and outside, $\triangle P$) and strain L/R_p: $\Delta P = \frac{2\pi}{3\varphi_0} E_t \frac{L}{R_p}$, where L is the length of tissue aspirated from the mouth of the pipette, R_p is the pipette's inner radius, and φ_o is a shape factor ~2 (Theret et al., 1988).

2.4.8 *Ex vivo* drug perturbations

For actomyosin perturbation experiments, E4 heart tissue was incubated in 25 μM blebbistatin (EMD Millipore, #203390, stock solution 50 mg/ml in DMSO), 1 μM Omecamtiv Mecarbil (OM, Cytokinetics) or 0.3 - 1 μM MYK-581 (gift from MyoKardia) in heart media at 37˚C. Drug-treated hearts were compared to a control sample treated with an equal concentration of vehicle solvent DMSO in heart media. Drug solutions were gently washed out with pre-warmed chick heart media x3 for recovery experiments. For collagen matrix perturbations, E4 heart tissue was incubated in 0.3 - 1 mg/ml concentrations of collagenase (Sigma, #C7657) for ~45 min, or 20 mg/mL transglutaminase (Sigma, T5398) for up to 3 hrs at 37˚C. Enzyme activity was blocked by replacing with chick heart media containing 5% BSA. For MMP inhibition during blebbistatin treatment, hearts were incubated with 10 μM GM6001 (EMD Millipore, #CC1010) or with 30 μM of ARP100 (Santa Cruz, CAS 704888-90-4). 1 μM cycloheximide (CHX, Sigma, C7698-1G) was added to block protein synthesis during actomyosin and/or matrix perturbations. For transcriptional modulation of *LMNA* using retinoid compounds, hearts were incubated with 1 μM retinoic acid (RA, Fisher Scientific) or antagonist to retinoic acid (AGN-193109, Santa Cruz), for short (3 hrs) or long (72 hrs) treatment times. At least 8 E4 hearts were treated and pooled per lysate/experimental condition.

2.4.9 Alkaline Comet assay

Comet assays was performed according to manufacturer's protocol (Cell Biolabs). Briefly, cells were trypsinized, mixed with liquefied agarose at 37°C, placed drop-wise onto the supplied glass slide, and incubated for 15 min at 4°C for the agarose to gel. Lysis buffer from the kit was then added to the solidified gel and incubated for 45 min, followed by an additional 30 min incubation with alkaline solution. Electrophoresis was performed at 300 mA for 30 min followed by a 70% ethanol wash, before samples were

air dried overnight. Finally, DNA dye in the kit was added to each sample for 15 minutes, followed by epifluorescence imaging as described above.

2.4.10 Transduction of GFP-phosphomimetic mutants S22A and S22E

GFP-Lamin-A S22A and S22E plasmids were constructed by standard site directed mutagenesis (Stratagene). Phosphomutant constructs were packed into a lentiviral delivery system and transduced into lamin-A knockdown A549s. Transduction efficiencies ranged from 60-90%. Transduced A549 cells were treated with cycloheximide at a concentration of 500 µM diluted in Ham's F-12 nutrient media (Thermo Fisher) for 3 hours. MMP-2 inhibitor ARP-100 was used at 30 µM concentration for 3 hours as well. DMSO added to media in equal volume as the drug, was used as control in both cases. The cells were then washed in PBS and fixed with 4% formaldehyde (Sigma-Aldrich) in PBS for 10 min at RT followed by washing in 0.1% BSA diluted in PBS 3X for 5 min. Blocking was performed in 5% BSA in PBS. Lamin-A/C (4C11) Mouse mAb (Cell Signaling) was used as the primary antibody. It was diluted 1:500 from stock concentration and incubated overnight at 4°C followed by washing in 0.1% BSA diluted in PBS 3X. Donkey secondary antibody was used at 1:500 dilution (Alexa Fluor dye 647) in 1% BSA diluted in PBS, along with Hoechst diluted at 1:2000. Imaging for quantitative immunofluorescence of lamin-A, GFP was performed using an inverted microscope (IX-71; Olympus) with either 20X (Olympus, NA-0.75) or 40X (NA-0.60) objectives, and a cooled CCD camera (Cascade; Photometrics) and image acquisition performed with Fiji ImageJ software.

2.4.11 siRNA knockdown and GFP-repair factor rescue

All siRNAs used in this study were purchased from Dharmacon (ON-TARGETplus SMARTpool; siBRCA1, L-003461-00; siBRCA2, L-003462-00; siKu80, L-010491-00; siRPA1, L-015749-01; siLMNA, L-004978-00 and non-targeting siRNA, D-001810-10). GFP-KU70 and GFP-KU80 were gifts from Dr. Stuart L Rulten from University of Sussex, Brighton, UK (Grundy et al., 2013), and GFP-53BP1 was a gift from Dr. Roger Greenberg from University of Pennsylvania (Cho et al.,

2014). U2OS cells were plated 24 hours prior to transfection. Lipofectamine/nucleic acid complexes were prepared according to the manufacturer's instructions (Lipofectamine 2000, Invitrogen), by mixing siRNA (25 nM) or GFPs (0.2-0.5ng/ml) with 1 µg/ml Lipofectamine 2000. Final solutions were added to cells and incubated for 3 days (for siRNAs) or 24 hours (for GFPs) in corresponding media containing 10% FBS.

2.4.12 Human iPS-CM differentiation and culture

Normal human iPS cells (gift from Dr. Joseph Wu, Stanford CVI Biobank) were cultured following the protocol provided. Briefly, Matrigel (BD Matrigel, hESC qualified: #354277) was suspended in cold DMEM/F12 medium 1:200 dilution (DMEM/F12 medium #10-092-CM-Fisher), mixed gently, and 1ml of this suspension was added to one 6-well plate (Corning Catalog #353046) and incubated for 1hr at RT to allow Matrigel to coat the surface. The solution was gently aspirated and small aggregates of human iPS cells were added to each well in mTesr1 medium containing 10 µM of ROCK inhibitor (Y27632, 2HCl – 50 mg: #50-863-7-Fisher). Culture medium was replaced daily (no ROCK inhibitor) until the cells reached ~85% confluency.

hiPS cells were differentiated into cardiomyocytes (hiPS-CMs) using the "Cardiomyocytes differentiation and maintenance kit' from Stem Cell technologies (#05010 & #05020). The differentiation process was followed as described by the manufacturer's protocol. Briefly, the mTesr1 medium with ROCK inhibitor (10 µM) was replaced with differentiation medium A, cultured for 2 days (Day 0), then subsequently to medium B for 2 days (Day 2) and again switched to medium C twice (Day 4 & 6). From Day 8 onwards, maintenance medium (Day 8) was added/refreshed every 2 days until spontaneous CM beating was observed through imaging.

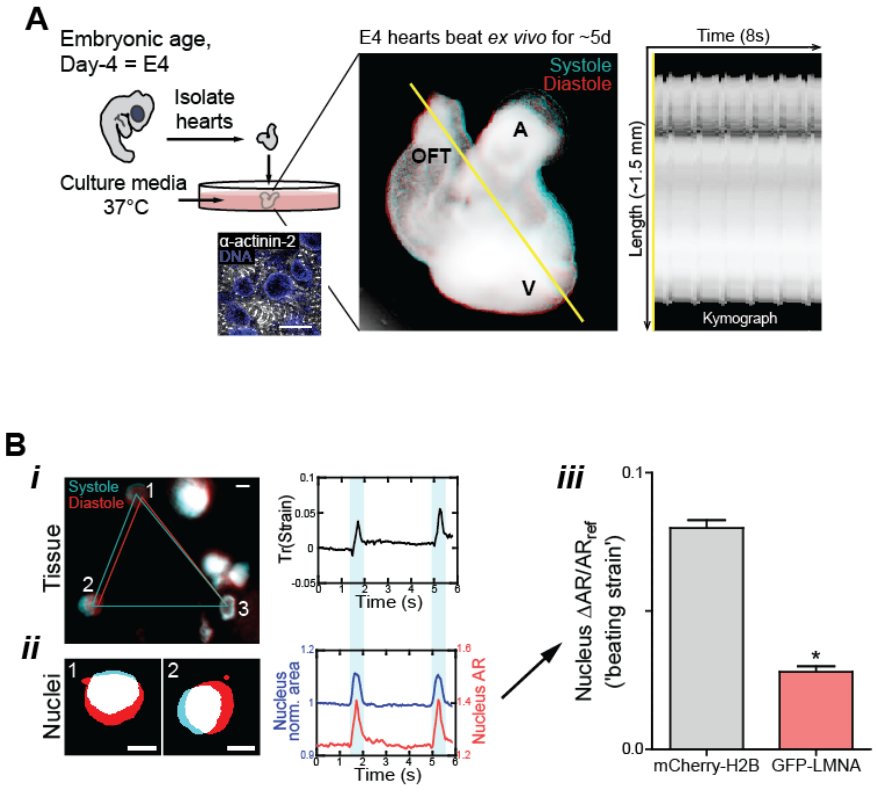

Figure 2.1. Nuclear 'beating' in isolated hearts is suppressed by forced overexpression of lamin-A

(**A**) Embryonic chick hearts isolated from day 4 (E4) embryos beat at 1-2 Hz *ex vivo* for up to 5 days in culture medium. Red and cyan indicate snapshots of diastole and systole, respectively. A=atrium, V=ventricle, OFT=outflow tract. (**B**) (***i***) Representative snapshots of beating E4 tissue with GFP-LMNA transfection. Right: Trace of tissue strain tensor quantified using transfected nuclei as fiduciary markers, as detailed in (Taber et al., 1994). (***ii***) Snapshots of individual nuclei 'beating' *ex vivo*. Nuclear strain quantified by tracing nuclear area and aspect ratio (AR) with time reveals precise synchrony with tissue-level contractions. (***iii***) Stiffer nuclei overexpressing GFP-LMNA deform less than those transfected with mCherry-H2B control. Scale bar = 5 μm.

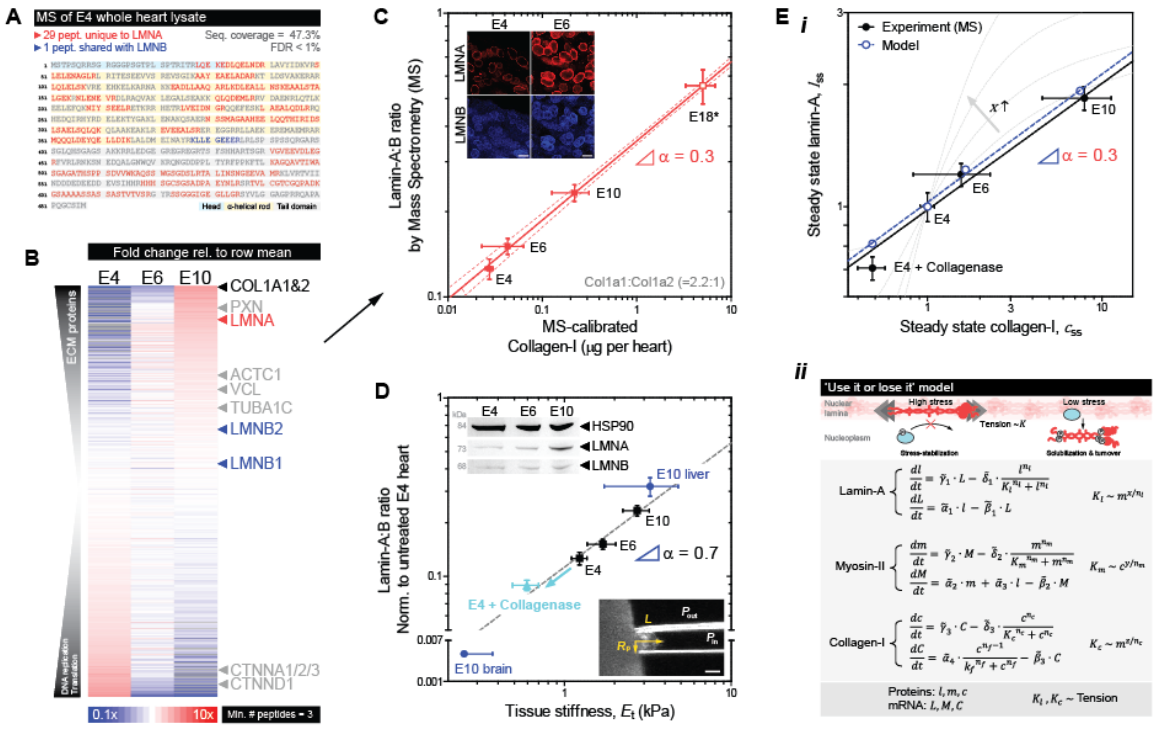

Figure 2.2. Lamin-A expression begins early, increases with collagen-I & with stiffening of embryonic heart, and fits a 'use it or lose it' model

(**A**) LC-MS/MS of E4 whole heart lysates detect 29 peptides unique to lamin-A. (**B**) Heatmap of all proteins detected by MS, ranked by the fold-change relative to the average. Collagen-I and lamin-A rank among the top proteins upregulated from E4 to E10, while lamins-B1 and B2 remain comparatively constant. (**C**) Lamin-A:B ratio determined by MS fits power-law scaling versus MS-calibrated collagen-I (µg per heart) (R^2 = 0.9997), with a scaling exponent α ~ 0.3 comparable to that found for diverse adult tissue proteomes (α ~ 0.4) (Cho et al., 2017; Swift et al., 2013). *E18 datapoint obtained from the PRoteomics IDEntifications (PRIDE) database (Vizcaino et al., 2016) fits the trend within the 95% confidence interval, but was excluded from curve-fitting. Upper inset: Confocal immunofluorescence images of lamin-A and B1/B2 in embryonic hearts. Scale bar = 10 µm. (**D**) Lamin-A:B ratio in developing hearts exhibits power-law scaling versus tissue microelasticity E_t (or 'stiffness') measured by micropipette aspiration (lower right inset), with a scaling exponent α ~ 0.7 again consistent with that for adult tissue (α ~ 0.6) (Swift et al., 2013). Blue: brain and liver tissue measurements at E10. Cyan: e*x vivo* tissue softening by collagenase treatment results in a corresponding reduction in lamin-A. Upper left inset: Immunoblot densitometry measurement of lamin-A and B in embryonic heart lysates at E4, E6, and E10 (n>6 hearts per lysate). (**E**) 'Use it or lose it' model of tension-inhibited protein turnover (Dingal and Discher, 2014) fits steady state lamin-A_{ss} vs collagen-I_{ss} scaling (α = 0.3) in heart development. Lamin-A turnover is dictated by $K_l \sim m^{x/nl}$, for some x that represents sensitivity of lamin-A degradation to myosin-generated stress.

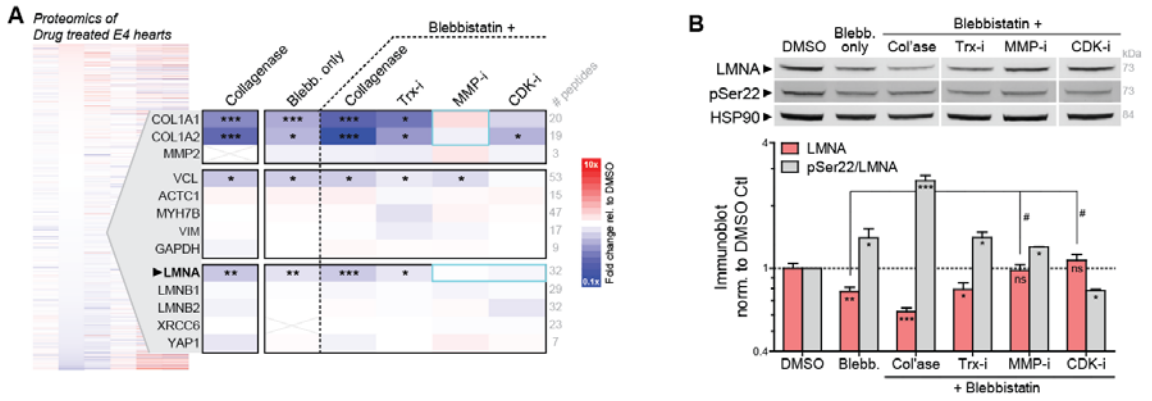

Figure 2.3. Lamin-A mechanosensitivity is maintained even with inhibition of protein synthesis, but lost w/ inhibition of phosphorylation or of MMPs

(**A**) Proteomic profiling of *ex vivo* drug perturbations. Responses for proteins of interest in the extracellular matrix (ECM), cytoskeleton, and nucleus are shown as a heatmap based on MS intensity fold-change relative to DMSO control. 'Trx-'' = inhibitor of protein transcription/translation (cycloheximide, CHX); 'MMP-i' = broad spectrum pan-MMP inhibitor (GM6001); 'CDK-i' = CDK inhibitor (RO3306, at >3.5 μM doses to inhibit many CDKs). (**B**) Immunoblot validation of lamin-A trends seen in MS profiling of drug perturbations (n>6 hearts per lysate). Additional immunoblot against phosphorylated Ser22 shows that normalized phosphorylation ('pSer22/LMNA') increases with blebbistatin-inhibition of actomyosin stress or with collagenase-softening of tissue, but decreases with CDK-i treatment. (**p*<0.05, ** *p*<0.01, ****p*<0.001)

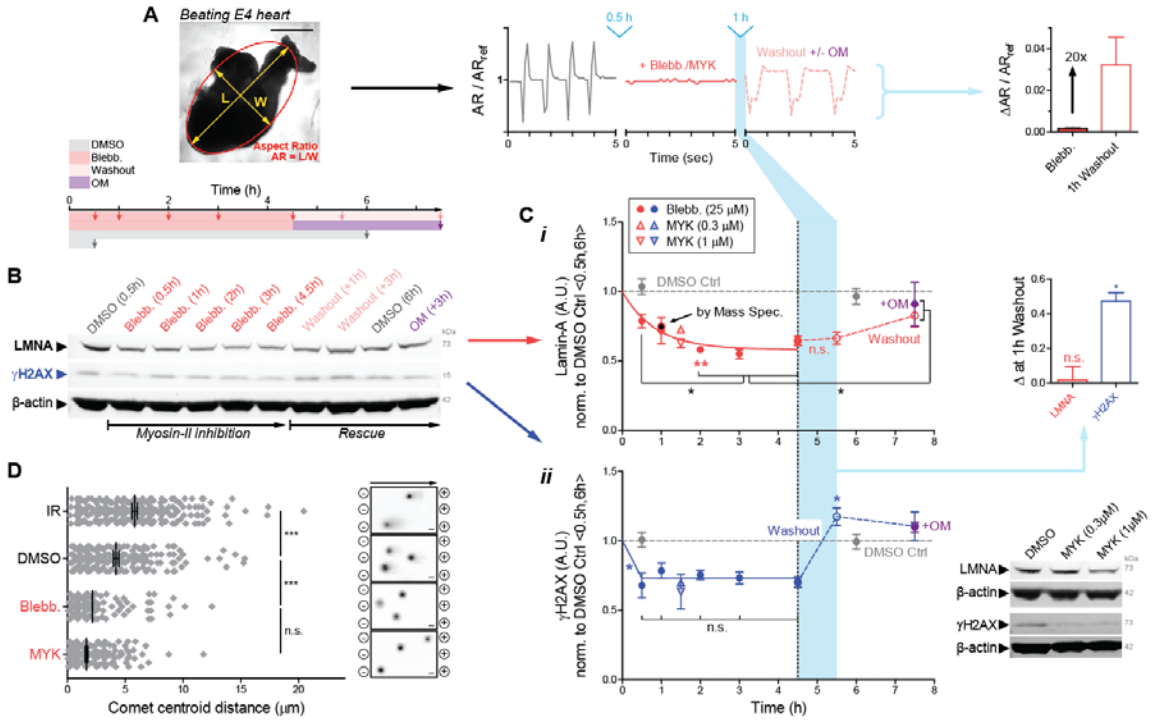

Figure 2.4. Myosin-II inhibition results in rapid 1-2h lamin-A turnover & suppression of DNA damage in intact hearts

(**A**) Beating strain of E4 hearts quantified by tracing changes in aspect ratio (AR). Myosin-II inhibition by blebbistatin or MYK causes hearts to stop beating within 30 min. Effects are rapidly reversible upon washout of drug, with or without OM. (**B**) Immunoblot of E4 hearts treated with blebbistatin for varying durations (0.5 - 4.5h), followed by a short (1h) or long (3h) rescue by washout, with or without OM. Arrows indicate time points at which hearts were harvested and lysed for immunoblots. (**C**) (***i***) Immunoblot densitometry analysis reveals lamin-A decreases rapidly (half life ~ 45 min) upon inhibition of actomyosin stress (n=8 hearts per lysate). In contrast, lamin-A recovery upon washout is slow (>3h). (***ii***) Inhibition of actomyosin contractility also results in a reduction in DNA damage as measured by γH2AX. Light blue highlights: rapid recovery in contractility upon washout of blebbistatin (A, right) results in a sharp increase in DNA damage (at t=5.5h) (*ii*), while lamin-A remains low (*i*). Right bar graph inset indicates fractional increase relative to t=4.5h (pre-washout)). Bottom right inset: MYK treatment for 1.5 h at two different doses show consistent effects on both lamin-A and γH2AX. (*p<0.05, ** p<0.01). (**D**) Electrophoretic Comet assay of myosin-perturbed hearts validate γH2AX immunoblot quantitation of DNA damage trends ((C-*ii*)). Gamma-ray irradiation ('DMSO + IR') was used as a positive control for DNA damage.

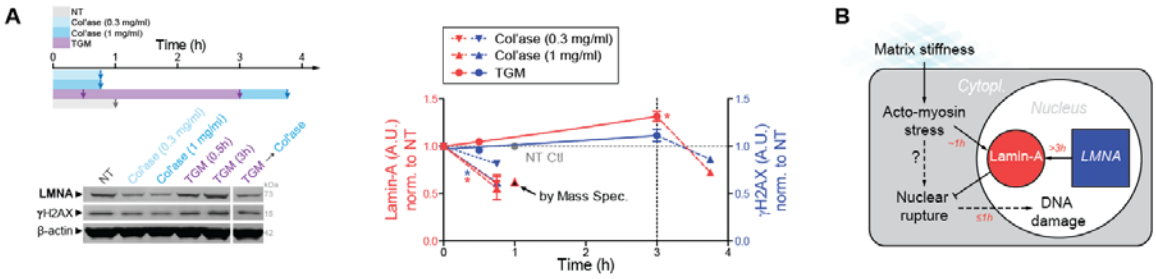

Figure 2.5. Matrix softening by collagenase & crosslinking by TGM impact lamin-A levels & DNA damage

(**A**) Immunoblot of hearts treated with collagenase and transglutaminase (TGM) (n=8 hearts per lysate). Matrix softening by collagenase causes a rapid reduction in lamin-A and γH2AX consistent with low stress, while cross-linking by TGM leads to a slower increase only after >3h. TGM effects on lamin-A and γH2AX are reversible upon degradation collagens. (**p*<0.05). (**B**) Schematic diagram of proposed mechanosensing pathway.

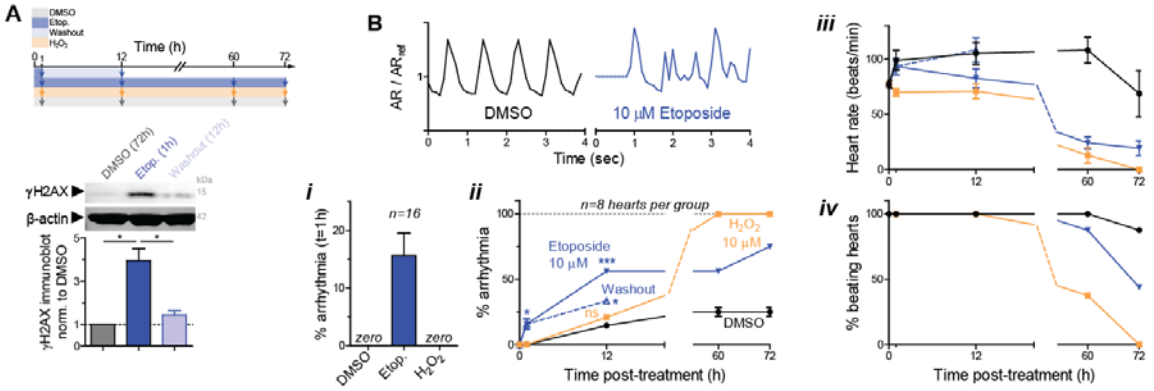

Figure 2.6. Acute DNA damage causes aberrant beating and subsequent heart failure

(**A**) 1h etoposide treatment in embryonic hearts induces a marked ~4x increase in DNA damage, which is reversed with 12h washout of drug (n=8 hearts per lysate). (**p*<0.05). (**B**) Acute DNA damage by etoposide results in arrhythmia (top: representative '$\Delta AR/AR_{ref}$' beating curve). (***i*,*ii***) % arrhythmic hearts increases significantly within 1h upon etoposide treatment and continues to rise until 72h. (***iii*,*iv***) Continued exposure results in a decrease in beating rate (*iii*) and premature heart failure compared to DMSO control (*iv*). Oxidative stress induced by H_2O_2 also causes arrhythmia but with distinct kinetics. (**p*<0.05, ** *p*<0.01, ****p*<0.001)

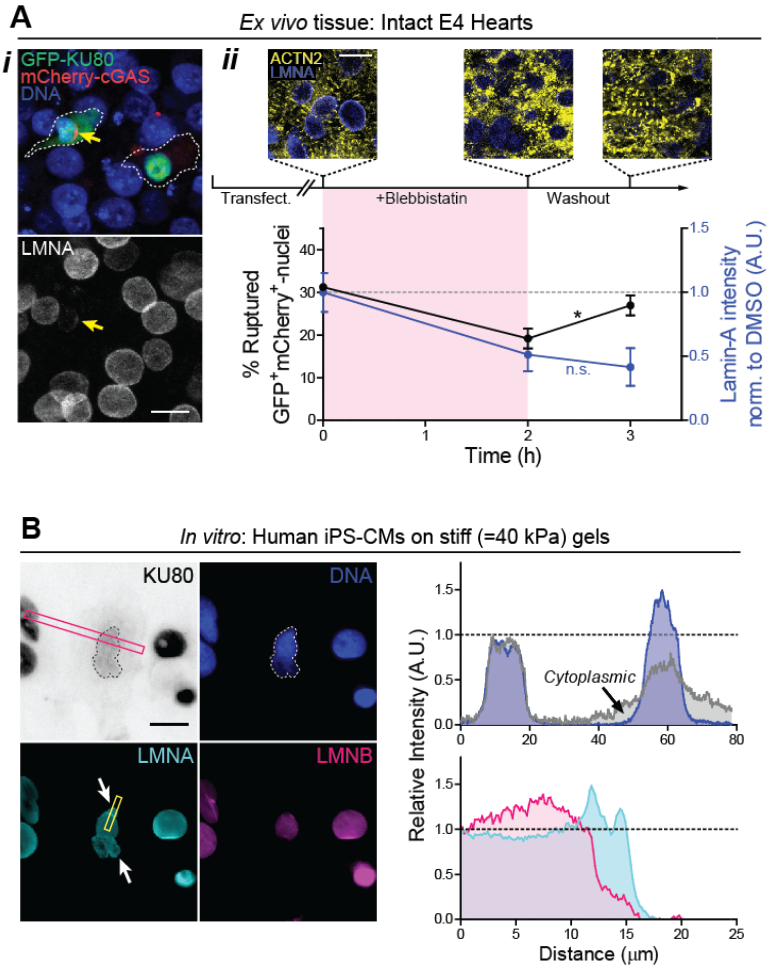

Figure 2.7. Nuclei in intact embryonic hearts and hiPS-CMs on stiff matrix show rupture with cytoplasmic leakage of DNA repair factors

(**A**) (***i***) Confocal images of E4 hearts doubly transfected with GFP-KU80 and mCherry-CGAS. Yellow arrow: representative cell with low lamin-A and ruptured nuclear envelope, as indicated by cytoplasmic mis-localization of GFP-KU80 and formation of mCherry-cGAS puncta at the nuclear envelope. Scale bar = 10 μm. (***ii***) Confocal images of z-disc striation (α-actinin-2) in E4 hearts treated with blebbistatin (2h), before and after washout (+1h). %-Ruptured $GFP^{+}mCherry^{+}$ (double positive) nuclei decreases with inhibition of contractility, but increases upon washout of blebbistatin while lamin-A remains low. (**B**) Human iPS-derived cardiomyocytes ('hiPS-CMs') cultured on stiff 40 kPa matrices for 24h. On stiff substrates, a small fraction of hiPS-CMs exhibit cytoplasmic mis-localization of the DNA repair factor, KU80. Nuclei of cells with cytoplasmic KU80 also have lamin-A-rich, lamin-B-devoid blebs along the long axis, at points of high curvature (white arrows). Scale bar = 10 μm.

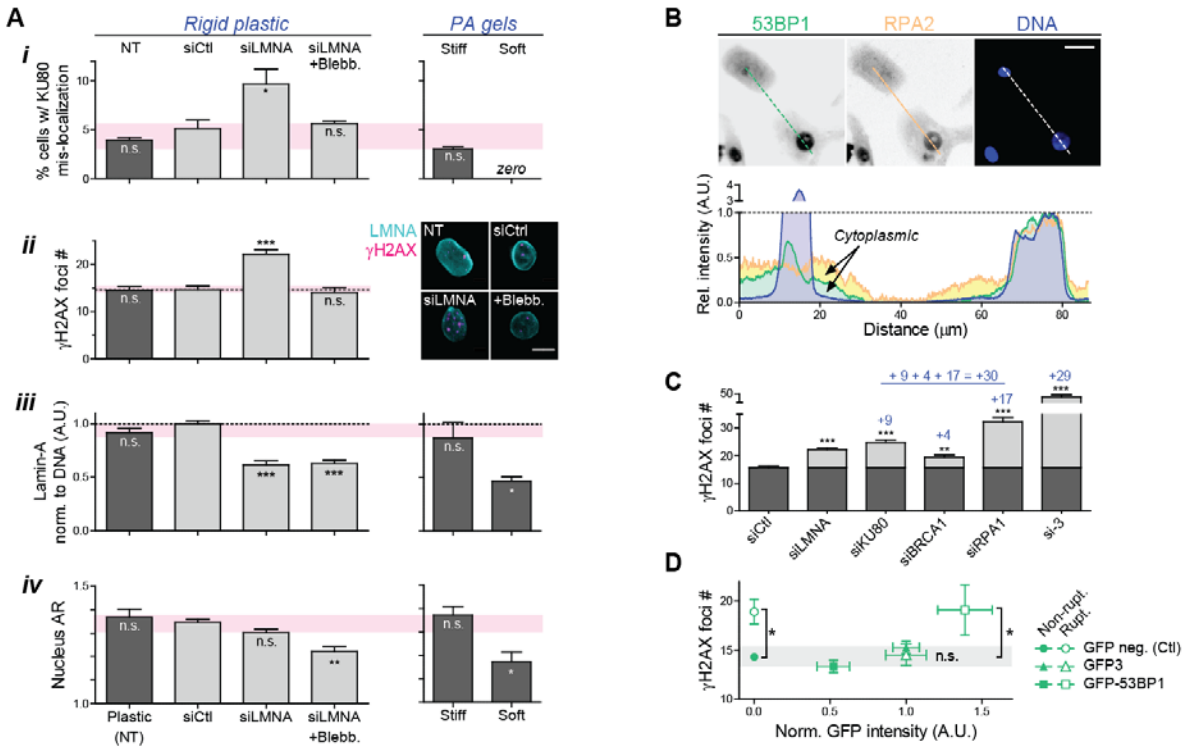

Figure 2.8. siLMNA knockdown increases rupture & DNA damage, dependent on myosin-II. Overexpression of repair factors rescues excess DNA damage in ruptured nuclei

(**A**) (***i***,***ii***) hiPS-CM culture on soft 0.3 kPa matrices greatly reduces the fraction of cells with cytoplasmic mis-localization of KU80, consistent with a decrease in nuclear stress. siLMNA knockdown (~40% (***iii***)) on rigid plastic, on the other hand, increases %-ruptured nuclei with mis-localized KU80 (*i*) and DNA damage by γH2AX foci count (right inset images) (*ii*). Myosin-II inhibition by blebbistatin causes nuclei to become more rounded (*iv*) and rescues frequency of nuclear rupture (*i*) and γH2AX foci down to basal levels (*ii*), consistent with trends observed for soft matrix. (**B**) Cytoplasmic mis-localization is not limited to KU80, but applicable to other DNA repair factors including 53BP1 and RPA2 (top: immunofluorescence images, bottom: intensity profiles along white dashed line). Scale bar = 10 μm. (**C**) siRNA KD of various repair factors (KU80, BRCA1, RPA1, and a combination of the 3 ('si3')) result in significant increases in γH2AX foci count, consistent with partial loss from the nucleus. (**p*<0.05, ** *p*<0.01, ****p*<0.001). (**D**) Over-expression of relevant DNA repair factors (GFP-KU70, KU80, BRCA1) rescue only the excess DNA damage in siLMNA cells, comparing ruptured nuclei vs non-ruptured nuclei. Closed: non-ruptured nuclei; Open: ruptured nuclei.

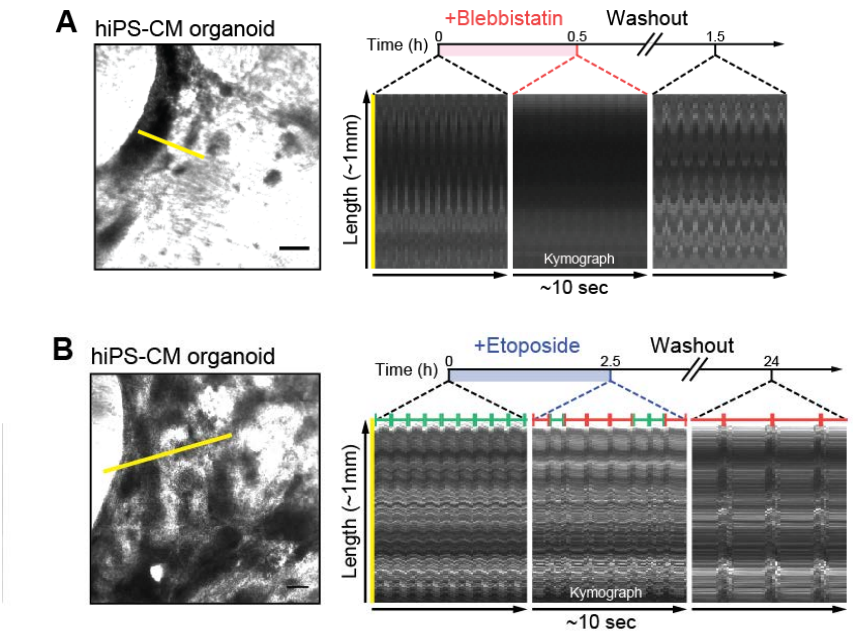

Figure 2.9. Acute DNA damage in hiPS-CM organoids causes aberrant beating

(**A**) Kymograph of beating hiPS-CM organoids generated by tracing length along yellow line with time. Blebbistatin treatment results in reversible inhibition of contractility. (**B**) Etoposide-induced DNA damage causes arrhythmia in hiPS-CM organoids with irregular short (green) and long (red) contractions.

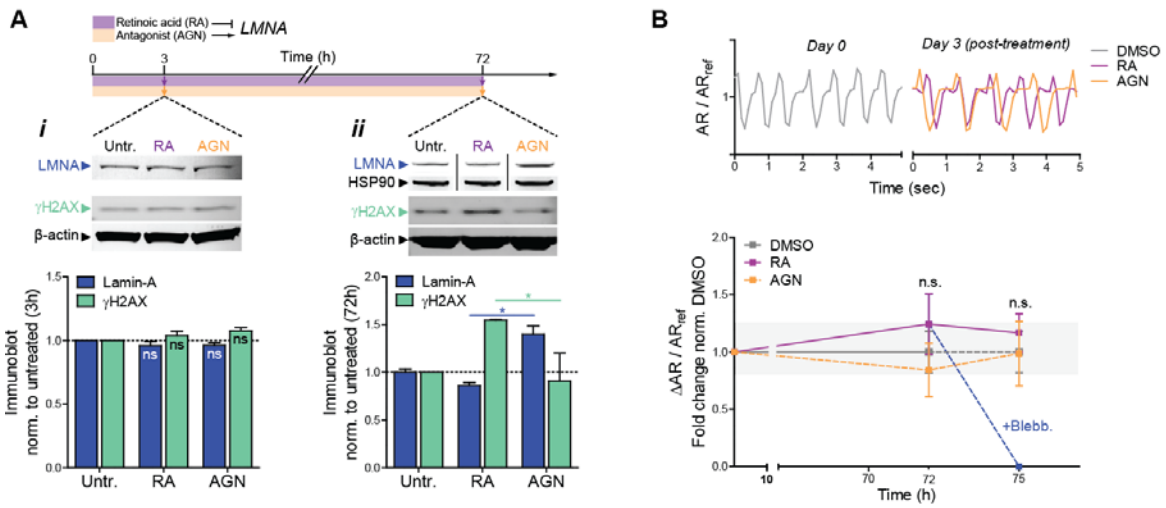

Figure 2.10. Transcriptional regulation of LMNA by retinoids results in anti-correlated changes in γH2AX after 72 hrs

(**A**) (***i***) Retinoic acid (RA) and antagonist to retinoic acid (AGN) treatment in intact embryonic hearts have no observable effect on lamin-A levels or DNA damage (γH2AX) at 3h. (n=6 hearts per condition). (***ii***) Significant changes in lamin-A and γH2AX are detectable only after 72h treatment, consistent with slow transcriptional modulation. A reduction in lamin-A upon RA treatment (72h) is accompanied by an increase in DNA damage as measured by γH2AX, while AGN treatment leads to an upregulation of lamin-A coupled to suppression of DNA damage. (*p<0.05). (**B**) RA and AGN treatment does not significantly affect contractility of hearts even after 72h of treatment.

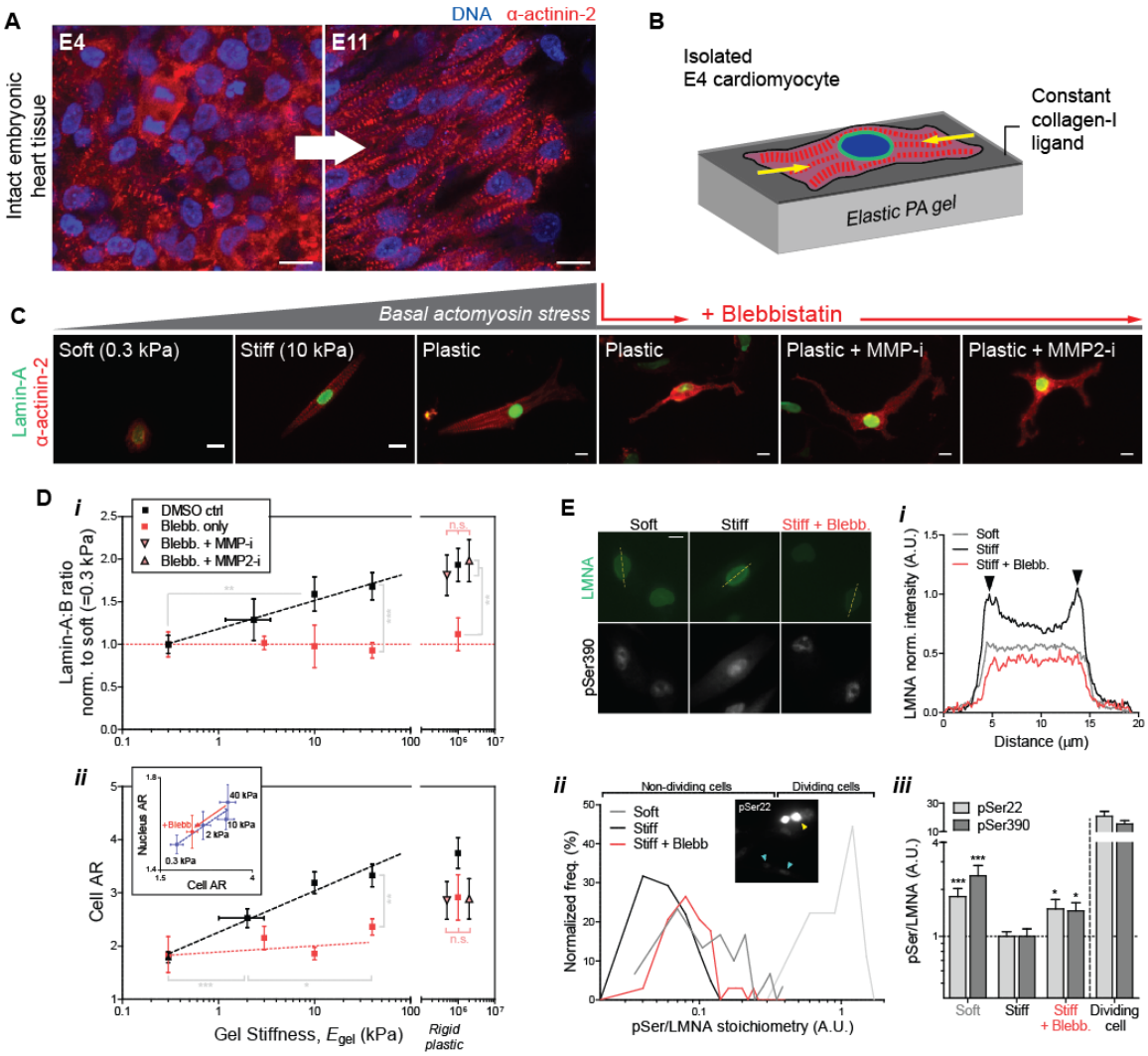

Figure 2.11. Lamin-A in isolated embryonic CMs is sensitive to substrate stiffness and actomyosin stress

(**A**) Confocal Airyscan images of embryonic heart tissue at E4 and E11. CMs undergo significant spreading, cell/nuclear elongation, sarcomere assembly, and anisotropic alignment during development. Scale bar = 10 μm. (**B**) Schematic diagram illustrating isolated E4 CMs cultured on polyacrylamide (PA) gels of varying stiffness (0.3 -40 kPa), coated with an equal concentration of collagen-I ligand. (**C**) Representative images of well-separated E4 CMs cultured for 24h on collagen-I-coated PA gels. As seen in developing tissue (A), isolated CMs exhibit increased spreading, elongation, and sarcomere striation order with increasing stiffness. Addition of blebbistatin on rigid plastic causes CMs to become either rounded or dendritic, with significant disruption of sarcomeric striations. MMP inhibitors have no effect on morphology. Scale bar = 10 μm. (**D**) (***i***) Lamin-A:B intensity ratio increases monotonically with gel stiffness. Blebbistatin treatment abolishes lamin sensitivity to matrix stiffness (red), but effects are rescued by MMP2-i or MMP-i. Datapoints for 'Blebb. + MMP-i' and 'Blebb. + MMP2-i' on rigid plastic (~1 GPa) were separated from 'DMSO ctrl' for better depiction of individual points. (***ii***) Cell and nuclear AR (inset) likewise increase monotonically as CMs become more polarized and elongated on stiffer gels.

Blebbistatin causes a reduction in cell/nuclear AR, but MMP-i and MMP2-i do not affect morphology. (**E**) (***i***) Lamin-A immunofluorescence signal is more nucleoplasmic in CMs cultured on soft (0.3 kPa) compared to stiff (40 kPa) matrices. Addition of blebbistatin to CMs on stiff matrices ('Stiff + Blebb.') also results in higher nucleoplasmic signal, as seen with soft matrix. Scale bar = 10 μm. (***ii***) Histogram of normalized phosphorylation ('pSer/LMNA') for two phospho-sites, pSer22 and pSer390. pSer/LMNA is higher in CMs cultured on soft gels ('Soft', grey) and blebbistatin-treated CMs on stiff gels ('Stiff + Blebb.', red). pSer/LMNA for rare mitotic CMs (yellow) are typically 10~20-fold higher than in interphase cells (cyan). (***iii***) Average pSer/LMNA ratios quantified separately for pSer22 and 390.

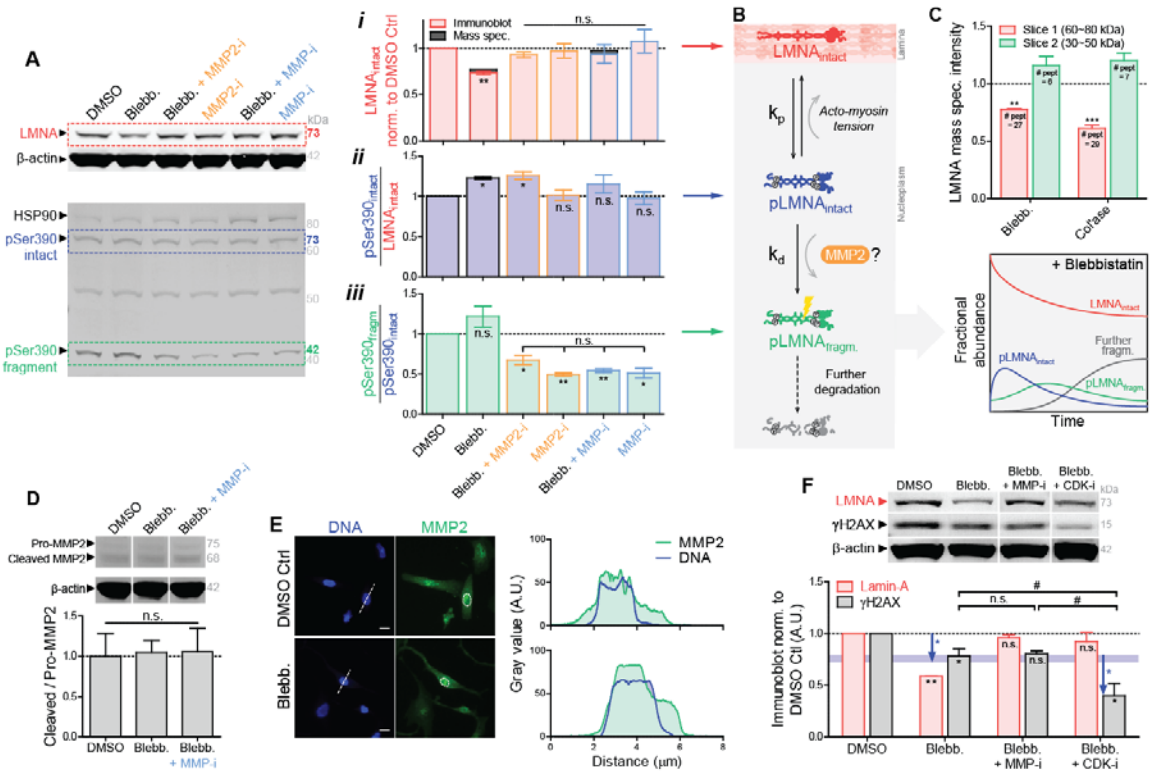

Figure 2.12. Nuclear MMP2 degrades lamin-A upon myosin-II inhibition, unless lamin-A phosphorylation is inhibited in intact heart

(**A**) Immunoblots of intact embryonic hearts treated with blebbistatin and MMP inhibitor drugs, probed for lamin-A (upper) and phosphorylated Ser390 ('pSer390'; lower immunoblot). Lower pSer390 immunoblot shows visible bands not only at the intact lamin-A MW (73 kDa), but also at 42 kDa, consistent with fragment bands reported in the literature (Baghirova et al., 2016; Prudova et al., 2010) and predicted *in silico* (Song et al., 2012). **(*i*)** The rapid decrease in lamin-A induced by blebbistatin is rescued upon MMP inhibition, consistent with MS quantitation (Fig.1H) (n=6 hearts per lysate). ARP100 (an MMP2-specific inhibitor) replicates the effects of the pan-MMP inhibitor, GM6001 (upper immunoblot). **(*ii*)** Blebbistatin inhibition of actomyosin stress causes an increase in normalized phosphorylation at Ser390 ('$pSer390_{intact}/LMNA_{intact}$'): pSer390 signal (blue) normalized to total lamin-A (magenta) at 73 kDa. **(*iii*)** However, blebbistatin does not significantly affect pSer390 signal ratio between the fragment 42 kDa band (orange) and intact 73 kDa band (magenta) ('$pSer390_{fragm.}/pSer90_{intact}$'). $pSer390_{fragm.}/pSer90_{intact}$ is only lowered upon inhibition of MMP2. (*p<0.05, ** p<0.01). (**B**) Proposed two-step reaction scheme for lamin-A protein dynamics. Actomyosin tension on the nucleus inhibits lamin-A phosphorylation and subsequent degradation by MMP2. Lower right schematic plot illustrates hypothesized time-dependent changes in the fractional abundance of each species including intermediates. (**C**) MS validation of lamin-A degradation. MS detects with high abundance multiple (>6) peptides unique to lamin-A in the 42 kDa fragment range ('Slice 2') in both blebbistatin and collagenase-treated hearts. (**D**) Neither blebbistatin nor MMP-i affect catalytic activation of MMP2, as determined by immunoblot quantitation of 'cleaved / pro-MMP2' ratio. (**E**) Immunofluorescence shows high nucleoplasmic MMP2 signal in embryonic CMs. Nuclear vs cytoplasmic localization is unaffected by actomyosin contractility (blebbistatin treatment). Scale bar = 10 μm. (**F**) MMP inhibition rescues the blebbistatin-induced decrease in lamin-A, but does not further suppress γH2AX

levels (n=6 hearts per lysate). γH2AX is further decreased upon co-treatment with CDK-i, which inhibits lamin-A phosphorylation (similar to GFP-S22A mutant). (*p<0.05, ** p<0.01)

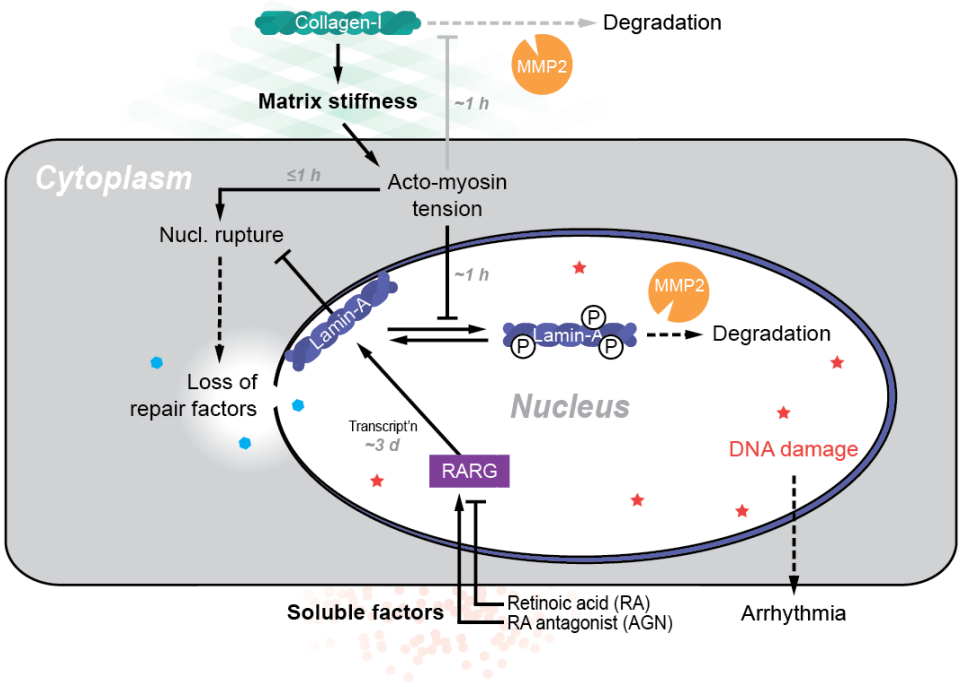

Figure 2.13. Lamin-A mechanosensing protects the genome from stress-induced loss of DNA repair factors, hence excess DNA damage

Schematic diagram summarizing lamin-A's mechanosensing circuit, with a 'use it or lose it' mechanism of tension-inhibited turnover also applicable to collagen-I.

CHAPTER 3
Progerin phosphorylation in interphase is lower and less mechanosensitive than lamin-A,C in iPS-derived mesenchymal stem cells

This chapter appears in *Nucleus,* 9(1), 230-245 (2018).

HGPS patient-derived iPS-MSCs were differentiated and cultured by Dr. Manorama Tewari.
Immunoblots of late passage HGPS iPS-MSCs were performed by Amal Abbas.
Transwell migration experiments were performed by Yuntao Xia and Dr. Jerome Irianto.
Portions of retinoid experiments were done by Dr. Irena L. Ivanovska.

Abstract

Interphase phosphorylation of lamin-A,C depends dynamically on a cell's microenvironment, including the stiffness of extracellular matrix. However, phosphorylation dynamics is poorly understood for diseased forms such as progerin, a permanently farnesylated mutant of LMNA that accelerates aging of stiff and mechanically stressed tissues. Here, fine-excision alignment mass spectrometry (FEA-MS) is developed to quantify progerin and its phosphorylation levels in patient iPS cells differentiated to mesenchymal stem cells (MSCs). The stoichiometry of total A-type lamins (including progerin) versus B-type lamins measured for Progeria iPS-MSCs prove similar to that of normal MSCs, with total A-type lamins more abundant than B-type lamins. However, progerin behaves more like farnesylated B-type lamins in mechanically-induced segregation from nuclear blebs. Phosphorylation of progerin at multiple sites in iPS-MSCs cultured on rigid plastic is also lower than that of normal lamin-A and C. Reduction of nuclear tension upon i) cell rounding/detachment from plastic, ii) culture on soft gels, and iii) inhibition of actomyosin stress increases phosphorylation and degradation of lamin-C > lamin-A > progerin. Such mechano-sensitivity diminishes, however, with passage as progerin and DNA damage accumulate. Lastly, transcription-regulating retinoids exert equal effects on both diseased and normal A-type lamins, suggesting a differential mechano-responsiveness might best explain the stiff tissue defects in Progeria.

3.1 Introduction

Hutchinson-Gilford Progeria Syndrome ('HGPS' or 'Progeria') is a premature aging disease that resembles normal aging in many key respects (Burtner and Kennedy, 2010; Gonzalo et al., 2017; Gordon et al., 1993). Shared defects include atherosclerosis, stiffening of skin, muscle attrition, weakening of bones, and fibrosis across many solid tissues (Gordon et al., 1993). However, tissues most severely affected by Progeria are those which are mechanically stressed and stiff, whereas soft tissues including brain, bone marrow, and blood appear unaffected (Worman, 2012) (**Figure 3.1A**). This stiff versus soft dichotomy seems independent of lineage and developmental origin, and raises the question of whether a defective mechanical response contributes to the pathology of Progeria.

Progeria is typically caused by a point mutation in one allele of *LMNA* that activates a cryptic splice site to produce 'progerin', a C-terminal mutant that lacks 50 amino acids (Eriksson et al., 2003; Vidak and Foisner, 2016) and thereby retains a farnesyl group that is cleaved off in normal lamin-A (Davies et al., 2009) (**Figure 3.1B**). Farnesylation favors binding to the inner lipid leaflet of the nucleus (Capell et al., 2005) and, consistent with membrane viscosity impeding diffusion (Goodwin et al., 2005), the permanently farnesylated B-type lamins show very low molecular mobility (as GFP-fusions) (Dahl et al., 2006; Moir et al., 2000) similar to prelamin-A and progerin. In contrast, mature lamin-A and its truncated spliceform, lamin-C, are both mobile and exchange dynamically between the lamina and the nucleoplasm (in '3D') (Dahl et al., 2006). Movement along or within the lamina (in '~2D') is relatively hindered; however, interphase phosphorylation of lamin-A/C at multiple residues clearly enhances mobility in either direction/mode by promoting rapid disassembly of filaments and solubilization into the nucleoplasm (Kochin et al., 2014). In particular, phosphorylation at serines 22, 390, and 392 near the head and tail domains has been shown to exert dominant effects on nucleoplasmic localization. While the precise functions of phosphorylated, nucleoplasmic lamin-A/C during interphase are still unclear (Naetar et al., 2017; Torvaldson et al., 2015), phospho-solubilization promotes lamin-A/C interaction with several key regulatory factors (e.g. LAP2α (Dechat et al., 2000)) and significantly alters the mechanical properties of the nucleus (Buxboim et al., 2014).

Given the many structural and protective functions of the lamins at the nuclear periphery (Aebi et al., 1986; Cho et al., 2017; Dahl et al., 2008; Gruenbaum and Foisner, 2015; Turgay et al., 2017), regulation of mobility and assembly dynamics by such post-translational modifications (PTMs) suggests some mechanical relation to the stiff tissue defects seen in Progeria.

Contributions to disease from cell-extrinsic factors such as 'tissue stiffness' is consistent with surprising conclusions from mosaic mouse models (de la Rosa et al., 2013b): mice with 50% of cells expressing farnesylated lamin-A in all tissues maintain a normal lifespan, while mice with 100% of cells expressing farnesylated lamin-A die within weeks of birth. Conventional cultures of these cells on rigid tissue culture plastic leads to premature senescence and/or apoptosis, as is also observed with related progeroid cells having low amounts of normal lamin-A/C (Hernandez et al., 2010), but the *in vitro* phenotype is rescued by cultures on almost any type of extracellular matrix (ECM) (Csoka et al., 2004; Hernandez et al., 2010), which is typically softer than plastic by many orders of magnitude. Furthermore, with cells depleted of lamin-A/C, migration through small rigid pores has shown that nuclear stress induces apoptosis (Harada et al., 2014). Failure to dynamically remodel the nuclear envelope and protect the nucleus from mechanical stress might thus provide some explanation for why defects in HGPS patients are limited to stiff tissues.

Soft tissues (e.g. marrow) as well as stiff tissues (e.g. muscle) almost always have within a perivascular niche a population of mesenchymal stem cells (MSCs), which are key contributors to fibrosis (Kramann et al., 2015). Fibrosis is in turn a mechanosensitive process that affects MSC nuclei (Dingal et al., 2015; Li et al., 2017), and is major a hallmark of both normal and premature aging of solid tissues. Understanding MSC responses to microenvironmental properties can therefore provide fundamental insight into processes of relevance to many tissues and organs affected in disease or not. In standard cultures, MSCs (and closely related vascular smooth muscle cells (Liu et al., 2011)) that are differentiated from HGPS patient-derived iPS cells (HGPS iPS-MSCs) exhibit the highest levels of progerin, nuclear abnormalities, and DNA damage (Zhang et al., 2011). However, any effect of matrix stiffness or mechanical stress remains unknown.

Cytoskeletal tension on the nucleus suppresses interphase phosphorylation of normal A-type lamins (Buxboim et al., 2014; Swift et al., 2013), which otherwise promotes their

solubilization into the nucleoplasm and subsequent degradation(Bertacchini et al., 2013; Buxboim et al., 2014; Dingal and Discher, 2014; Naeem et al., 2015). In particular, lamin-A/C phosphorylation is low in cells on rigid surfaces that lead to stress fibers (such as tissue culture plastic), but increases rapidly (<1 hr) upon enzymatic detachment which disrupts the cytoskeleton and leads to cell and nuclear rounding (as seen during mitosis) (Sen and Kumar, 2009). Soft ECM similarly causes cell/nuclear rounding and increases phosphorylation of lamin-A and C. Whether the presence of a C-terminal farnesyl group can affect mechanosensitive phospho-solubilization of A-type lamins is unclear, but de-farnesylation is reportedly required for phosphorylation at serine 22 (Moiseeva et al., 2016). Here, we develop a new mass spectrometry (MS)-based method for quantitation of intact lamins and their phosphorylation states in HGPS iPS-MSCs that are exposed to different mechanical environments.

3.2 Results

3.2.1 Stoichiometries of lamins in HGPS-derived iPS-MSCs are quantified by FEA-MS

Progerin is the product of one of two alleles and might naively be expected to compose half of all A-type lamin protein, but past immunoblots of human progeria cells or tissues show disproportionately less progerin compared to normal lamin-A/C (McClintock et al., 2007; Scaffidi and Misteli, 2005). Quantitative immunoblotting for protein levels is of course extremely powerful, but precise measurements of protein stoichiometry can be a particular challenge unless an antibody binds with equal affinity to each protein band. We therefore developed a label-free mass spectrometry (MS)-based method for simultaneous quantitation of progerin, the normal lamins, and their phosphorylation states in HGPS patient-derived iPS-mesenchymal stem cells (HGPS iPS-MSCs). Briefly, fine-excision alignment mass spectrometry (FEA-MS) exploits molecular weight differences (ΔMW) between A-type lamins (Fig.1B, upper right box) by sectioning SDS-PAGE gels into narrow slices (<1 mm^3) along the electrophoresis direction (**Figure 3.2A**). A custom device with equally spaced blades allows for precise sectioning of the gel into seven or more slices per lane spanning the lamin MW range (60~80 kDa) (Fig.2A). Known amounts of

synthetic phospho-peptides (each containing a phosphorylated serine residue: 'pSer22' and 'pSer390') and their non-phosphorylated forms ('Ser22' and 'Ser390') are injected into samples from adjacent replicates (Fig.2A, upper right), which adds precision to MS peak alignment and calibrated quantitation (see *Materials and Methods*). FEA-MS sample lanes are flanked by replicate lanes for immunoblotting.

Isoform-specific peptides (Fig.1B, lower right Venn diagram) were used to generate separate intensity plots for lamin-A ('LA'), progerin ('P'), and lamin-C ('LC') in slices 2-6 (**Figure 3.2B** & **Figure B.1A**). Signal-to-noise ratios calculated for isoform-specific peptides proved highest at the respective peaks (**Figure B.1B**). Summed MS intensities gave A-type lamin isoform stoichiometries of (LA : P : LC) = (1 : 0.5 : 1.7) in HGPS iPS-MSCs (**Figure 3.2C**; **Figure B.1C,D**), in agreement with densitometry of Western blots (**Figure 3.2D,E**). We showed previously that the iPS-MSCs studied here have a normal karyotype (Irianto et al., 2017) with one allele expressing normal (LA + LC) and one expressing progerin (P), and so normal-to-diseased protein ratios of (2.7 : 0.5) likely suggest differences in protein or mRNA stability.

The total MS intensity of A-type lamins was also 8-fold greater than that of B-type lamins (lamin-B1, 'LB1', plus lamin-B2, 'LB2') (**Figure 3.2F** & **G-*i*, Figure B.1E**), such that lamin-A:B ~ 8:1. Normal primary bone-marrow derived human MSCs (hMSCs) have a similar lamin-A:B ~ 10:1 (Swift et al., 2013), which is consistent with iPS differentiation toward MSCs. On the other hand, expression of progerin in these HGPS iPS-MSCs effectively decreased the (non-farnseylated : farnesylated) lamin ratio to ~3:1 (**Figure 3.2G-*ii***). Since lamin-A:B is a key determinant of nuclear response to mechanical stress (Harada et al., 2014; Swift et al., 2013), the latter stoichiometry raised questions of how progerin responds to various mechanobiological perturbations.

3.2.2 Progerin and lamin-B's are both depleted from mechanically-induced nuclear blebs

To assess whether C-terminal farnesylation causes progerin to respond differently to mechanical stress, HGPS iPS-MSCs were seeded onto transwell membranes for migration through 3 μm

pores (**Figure 3.3A**), which are typical of pores in stiff tissues[25]. Despite the well-documented reduction in motility and disrupted nucleus-cytoskeleton connections in Progeria cells (Booth-Gauthier et al., 2013; Haque et al., 2010; Wang et al., 2012), the patient-derived iPS-MSCs were fully capable of migrating through narrow constrictions. The cells that migrated to the bottom of the transwells (~40% of cells in 48h) further exhibited nuclear blebs that are typical of mechanically-induced nuclear envelope rupture (Harada et al., 2014; Irianto et al., 2017) (**Figure 3.3B**). With these cells, however, progerin could not be easily distinguished from normal LA and LC due to antibody cross-reactivity. Human A549 lung carcinoma cells with a low *LMNA* background (via shLMNA) were therefore transfected with GFP-LA or GFP-progerin and seeded onto the same transwell membranes to assess any differences in their migration-induced response. *LMNA* knockdown in A549s resulted in a higher number of cells that migrated compared to wild type ('WT') (**Figure B.2A**), consistent with past studies demonstrating that a soft nucleus facilitates migration through narrow pores(Harada et al., 2014). Migrating cells as (fraction of cells migrating to bottom) was rescued to baseline upon transfection with WT GFP-LA, but was further reduced with expression of GFP-progerin (Figure B.2A).

As with the patient-derived iPS-MSCs, the GFP-LA expressing A549s that managed to migrate to the bottom of the transwells exhibited mechanically-induced nuclear blebs (**Figure 3.3C**). Blebs were again depleted of B-type lamins but were enriched in lamin-A/C immunofluorescence signal, which accounts for endogenous LA & C as well as transfected GFP-LA (**Figure 3.3D**). No such enrichment was seen however with GFP fluorescence (accounting for LA only), suggesting that the ~3-fold enrichment in anti-lamin-A/C might be a result of preferential accumulation of endogenous LC (Figure 3.3D, immunoblot inset). Nuclear blebs in the shLMNA + GFP-progerin cells showed progerin depletion as well as a dominant negative effect on LA and LC (Figure 3.3C,D). Progerin's absence from blebs suggested that it responds more similarly to lamin-B's than LA or LC upon nuclear constriction and/or rupture. Permanent C-terminus farnesylation is one possible explanation, but the mobility and localization of A-type lamins can also be regulated dynamically by interphase phosphorylation, which promotes solubilization of filaments from the lamina into the nucleoplasm (Kochin et al., 2014). Confocal

immunofluorescence with an anti-phospho-LA/C-Ser22 antibody ('pSer22') indeed revealed significant nucleoplasmic signal, but the localization and overall levels of phosphorylated A-type lamins were unaffected by constricted migration (**Figure 3.3E,F**) regardless of DNA content ('2N' vs '4N', Fig.3F upper inset). Migration resulted in a decrease in % 4N cells (**Figure B.2B**), consistent with recent reports showing pore migration suppresses late cell cycle (G2) (Pfeifer et al., 2017), and the same cells showed slightly higher pSer22 as expected(Akopyan et al., 2014). Due to the cross-reactivity of the pSer22 antibody, however, any differences in phosphorylation responses of progerin relative to normal LA/C remained unclear and were best assessed by FEA-MS and immunoblots.

3.2.3 Basal phosphorylation of progerin and lamin-A is 2-fold lower than that of lamin-C

To clarify any isoform-specific differences in interphase phosphorylation of A-type lamins including endogenous progerin, we examined HGPS iPS-MSCs on rigid culture plastic. The iPS-MSCs were first analyzed by immunofluorescence, which again revealed characteristic nuclear blebs that were enriched in A-type lamins and depleted of B-type lamins (**Figure 3.4A**), consistent with images after pore migration of both iPS Progeria cells and normal A549 cells (Figure 3.3). Phosphorylated A-type lamins were again found mostly in the nucleoplasm (Figure 3.4A-*i*) and appeared capable of diffusing into lamin-B-depleted nuclear blebs (Figure 3.4A-*ii*). Nucleoplasmic signal in the vast majority of the population was clearly attributable to interphase phosphorylation, as very few cells (<1%) were mitotic with the expected cytoplasmic distributions of lamin-A/C and pSer22 (**Figure 3.4B**).

For more rigorous quantitation of phosphorylation of the three A-type lamin isoforms, we then calibrated our FEA-MS analysis with synthetic versions of tryptic peptides that have well-documented phospho-serines at Ser22 and Ser390, which are near the head and tail domains of lamin-A/C, respectively (Torvaldson et al., 2015). Injections of known amounts of both phosphorylated ('pSer22' and 'pSer390') and non-phosphorylated ('Ser22' and 'Ser390') peptides into adjacent replicate lanes (Figure 3.2A) allowed for MS peak alignment and transfer of

identifications from the 'spike-in' lanes to the 'endogenous' sample lane containing no synthetic peptide. Intensities of injected synthetic peptides exhibited robust linearity versus spike-in amounts over several orders of magnitude (all $R^2 > 0.97$ in slices #3-5;

Figure B.3A), which provides confidence in MS quantitation.

Analysis by FEA-MS revealed that progerin (P) phosphorylation is slightly lower than that of intact LA, and is ~2-fold lower than that of intact LC in HGPS iPS-MSCs (**Figure 3.4C**). All three A-type lamin isoforms exhibited phosphorylation stoichiometries ('% phosphorylation') of 0.5~10% (**Figure 3.4D**). This was determined by three different normalization methods: the ratio of phosphorylated peptide intensity divided by 1) the intensity of its non-phosphorylated counterpart (e.g. 'pSer22/Ser22'), 2) the mean intensity of all lamin-A/C peptides (e.g. 'pSer22/$LMNA_{mean}$'), and 3) the median of all lamin-A/C peptides (e.g. 'pSer22/$LMNA_{median}$') (

Figure B.3B). All three normalization methods produced consistent trends showing phosphorylation of LC > LA ≥ P (Fig.4B, inset). In addition to the Ser22 and Ser390 spike-in sites, FEA-MS also detected a doubly phosphorylated peptide with 'pSer404&407', which followed similar trends as Ser390, a neighboring tail-domain phospho-site (Figure 3.4C,D;

Figure B.**3**B-*iii*). LC having the highest phosphorylation is consistent with LC being the most mobile and mechanosensitive A-type isoform *in vitro* (Broers et al., 2005; González-Cruz et al., 2018; Pugh et al., 1997). On the other hand, phosphorylation of LB1 and LB2 at analogous sites was not detected (**Table S1**) despite abundant signal from the non-phosphorylated control peptides. Undetectably low phosphorylation of the B-type lamins is consistent with the hypothesis that C-terminal farnesylation somehow suppresses phosphorylation and solubilization of lamins, as likewise suggested by progerin and LB1/B2's depletion from mechanically-induced nuclear blebs (Fig.3B,C).

Western blots for anti-pSer22 validated the above FEA-MS trends, showing the highest normalized phosphorylation of LC (anti-pSer22 densitometry signal divided by that of total anti-lamin-A/C: 'pSer22/LMNA'), followed by LA, then P (**Figure 3.4E,F**). Low MW bands (30-40 kDa) that immunostained for lamin-A/C also stained intensely with anti-pSer22 (as plotted for the lowest band at ~30 kDa, purple box; Figure 3.4F); this is consistent with previous studies of

interphase phosphorylation favoring degradation into smaller fragments (Bertacchini et al., 2013; Buxboim et al., 2014; Dingal and Discher, 2014; Naeem et al., 2015). Since phosphorylation of A-type lamins increases upon release of cytoskeletal tension on the nucleus (Buxboim et al., 2014; Swift et al., 2013), these measurements raised questions of whether responses to mechanical perturbations are also isoform-dependent.

3.2.4 Phosphorylation of A-type lamins increases with low tension but mechanosensitivity is lost with passage of iPS-MSCs

To assess whether the difference in baseline phosphorylation levels across A-type lamin isoforms influence their responses to mechanical stress, well-spread HGPS iPS-MSCs on rigid plastic were treated with low concentrations of trypsin for tens of minutes to induce cell rounding and detachment from the substrate (**Figure 3.5A**). In culture, lamin-A/C levels in adult cells including primary hMSCs decrease rapidly (<1h) upon cell rounding, with increased phosphorylation and turnover of lamin-A/C dependent on actomyosin contractility (Buxboim et al., 2014). Lower mechanical tension on the nucleus (e.g. cell/nuclear rounding) increases phosphorylation and solubilization of lamin-A/C into the nucleoplasm, which in turn favors its degradation (Bertacchini et al., 2013; Buxboim et al., 2014; Naeem et al., 2015). Intact A-type lamins in early passage (P2) HGPS iPS-MSCs likewise decreased in level upon cell rounding and detachment by trypsinization (up to 45 min), with correspondingly higher phosphorylation at Ser22 (**Figure 3.5A-*i***). Low MW (~40 kDa and lower) degradation fragment bands were again clearly visible and increased in intensity with cell/nuclear rounding (Figure 3.5A-*i*, immunoblot), correlating with elevated pSer22 signal but anti-correlating with the *decrease* in intact lamins. Effects were most pronounced once again for LC > LA > P. However, the rapid response to cell rounding was lost at high passage (>P7) (**Figure 3.5A-*ii***).

Cell and nuclear rounding can also be achieved and sustained for days by culturing cells on soft gels as opposed to stiff gels which promote cell spreading per conventional cultures on glass or plastic. Quantitative immunoblotting of P7 iPS-MSCs cultured on soft or stiff collagen-coated gels showed decreases in LC > LA > P on soft gels relative to stiff (**Figure 3.5B** &

Figure B.4A), and a ~40 kDa fragment band was evident only in cells on soft gels, consistent with degradation under these sustained low tension conditions. Immunofluorescence showed normal primary hMSCs are more mechano-responsive, at least at low passage (Figure 3.5B: gray bar, adapted from Dingal et al. (Dingal et al., 2015)) and likewise showed a clear mechano-response in lower passage iPS-MSCs (

Figure B.4B).

To further clarify the effects of tension on lamin phosphorylation and degradation, low-passage (P2) iPS-MSCs on rigid culture plastic were treated for 2h with the myosin-II inhibitor, blebbistatin, and analyzed by immunofluorescence (**Figure 3.5C**). Treatment with blebbistatin caused nuclear rounding (smaller projected area, **Figure 3.5D**) and significantly reduced the fraction of nuclei with blebs (Figure 3.5C and **Figure 3.5E-*i*,*ii***), consistent with inhibition of actomyosin tension. Reduced actomyosin stress also caused a rapid decrease in A-type lamin levels (but not B-type lamins) (**Figure 3.5F**), concomitant with an increase in normalized phosphorylation (in both '2N' and '4N' cells) (**Figure 3.5G-*i***). Furthermore, the fraction of 2N vs 4N cells remained unaffected with blebbistatin treatment (**Figure 3.5G-*ii***), removing the possibility of any confounding effects of cell cycle shift. Once again, higher passage (P7) iPS-MSCs were unaffected (

Figure B.4C).

Loss of sensitivity with passage coincided with (i) an increase in cell and nuclear area (**Figure 3.5H,I**), (ii) accumulation of progerin (**Figure 3.5J**, top), and (iii) a greater number of cells with γH2AX foci, which is a marker of DNA damage (Figure 3.5H,J-bottom). The findings thus suggest that regulation of the intact A-type lamins (LC > LA > P) by tension-mediated phosphorylation and turnover diminishes with passage number and possibly with cell senescence, which has been shown in many contexts to be accelerated with accumulation of progerin (Benson et al., 2010; Cao et al., 2011; Wheaton et al., 2017). The rapid and distinct mechano-responses at the level of protein for the normal and diseased A-type lamin isoforms raised questions of whether or not they also respond differently to transcriptional regulation.

3.2.5 Lamin-A, progerin, and lamin-C respond equally to transcriptional regulation by retinoids

Progerin protein levels measured by FEA-MS were clearly below the levels expected from allele ratios (Figure 3.1B), and were also found to be less mechanosensitive than normal LA/C after both acute and sustained perturbations (Figure 3.5A-G). It is conceivable that through some allele-specific mechanisms (such as positioning the mutated sequence more in heterochromatin) progerin expression occurs at an unperturbable, low level similar to lamin-B1/B2 in the MSCs. It is also conceivable that splicing mechanisms are differentially regulated (Figure 3.1B). HGPS iPS-MSCs were therefore cultured on soft or stiff collagen-coated gels and treated with retinoid compounds that are known to regulate *LMNA gene* expression. All-trans retinoic acid ('RA') and CD1530 are retinoid agonists that repress *LMNA* promoter activity (Ivanovska et al., 2017; Swift et al., 2013), while antagonist ('AGN') and CD2665 upregulate *LMNA* promoter activity. RA is a vitamin-A metabolite with potent effects in differentiation that is normally ~10 nM in serum. Treatment of early passage (P2) HGPS iPS-MSCs with 1 μM CD1530 or CD2665 revealed significant changes in *LMNA* expression on stiff gel cultures but not on soft (**Figure 3.6A**), consistent with recent reports demonstrating that a stiff matrix is required in order to sensitize cells to these compounds (Ivanovska et al., 2017). Quantitative densitometry of A-type lamins in RA/AGN treated cells cultured on rigid plastic further revealed that regulation by retinoids is not isoform-specific in these early passage (P2) HGPS iPS-MSCs (**Figure 3.6B** &

Figure B.4D): LA, P, and LC all responded equally, resulting in ~30% repression with RA and up to ~10% upregulation with AGN. These results agree with recent reports (Lo Cicero et al., 2016) and suggest that regulatory perturbations of the mutated *LMNA* gene and transcript are similar to the normal allele, with effects likely independent of phospho-degradation (

Figure B.**4**E). Nonetheless, as seen with mechano-regulation (Figure 3.5A-E), sensitivity to retinoids diminished with passage (**Figure 3.6C**), indicating that expression responses to both soluble and insoluble microenvironmental cues are blunted over time.

3.3 Discussion

FEA-MS complements and extends antibody-based methods for quantifying stoichiometries of lamins and phosphorylation states in HGPS patient-derived cells that are differentiated to MSCs with abundant lamin-A. Additional steps in the workflow could improve quantitation (e.g. injection of synthetic peptides unique to each isoform), but our measurements of LA : P : LC (1: 0.5 : 1.7) and %-phosphorylation (0.5-10%) proved consistent with immunoblot trends (Figure 3.2B-E, Figure 3.3A-C) and with total lamin-A:B stoichiometry in primary MSCs (Figure 3.2G). New phospho-specific antibodies should be useful for further assessments, including degradation involving pSer404 (

Figure B.**4**E). The ratio of normal : mutant A-type lamins, (LA + LC) : P, was found to be far below 1:1 despite the iPS-MSCs having a normal karyotype (Irianto et al., 2017), suggesting differences in mRNA stability (Rodriguez et al., 2009) and/or inefficiencies in the activation of the cryptic progerin splice site(Reddel and Weiss, 2004). Progerin protein also interacts more strongly with the proteasome (Kubben et al., 2010) and is suggested to be a selective target of autophagy (as is prelamin-A) (Cenni et al., 2011; Dou et al., 2015; Pellegrini et al., 2015), which could favor a basal rate of degradation. However, intact progerin was found here to be least responsive in its dynamic mechanosensitive phosphorylation and degradation (**Figure 3.7**). These molecular observations in a model cell type found in most organs begin to provide some insight into why Progeria(Gordon et al., 1993) primarily afflicts tissues that we pointed out are normally stiff and more stressed mechanically (Figure 3.1A), whereas soft tissues including brain, bone marrow, and blood are unaffected (Worman, 2012).

Mechanically induced nuclear blebs after constricted migration were depleted of progerin, which appeared to behave more like B-type lamins rather than LA or LC (Figure 3.3C,D). This observation is consistent with nuclear blebs seen in HGPS cells in culture (Goldman et al., 2004; Taimen et al., 2009) (Figure 3.4A,B). GFP-progerin also prevented the enrichment of endogenous LA and LC to nuclear blebs, suggesting a dominant negative effect on lamin mobility and remodeling dynamics. The findings are consistent with reports showing decreased nucleoplasmic localization of A-type lamins in HGPS fibroblasts (Vidak et al., 2015). Super-resolution imaging

suggests A-type lamins form distinct filament networks (Shimi et al., 2015; Xie et al., 2016), but the dominant negative effect seen here could reflect interactions between progerin and LA/C that are stronger than those between A-type and B-type lamins; in addition to 'hetero-filaments' of mixed LA-P or LC-P filaments, shared binding partners (Haque et al., 2006; Wilson and Foisner, 2010) might also suppress mobility under mechanical perturbations.

Consistent with low mobility of progerin, its steady state phosphorylation in iPS-MSCs on rigid culture plastic proved slightly lower than that of intact LA and far lower than that of LC. Turnover of progerin also exhibited lower sensitivity to mechanical perturbations than that of LA or LC: upon cell/nuclear rounding in early passage iPS-MSCs (Figure 3.5A&G), all three A-type isoforms decreased in level with increased phosphorylation at Ser22. Of the three isoforms, intact LC was again most responsive to the reduction in nuclear stress, consistent with its highest baseline phosphorylation (Figure 3.4C-F), followed by LA, then P. One appealing explanation for progerin's lower sensitivity to mechanical regulation is that farnesylation limits stress-induced conformational changes in lamin dimers that increase their affinity for modifying enzymes (Buxboim et al., 2014; Swift et al., 2013). It is also clear from studies of Ser22Asp that such a phospho-mimetic is more nucleoplasmic and soluble than WT *LMNA* (Kochin et al., 2014), and results in a significantly softer nucleus (Buxboim et al., 2014). The low MW phospho-bands could therefore derive from intact LA/P/LC. Determining which A-type lamin yields such degradation peptides will be a challenge but is essential to clarifying the LC > LA > P mechanosensitive dynamics of the intact proteins.

Sensitivity of all A-type isoforms to matrix stiffness in 2D adhesion and 3D migration as well as to retinoid compounds (soluble transcriptional regulators) was blunted by passage, consistent with loss of mechano-sensitivity reported for primary MSCs (Dingal et al., 2015). A dampened response to extracellular inputs is consistent with an increasingly senescent phenotype that correlates with progerin accumulation, DNA damage, and enlargement of cells and nuclei in higher-passage MSCs (Figure 3.5C-E). Given that progerin is known to reduce force propagation to the nuclear interior (Booth et al., 2015), interfere with mitosis (Cao et al., 2007), compromise stem cell differentiation potential (Scaffidi and Misteli, 2008), and induce senescence

(Benson et al., 2010; Cao et al., 2011; Wheaton et al., 2017), these findings point to a potential positive feedback loop in which progerin drives a cell into premature senescence, which in turn favors further accumulation of progerin by limiting its sensitivity to upstream regulatory factors. The findings also imply that therapeutic efforts to modulate progerin levels *in vivo* (e.g. with farnesyl transferase inhibitors (Gordon et al., 2012)) could become increasingly ineffective over time, which provides further motivation and rationale for early and accurate diagnosis and intervention.

3.4 Materials and Methods

3.4.1 Differentiation and maintenance of patient-derived iPS-MSCs

Induced pluripotent stem cell (iPSC) lines derived from primary fibroblasts were obtained from 'The Progeria Research Foundation Cell & Tissue Bank', University of Ottawa. Differentiation of the iPSCs into mesenchymal stem cells (iPSC-MSCs) was achieved as described in Zou et al (Zou et al., 2013). Briefly, iPS culture medium was replaced with MSC medium (low glucose Dulbecco's modification of Eagle's medium (DMEM, Invitrogen) with 10% fetal bovine serum (FBS, Sigma Aldrich) and 1% penicillin/streptomycin) three days after splitting. The MSC culture medium was refreshed every 2 days. After 14 days of culture, the cells were trypsinized (0.25% trypsin/1 mM EDTA, Difco-Sigma) and expanded in MSC medium on 0.1% gelatin coated dishes (BD). Upon confluency (typically 3-5 days), cells were trypsinized (0.025% trypsin-EDTA) and regularly passaged at ~1:3 ratio. A morphologically homogeneous population of fibroblast-like cells became evident typically after the third passage, at which point the cells were assessed for MSC phenotypic characteristics and differentiation potential.

3.4.2 Fine-excision mass spectrometry (FEA-MS)

HGPS patient-derived iPS-MSC lysates (see Immunoblotting section) were injected into four middle lanes of an SDS-PAGE gel (15-well NuPAGE 4-12% Bis-Tris; Invitrogen) and four

additional lanes (two on each side) spaced by molecular weight (MW) standards (Fig.1B). Gel electrophoresis was run for 10 min at 100 V, then subsequently for >1 hr at 160 V to allow maximum possible separation of the lamin MW range (60 - 80 kDa). A custom device made of >8 equally spaced blades (1 mm apart) was used to excise the SDS-PAGE into 7 narrow slices per lane (~1 mm^3 in volume) vertically along the direction of electrophoresis. The excised gel slices were prepared for LC-MS/MS processing following the protocol outlined in Swift et al. (Swift et al., 2013). Briefly, the gel slices were washed in 50% 0.2 M ammonium bicarbonate (AB), 50% acetonitrile (ACN) solution for 30 min at RT. The washed slices were lyophilized, incubated with a reducing agent (20 mM TCEP in 25 mM AB solution), then alkylated (40 mM iodoacetamide (IAM) in 25 mM AB solution). The gel sections were lyophilized again before in-gel trypsinization (20 mg/mL sequencing grade modified trypsin, Promega) overnight at 37°C with gentle shaking. The resulting tryptic peptides were extracted by adding 50% digest dilution buffer (60 mM AB solution with 3% formic acid). Known concentrations of phosphorylated lamin-A peptide standards (GenScript) containing well-documented phospho-serine residues ('pSer22' and 'pSer390') and their non-phosphorylated counterparts ('Ser22' and 'Ser390') were spiked-into the final tryptic peptide solutions (0.001, 0.01, 0.1 µM into lanes #6, 7, 8, respectively), per Fig.1B. Samples were injected (~10 nL) into a high-pressure liquid chromatography (HPLC) system coupled to a hybrid LTQ-Orbitrap XL mass spectrometer (Thermo Fisher Scientific) via a nano-electrospray ion source.

Raw data from each MS sample was processed separately using MaxQuant (version 1.5.3.8, Max Planck Institute of Biochemistry). MaxQuant's built-in Label-Free Quantification (LFQ) algorithm was employed with full tryptic digestion and up to 2 missed cleavage sites. Peptides were searched against a human FASTA database compiled from UniProt, plus contaminants and a reverse decoy database. The software's decoy search mode was set as 'revert' and a MS/MS tolerance limit of 20 ppm was used, along with a false discovery rate (FDR) of 1%. The minimum number of amino acid residues per tryptic peptide was set to 7, and MaxQuant's 'match between runs' feature was used for transfer of MS2 peak identifications across samples. All other parameters were run under default settings. The MaxQuant output

tables were then fed into its custom bioinformatics suite, Perseus (version 1.5.2.4), for protein annotation and sorting.

The LFQ intensity for 'Prelamin-A/C' (normalized intensity value incorporating signal from all LMNA peptides) was plotted against gel slice # to generate an intensity line profile with two distinct peaks at slices 3 and 5, respectively. Isoform-specific peptides (those belonging to lamin-A only ('LA'), lamin-A or progerin ('LA/P'), and lamin-C only ('LC') in Fig.S1A; Venn diagram) were used to calculate pair-wise intensity ratios for each slice range (e.g. LA:LC ratio in slice #3). The pair-wise ratios were then used to generate isoform-specific intensity plots (Fig.S1A, middle plot) which, when summed, preserved the total A-type isoform abundance ('LA / P / LC' in gray). Final adjusted line profiles for each isoform ('LA*', 'P*', and 'LC', Fig.S1A, rightmost plot) were generated based on the symmetry of the LA and LC peaks: since LA (~74 kDa) was close to zero at all slices except #3 and LC ~ 0 at all slices but #5, progerin was also assumed to have one distinct peak at slice #4 with minimal contribution to 'LA/P' in slice #3. The ratio of LA signal at slice #2 / #3 (LA_2/LA_3) and that of LC signal at slice #4 / #5 (LC_4/LC_5) were thus averaged to estimate the fractional decrease of progerin signal from slice #4 to #3, to estimate progerin's signal in slice #3, P^*_3 (which was found to be ~ 0). Isoform stoichiometries were computed by summing intensities over all slices (1-7), or alternatively, by integrating the best-fit Gaussian functions.

3.4.3 Transwell migration

Cells were seeded at densities of ~300,000 cells/cm^2 onto the top side of transwell filter membranes (Corning Inc.) and left to migrate under normal culture conditions for 24 hrs. The number of migrated cells on the bottom of the membrane are proportional to the number of cells added on the top in a given set of experiments, which allows for comparisons across conditions by normalizing to a control sample.

3.4.4 *LMNA* knockdown and overexpression

A549 cells (a human lung carcinoma cell line) was cultured in Ham's F12 nutrient mixture (Gibco), supplemented with 10% FBS and 1% penicillin/streptomycin (Sigma). Overexpression of lamin-A was achieved by transfection with Lipofectamine 2000 (Invitrogen) for 24-hr. GFP-lamin-A and GFP-progerin were gifts from David M. Gilbert (Florida State University) and Tom Misteli (Addgene plasmid # 17653), respectively. For shRNA knockdown of LMNA, A549 cells were infected with lentiviral supernatants targeting lamin-A (TRCN000061833, Sigma) at a multiplicity of infection (MOI) of 10 in the presence of 80 μg/mL Polybrene (Sigma) for 24 hours. Transduced cells were then selected by treatment with 2 μg/mL puromycin (Sigma) for 30 days. Efficiency of knockdown was determined by immunoblot.

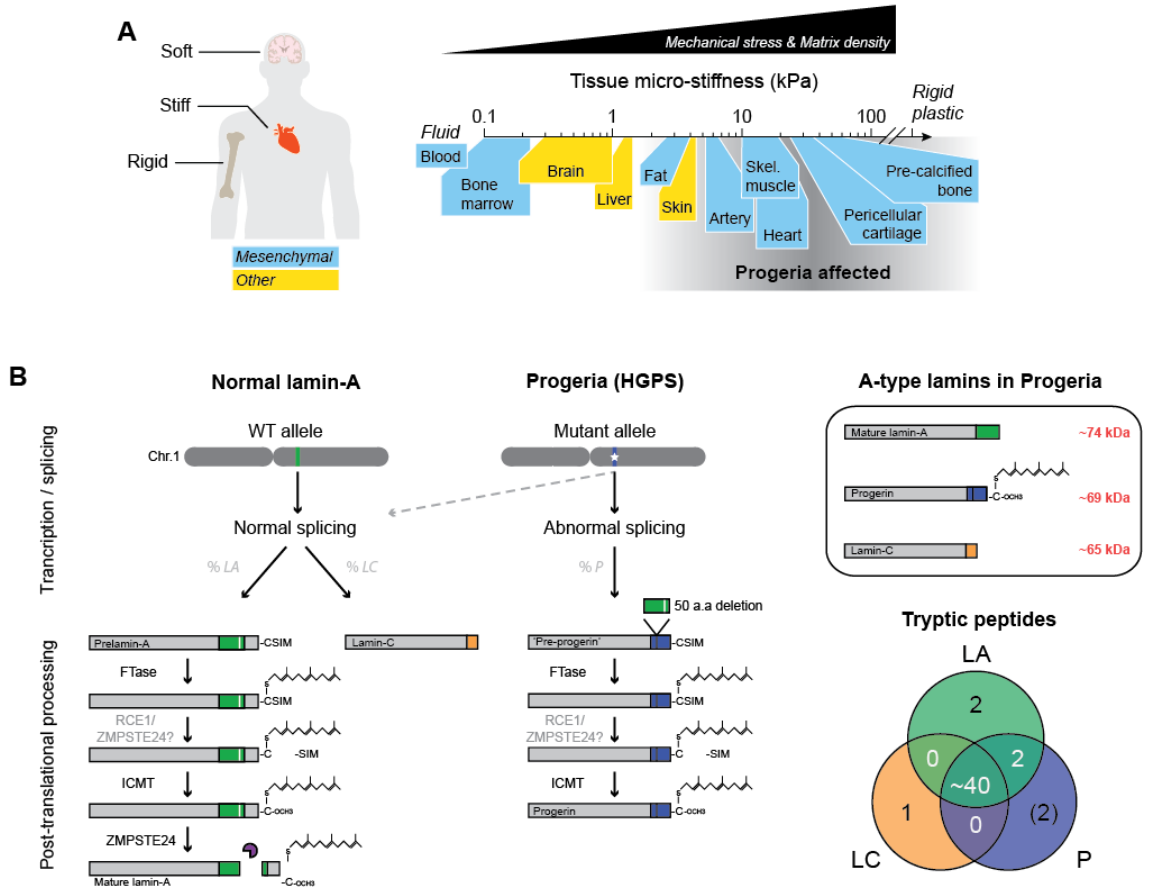

Figure 3.1. HGPS aging defects are most pronounced in mechanically stressed tissues.

(**A**) HGPS disproportionately affects stiff and mechanically stressed tissues (e.g. skeletal/cardiac muscle) while soft tissues (e.g. brain, marrow) appear normal, regardless of lineage or developmental origin. (**B**) Post-translational processing of normal lamin-A/C and progerin. The truncated mutant, progerin, retains a C-terminus farnesyl group. Upper right box: A-type lamin isoforms differ in molecular weight (MW) by ~5 kDa. Lower right: Venn diagram of unique and common A-type lamin peptides. The majority of the peptides are shared by all three isoforms, with the exception of isoform-specific peptides at the C-terminus. 'FTase' = Farnesyl transferase; 'RCE1' = Ras converting CAAX endopeptidase 1; 'ZMPSTE24' = Zinc metallopeptidase STE24; 'ICMT' = Isoprenylcysteine carboxyl methyltransferase.

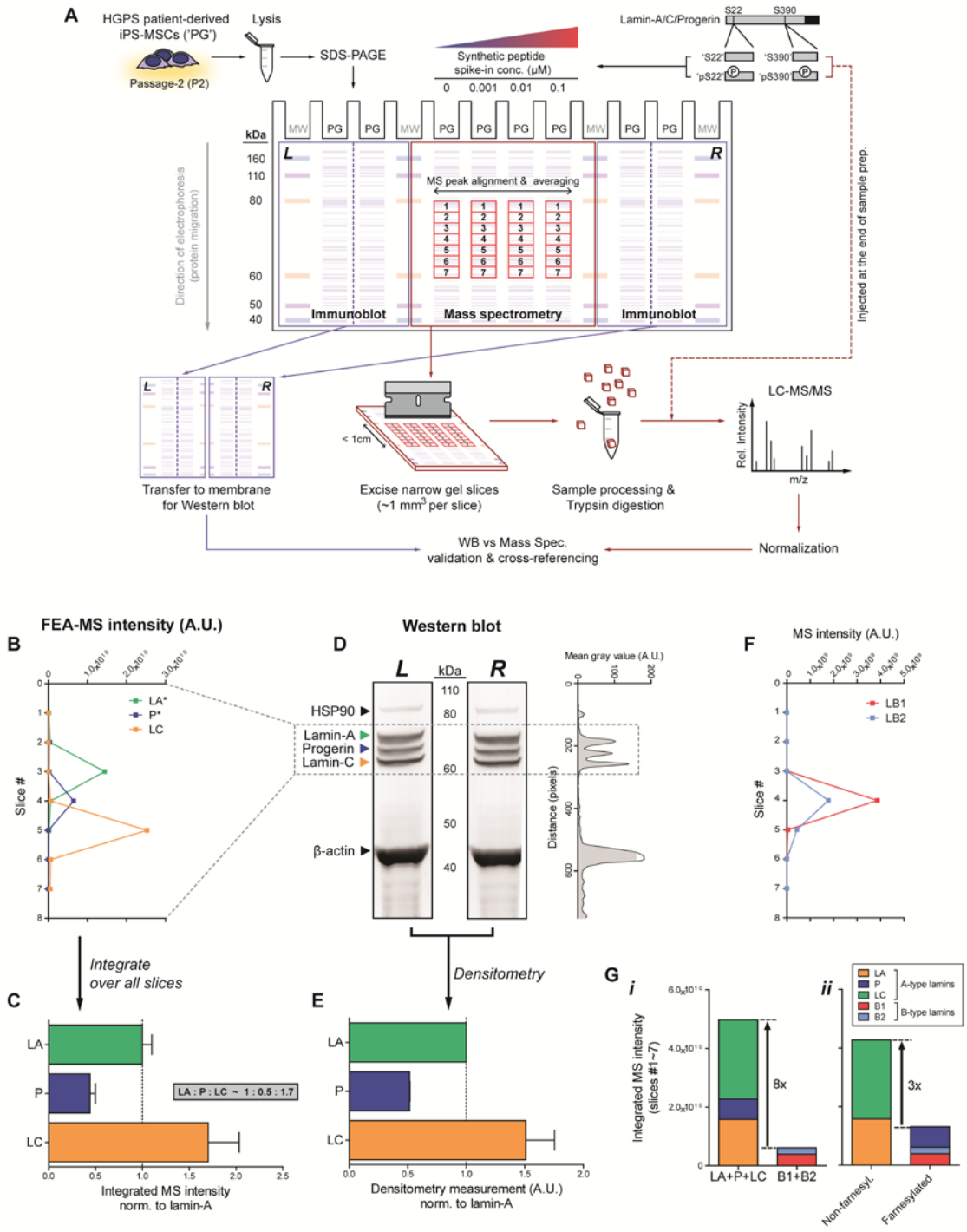

Figure 3.2. Quantification of lamin isoform stoichiometries by fine-excision alignment mass spectrometry (FEA-MS).

(**A**) FEA-MS pipeline. HGPS iPS-MSC lysates ('PG') are injected into 4 middle SDS-PAGE lanes. Known concentrations of synthetic phospho-peptide standards (each containing a well-known serine residue: 'pSer22' and 'pSer390') and their non-phosphorylated counterparts ('Ser22' and 'Ser390') are injected into adjacent lanes to allow for (i) better detection by MS peak alignment,

(ii) averaging over replicates, and (iii) calibrated quantitation of peptide/protein concentrations. An extended (>1h) SDS-PAGE run achieves sufficient separation of A-type lamin isoforms, allowing for excision of the gel into multiple narrow slices along the electrophoresis direction with a custom device of equally spaced parallel blades. FEA-MS sample lanes are flanked by 2 additional lanes on either side (left and right), which are used for parallel immunoblot analyses. 'MW' = molecular weight standards. (**B**) Intensity profiles of lamin-A ('LA'), progerin ('P'), and lamin-C ('LC') determined by FEA-MS and plotted vs slice #. (**C**) Summation of FEA-MS signal over all gel slices (#1-7) quantifies A-type lamin stoichiometries, LA : P : LC ~ 1 : 0.5 : 1.7. (**D**) Aligned left & right ('L' & 'R') flank Western blots for anti-lamin-A/C show three distinct bands for LA, P, and LC. Right inset: line profile plot of immunoblot densitometry signal. (**E**) Quantification of LA : P : LC by densitometry is consistent with that by FEA-MS. (**F**) Line profile plot of normalized MS intensities of B-type lamins ('B1' & 'B2'). (**G**) Stacked bar graph illustrating summed intensities of each isoform across all gel slices. (***i***) Total A-type lamins are >8-fold more abundant than B-type lamins, but (***ii***) the ratio of non-farnesylated : farnesylated lamins decreases to ~3 with progerin expression.

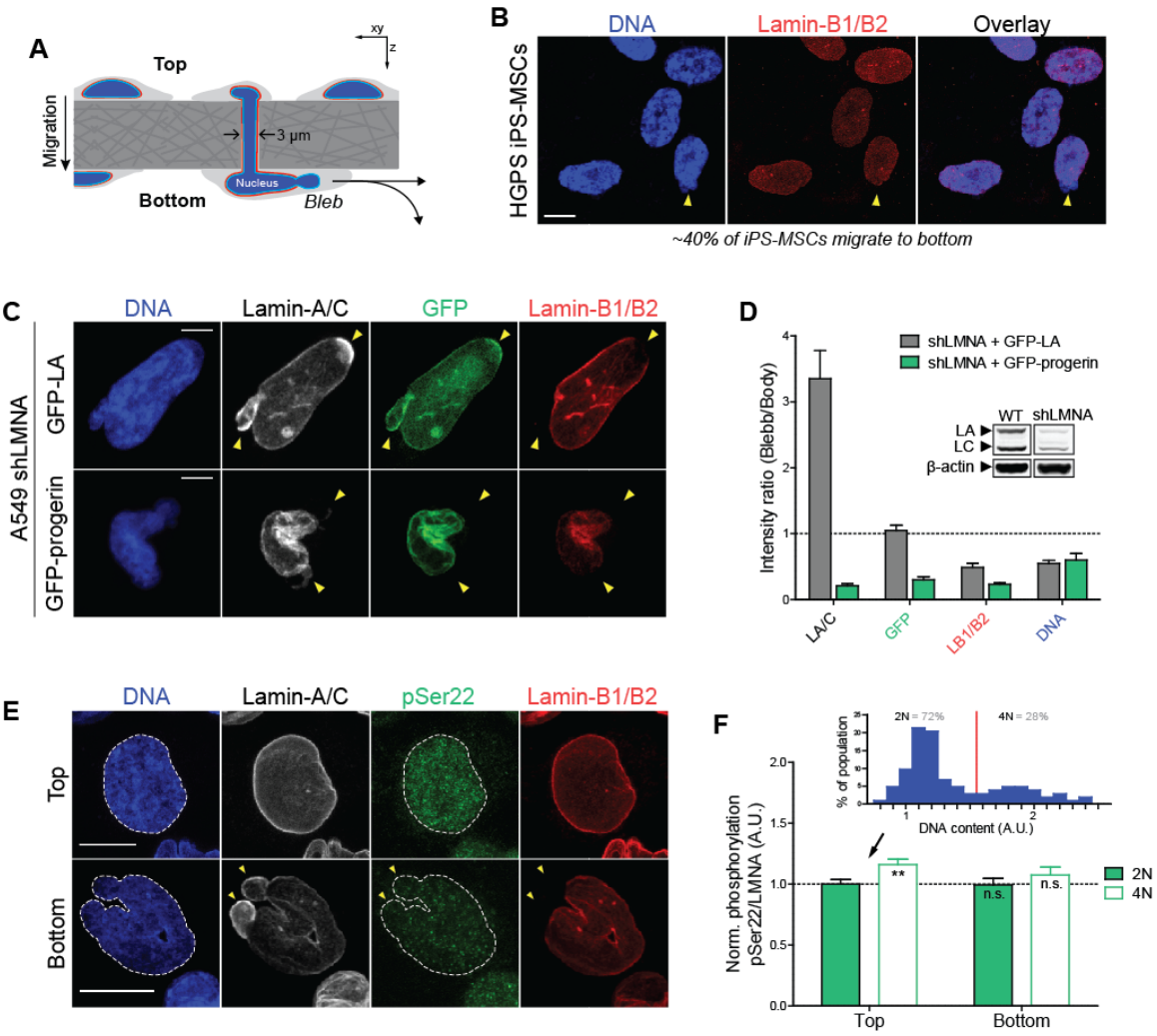

Figure 3.3. Farnesylated progerin, as with lamin-B1/B2, is depleted from nuclear blebs following constricted migration through narrow pores

(**A**) Cartoon illustrating transwell migration of cells. Pore diameter = 3 µm; Polystyrene membrane thickness ~10 µm. (**B**) Confocal images of HGPS iPS-MSCs that migrate to the bottom of narrow 3 µm pores (~40% of seeded cells migrate to bottom in 48h) show typical nuclear blebs with lamin-B1/2 depletion. Scale bar = 10 µm. (**C**) Representative images of nuclei exhibiting characteristic blebs following constricted migration. Lamin-A/C is enriched in sites of nuclear blebs (as seen by immunofluorescence and GFP signal), but GFP-progerin is depleted from blebs, as are the farnesylated lamins-B1 and B2. Scale bar = 5µm. (**D**) Quantitation of nuclear bleb/body fluorescence intensity ratio. Inset: immunoblot of WT and shLMNA cells showing residual LA and LC. (**E**) Confocal images of WT A549 cells at the top & bottom of the transwell membrane. Phosphorylated lamin-A/C ('pSer22') is seen in the nucleoplasm of interphase nuclei. Cells that migrate to the bottom show nuclear blebs with lamin-A/C enrichment and lamin-B1/B2 depletion (yellow arrowheads). Scale bar = 10 µm. (**F**) While lamin-A/C is phosphorylated ~10-15% higher in '4N' vs '2N' cells (inset), normalized phosphorylation (as 'pSer22/LMNA') does not change significantly before and after migration.

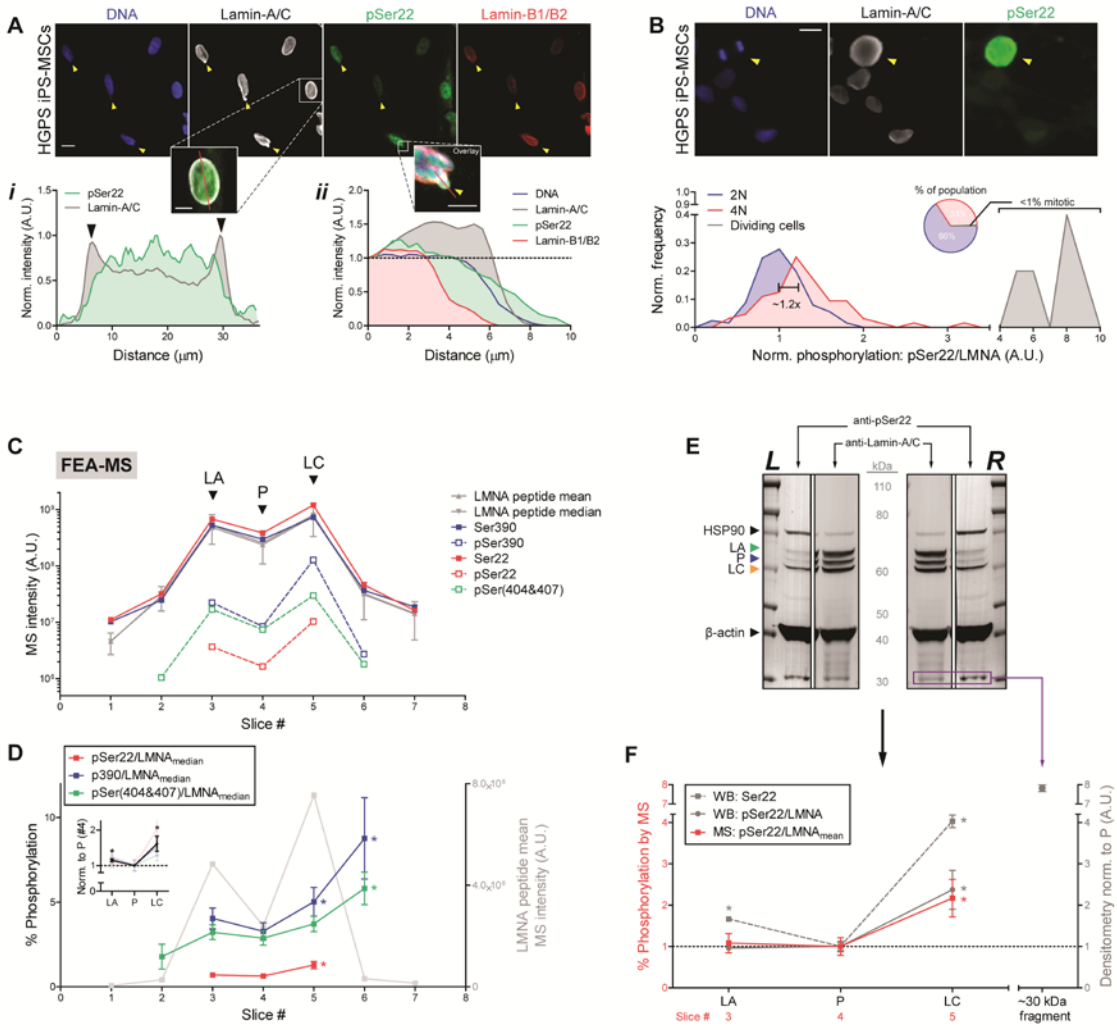

Figure 3.4. Progerin and lamin-A phosphorylation in HGPS iPS-MSCs is 2-fold lower than that of lamin-C.

(**A**) Immunofluorescence images of HGPS iPS-MSCs on rigid culture plastic showing lamin-A/C-enriched, lamin-B-depleted nuclear blebs (yellow arrowheads). Scale bar = 10 µm. (***i***) Intensity profile (along red line) of pSer22 primarily in the nucleoplasm and lamin-A/C at the nuclear periphery. (***ii***) Intensity profile (along red line) of a nuclear bleb enriched in lamin-A/C and depleted of lamin-B. (**B**) Immunofluorescence images of a dividing cell next to non-dividing cells. Bottom histogram illustrates normalized frequency distribution of pSer22/LMNA, with respect to DNA content ('2N' vs '4N'). Pie chart: mitotic cells with hyper-phosphorylated lamin-A/C are extremely rare (<1%). Scale bar = 10 µm. (**C**) Semi-log profile plot of A-type lamin peptide MS intensities. Intensities of non-phosphorylated (endogenous) peptides 'Ser22' and 'Ser390' are close to the average and median intensities of all lamin-A/C peptides (gray). (**D**) Normalized phosphorylation stoichiometries (signal of phosphorylated peptide divided by the median signal of all lamin-A/C peptides; e.g. '$pSer22/LMNA_{median}$') quantified for Ser22, Ser390, and the doubly phosphorylated pSer(404&407). Normalized phosphorylation of lamin-C (slices 5-7) is ~2-fold higher than that of LA or progerin (slices 1-4). Inset: average %-phosphorylation normalized to slice #4, which corresponds to the progerin peak. *$p < 0.05$. (**E**) Left and right SDS-PAGE 'flank'

lanes cut and analyzed in parallel by Western blot, using anti-lamin-A/C and anti-pSer22 separately. (**F**) Quantitation of normalized phosphorylation at Ser22 (densitometry signal of pSer22 divided by that of total lamin-A/C; 'pSer22/LMNA') is consistent with that by FEA-MS ('pSer22/$LMNA_{mean}$'). A low MW (~30 kDa) degradation fragment is visible in both blots (purple box, C) and is highly phosphorylated at Ser22.

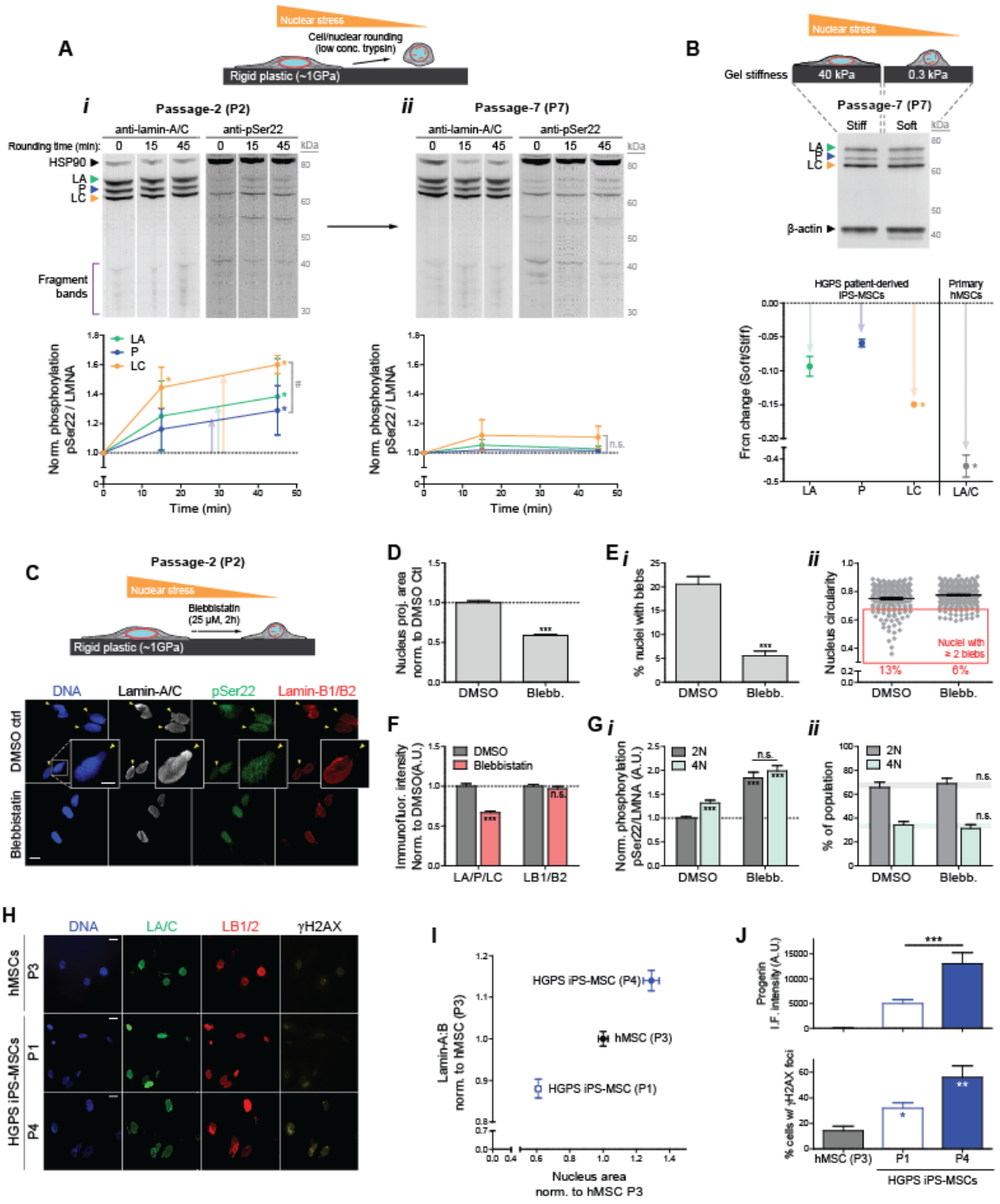

Figure 3.5. Low nuclear tension increases A-type lamin phosphorylation and degradation, but mechanosensitivity is lost with passage in HGPS iPS-MSCs

(**A**) (***i***) Full-length Western blots of cells rounded and detached from their substrate using low concentrations of trypsin, probed with anti-lamin-A/C (left) and anti-pSer22 (right). A-type lamins (LA, P, and LC) in the intact MW range (60-80 kDa) decrease with cell rounding, which anti-correlates with the increase in phosphorylation and the increase in low MW degradation fragment bands (≤ 40 kDa). Bottom plot: Normalized phosphorylation ('pSer22/LMNA') of intact LA, P, and

LC vs rounding time. (***ii***) Sensitivity to low tension (cell/nuclear rounding) is blunted with cell passage (P7). (**B**) Immunoblot of P7 HGPS iPS-MSCs cultured on stiff vs soft gels. Lower bar graph: fold change in densitometry signal (soft/stiff) of LA, P, and LC. Gray bar (right) indicates fold change of total A-type lamins in early passage primary hMSCs. (**C**) Cartoon and Immunofluorescence images of HGPS iPS-MSCs on rigid culture plastic treated with blebbistatin (25 μM, 2h) or DMSO control. (**D**) Nucleus 2D projected area decreases with blebbistatin treatment. (**E**) (***i***) Fraction (%) of cells with nuclear blebs. (***ii***) Nucleus circularity measurements. Nuclei with circularity < ~0.65 (red box) correspond to those with more than one bleb. (**F**) Immunofluorescence measurements of LA/P/LC (A-type lamin) abundance in DMSO vs blebbistatin treated iPS-MSCs. LB1/B2 (B-type lamins) remain unaffected by myosin-II inhibition. (**G**) (***i***) Normalized phosphorylation (as 'pSer22/LMNA') measured in DMSO vs blebbistatin treated iPS-MSCs. (***ii***) Fraction (%) of '2N' vs '4N' cells (by DNA content) remain unchanged with blebbistatin treatment. (**H**) Representative immunofluorescence images of LA/C, LB1/2, and γH2AX in HGPS iPS-MSCs (P1 and P4) and normal primary hMSCs. Scale bar = 10 μm. (**I**) Lamin-A:B ratio (total A : B-type lamin ratio) and cell/nuclear size increase with higher passage in iPS-MSCs. (**J**) Quantification of progerin intensity (using anti-progerin, top) and % cells with >1 γH2AX foci (bottom) determined by immunofluorescence.

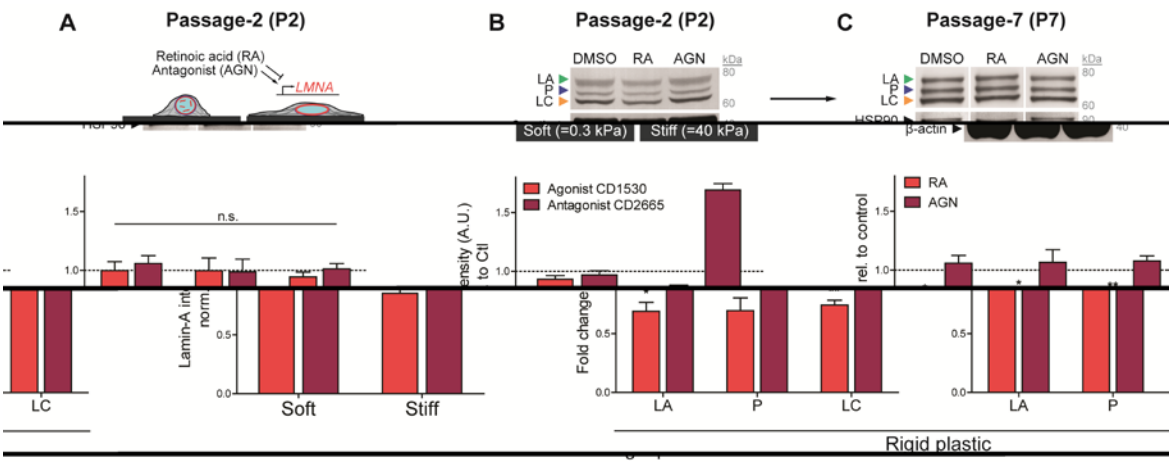

Figure 3.6. Transcriptional regulation of LA, P, and LC by retinoid compounds

(**A**) Top: cartoon illustrating HGPS iPS-MSCs on soft/stiff gels treated with retinoid compounds, all-trans retinoic acid (RA) and antagonist (AGN). Bottom: immunofluorescence quantitation of total A-type lamins after treatment with retinoids CD1530 (agonist) and CD2665 (antagonist) on soft or stiff gel cultures. (**B**) Western blot of early passage (P2) HGPS iPS-MSCs treated with 1 μM RA or AGN on rigid plastic. (**C**) Sensitivity to transcriptional regulation by retinoids decreases with passage.

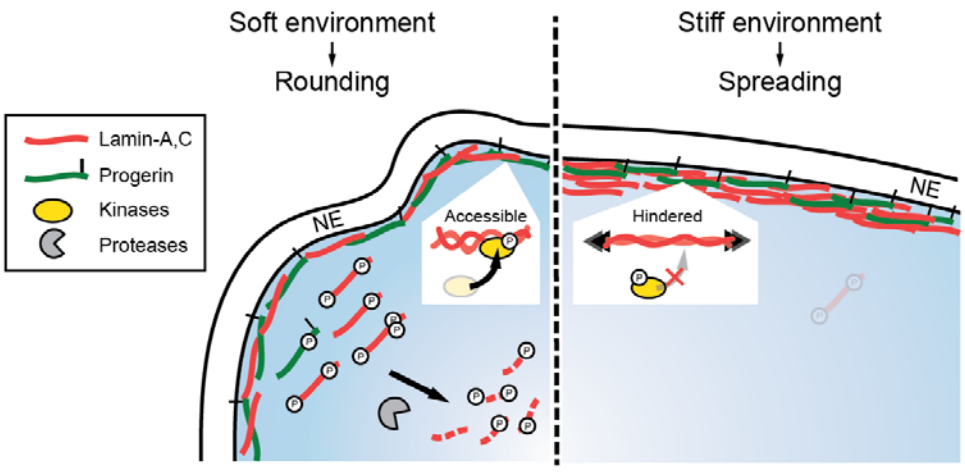

Figure 3.7. Progerin phospho-degradation is least responsive to mechanical perturbations.

Cartoon illustrating phosphorylation and turnover of A-type lamins in soft (rounded, low nuclear stress) and stiff (well-spread, high nuclear stress) environments.

CHAPTER 4
Conclusions and future work: Nuclear mechanosensing in cancer

Part of this Chapter is in preparation for submission to *Nucleus*.

4.1 Conclusions

Tissues such as bone, cartilage, and striated muscle are rigid and stiff, making them particularly robust to physical exertion during which they are subjected to mechanical stresses of varying duration, direction, and magnitude. Tissue-level strains are 'sensed' and transmitted into the nucleus via the cytokoskeleton, and recent evidence suggests such deformations might even be amplified within cells and their nuclei (Henderson et al., 2013). A strong correlation between tissue stiffness and the main structural protein of the nucleus, lamin-A, was recently discovered for diverse adult mouse tissues (Swift et al., 2013), suggesting a cell-intrinsic mechanosensitivity that confers protection against stress. The studies presented here surprisingly demonstrate that the lamin-A vs tissue stiffness correlations originate from the earliest stages of life, as soon as cells and tissues begin to differentiate in the developing embryo. In particular, in the first functional vertebrate organ – the beating embryonic heart – the increasing mechanical load of the rapidly stiffening myocardium (Majkut et al., 2013) necessitate an adaptive response to stress, and lamin-A fulfills this role by accumulating at the nuclear periphery under elevated mechanical tension (Figure 2.2). The increase proves mechano-protective against nuclear envelope rupture and DNA damage, which in excess can affect tissue-level function (Figure 2.6). Sensitivity to tissue mechanics is achieved by a 'use it or lose it' mechanism of tension-suppressed phosphorylation and turnover, which allows optimal lamin-A levels to be maintained in close coordination with the mechanical microenvironment. Defects in mechanosensitive turnover of lamin-A can thus be problematic for stiff and mature tissues that are subject to mechanical wear-and-tear, and one example is the aging-associated laminopathic mutant, progerin, whose phosphorylation-dependent turnover is shown here to be lower and less sensitive to stress relative to normal lamin-A and C (Figure 3.4, Figure 3.5). The ability of the nucleus to adaptively remodel in response to mechanical strain is thus critical for maintaining gnome integrity not only in embryonic development, but also in disease and aging of mature tissues.

4.2 Future directions

Given the broad 'universality' of lamin-A vs tissue stiffness correlations consistently observed in tens of proteomics and transcriptomics data generated by ourselves and by others, a reasonable next step is to examine more systematically whether any defects in lamin-A mechanosensing contribute to manifestation of specific diseases. Mis-regulation of lamin-A's response to mechanical stress could conceivably favor accumulation of excess DNA damage (perhaps beginning from early embryonic development), and thereby contribute to increased cell death, premature senescence, *de novo* mutations, and perhaps even more complex tissue-level phenomena such as tumorigenesis. Since lamin-A is also known to regulate a wide range of cellular processes including stem cell differentiation and chromatin organization, failure to maintain genomic stability might also further complicate defects in lamin-A's fine-tuning of cell fate and maturation.

Hundreds of *LMNA* point mutations to date are known to cause a number of cardiomyopathies (the most common being DCM) among many other musculoskeletal diseases (Worman and Bonne, 2007), but whether mechanically-induced DNA damage contributes to pathology remains unknown. Any detrimental effect of nuclear rupture and excess DNA damage would conceivably be accentuated in cardiac laminopathies, given the heart's limited regenerative/remodeling capacity upon acute injury or with mechanical wear-and-tear. Recent studies of laminopathic DCM mice have indeed begun to report significant nuclear blebbing (Lee et al., 2017), focal 'breaks' in the nuclear membrane (as imaged by EM) (Siu et al., 2012), cytoskeletal defects (Bollen et al., 2017), and fibrosis (Captur et al., 2018), all of which increase with electrical stimulation and enhanced contractility. The observations are consistent with envelope rupture under high mechanical strain (Figure 2.8), and so potential defects in lamin-A phosphorylation and/or assembly, and perhaps excess DNA damage, might also be expected for such blebbed laminopathic nuclei. Whether the blebs seen in these mutants form upon rupture of the nucleus (with lamin-A enrichment and lamin-B depletion), and whether the phenotype can be reversed to a certain extent with inhibition of cytoskeletal stress (e.g. myosin-II inhibition by blebbistatin) remain to be seen. If morphological parameters indeed prove consistent with

mechanically-induced rupture, the functional consequences of excess DNA damage and any contributions to disease pathology should be assessed.

As introduced in Chapter 3, nuclear blebbing and genomic instability are also major hallmarks of the premature aging disorder HGPS. Our MS analyses have shown that phosphorylation of the truncated mutant progerin is lower and less mechanosensitive than normal lamin-A and C, suggesting that the characteristic nuclear blebbing in HGPS cells (Butin-Israeli et al., 2012), as well as the well-documented increase in DNA damage (Liu et al., 2006), might in part result from aberrant lamin mechanosensing. Indeed, treatment of patient-derived cells with blebbistatin resulted in partial rescue of %-blebbed nuclei (Figure 3.5E), consistent with studies which demonstrate apoptosis/senescence defects in progeroid cells can be rescued by culture on soft matrix (de La Rosa et al., 2013a). While we have shown by correlation that average γH2AX foci count increases with progerin accumulation and with cell passage (Figure 3.5H-J), it remains to be seen whether rescue of nuclear morphology by blebbistatin (or perhaps soft matrix) can also impact DNA damage in these cells. Various mechanobiological perturbations should be performed (as done in the heart study in Chapter 2) to assess rigorously whether modulation of stress exerted on the nucleus can indeed help preserve genome integrity and ultimately improve cell function and/or survival in these cells.

Dramatic changes in nuclear morphology (Dey, 2010; Wolberg et al., 1999), levels of nuclear envelope components (Broers et al., 1993; Irianto et al., 2016b; Kaufmann et al., 1991), and localization of nuclear factors (Chow et al., 2012) have also been implicated in various types of cancers, which raise the question of whether lamin-A mechanosensing also plays a role in tumor development and/or metastasis. Given that tumors are typically much stiffer than normal adjacent tissue (Chin et al., 2016) with an excess of heavily bundled collagenous matrix, the tumor microenvironment presents complex structural and mechanical signals that could impact individual nuclei. A major hallmark and driver of hepatocellular carcinoma (HCC), for example, is extensive fibrotic matrix deposition that results in significant tumor stiffening, and in some extreme cases, cirrhosis. The increased stiffness of such tumors could in principle drive abnormal

accumulation of lamin-A levels, thereby affecting downstream regulation of differentiation, proliferation, and apoptosis.

To begin to assess whether lamin-A mechanosensing mechanisms would also apply to different cancers, we performed preliminary meta-analyses of publicly accessible tumor transcriptomes, as done for heart tissue '-omics' data in Chapter 1, Section 1.4. As described previously, *Col1a1* was used as a surrogate for tissue stiffness, and was again shown to exhibit robust scaling with *Col1a2* across most datasets, with an average scaling exponent $\alpha_{Col1a2} \sim 1$ (**Figure 4.1A-C**). The small subset of datasets that showed weak or inconsistent correlations between *Col1a1* & *Col1a2* ($\alpha_{Col1a2} < 0.7$ or $R^2 < 0.5$) were once again deemed 'unreliable', since the two collagen-I transcripts should in principle increase or decrease together as obligate subunits of the collagen-I triple helix. Analysis of *Lmna* levels revealed an average scaling exponent α_{Lmna} ~0.3 that is surprisingly consistent with that found for heart transcriptomes, suggesting lamin-A stiffness-sensing (and possible feedback to transcription) might indeed be applied to various types of cancer. A representative dataset for HCC tumors and normal adjacent tissue (Figure 4.1B) illustrates the elevated levels of collagen-I subunits and *Lmna* in HCC versus normal tissue. Similar analyses of other proteins of interest in the cytoskeleton (*Myh9*, *Acta2*), B-type lamins (*Lmnb1* & *b2*), as well as some known mechanosensitive transcription factors (*Yap1*, *Rarg*), also exhibited comparable correlations vs *Col1a1* as those in the heart -omics data, providing additional confidence in the potential 'universality' of stiffness-dependent scaling correlations.

It is important to note, however, that these tumor transcriptomics datasets exhibited much greater 'noise' compared to our meta-analysis of heart transcriptomes/proteomes, with error bars (SEM) that were often larger than the mean itself (Figure 4.1A). Significant noise likely reflects the heterogeneity in the mechanical properties tumors, as well as the numerous transcriptional and post-translational changes that could impact steady-state transcript and protein levels found in normal tissue. Similar average scaling exponents for *Lmna* (α_{Lmna} ~0.3) nonetheless prompted questions of whether such correlations could also be observed at the protein level. Human HCC tumor samples and adjacent 'uninvolved' liver tissue were thus collected from donors and were profiled by mass spectrometry (MS) (**Figure 4.2A**). MS-based proteomics of tumors revealed a

near 5-fold increase in collagen-I subunits COL1A1 and COL1A2, as well as significant increases in all other ECM components detected (**Figure 4.2B,C**). Elevated levels of collagenous matrix were also accompanied by an increase in lamin-A/C (**Figure 4.2D**), suggesting indeed that lamin-A/C accumulates in the stiffer, fibrotic HCC tumors. As reported previously for HCC (Sun et al., 2010), lamin-B1 was found to be >4-fold more abundant in the tumors compared to normal tissue (**Figure 4.2E**), possibly hinting at differences in ploidy. A well-documented diagnostic marker for HCC, alpha fetoprotein (AFP), was also quantified for validation, and was found indeed to be >100-fold more abundant in the HCC tumors versus adjacent tissue (**Figure 4.2E**).

The preliminary MS measurements are overall consistent with trends found for intact embryonic hearts (Chapters 1 and 2) and for diverse adult mouse tissues (Swift et al., 2013), and provide some initial evidence of lamin-A mechanosensing in at least one type of cancer known to be associated closely with fibrotic stiffening of tumors. Taken together with the mechanistic studies presented in Chapters 2 and 3, it is plausible that excess deposition of collagenous matrix drives abnormal stiffening of the liver, resulting in increased cytoskeletal contractility and steady-state accumulation of lamin-A/C. However, it remains to be investigated whether the same 'use it or lose it' mechanism of tension-suppressed turnover applies to HCC, given the abnormal increase also seen for lamin-B1, which in most other contexts remains unchanged in expression. Lamin-A/C mechanosensing mechanisms might further be mis-regulated in these tumors by aberrant transcription, chromosome copy number changes, altered tissue mechanics due to high lipid content, and general heterogeneity of the tumor microenvironment. Rigorous reductionist studies should be conducted with careful consideration of possible confounding/compensatory effects, in order to elucidate mechanisms and any functional consequences of lamin-A mechanosensing in cancer.

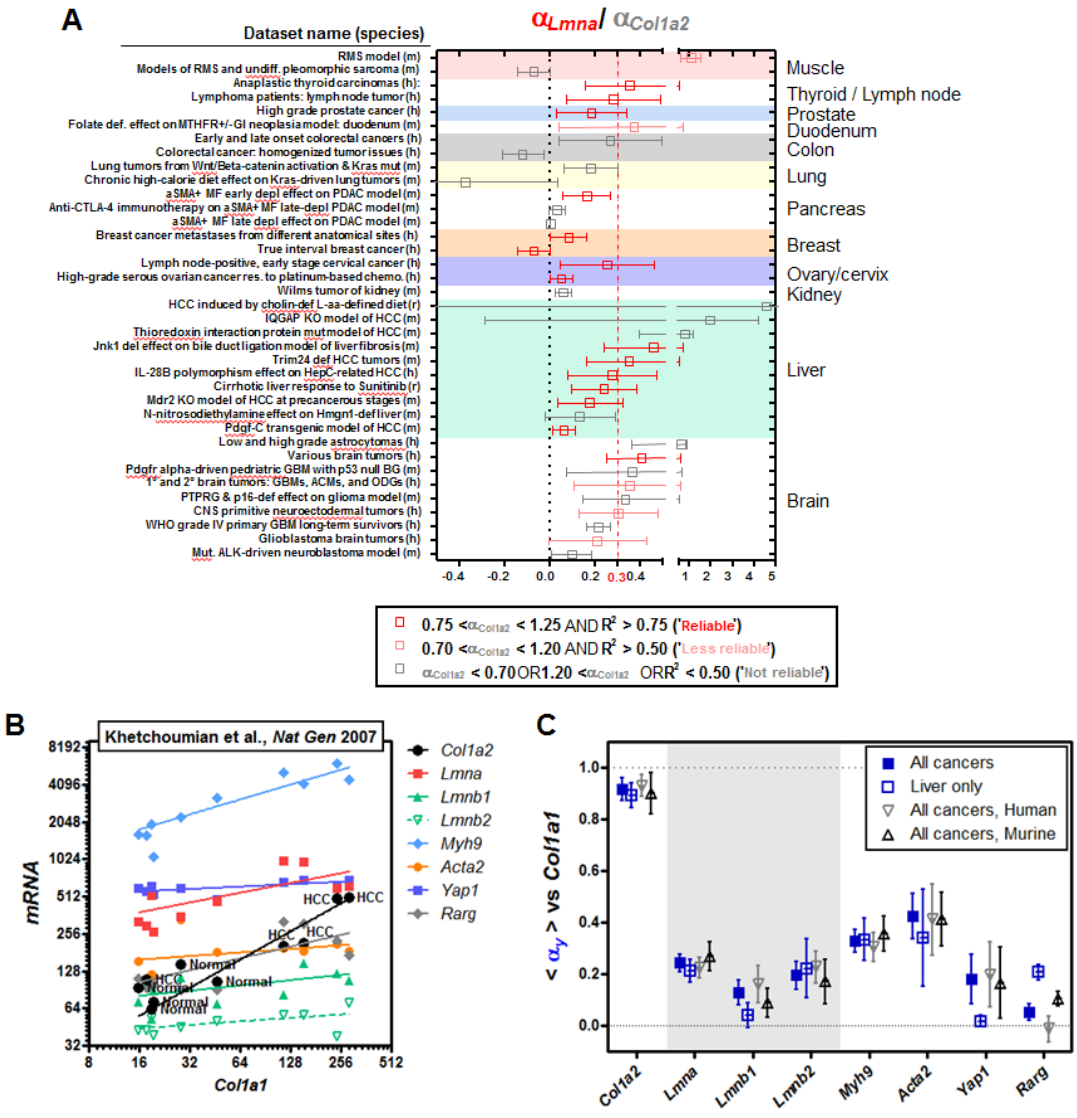

Figure 4.1. Stiffness-dependent *Lmna* scaling in diverse cancer transcriptomes

(**A**) Meta-analysis of >35 tumor transcriptomics datasets reveals average scaling exponent α_{Lmna} ~ 0.3 (from *Lmna* ~ *Col1a1*$^{\alpha_{Lmna}}$), consistent with that found for diverse heart transcriptomics datasets. (**B**) Representative log-log plot and (**C**) average scaling exponents for several transcripts of interest vs *Col1a1*.

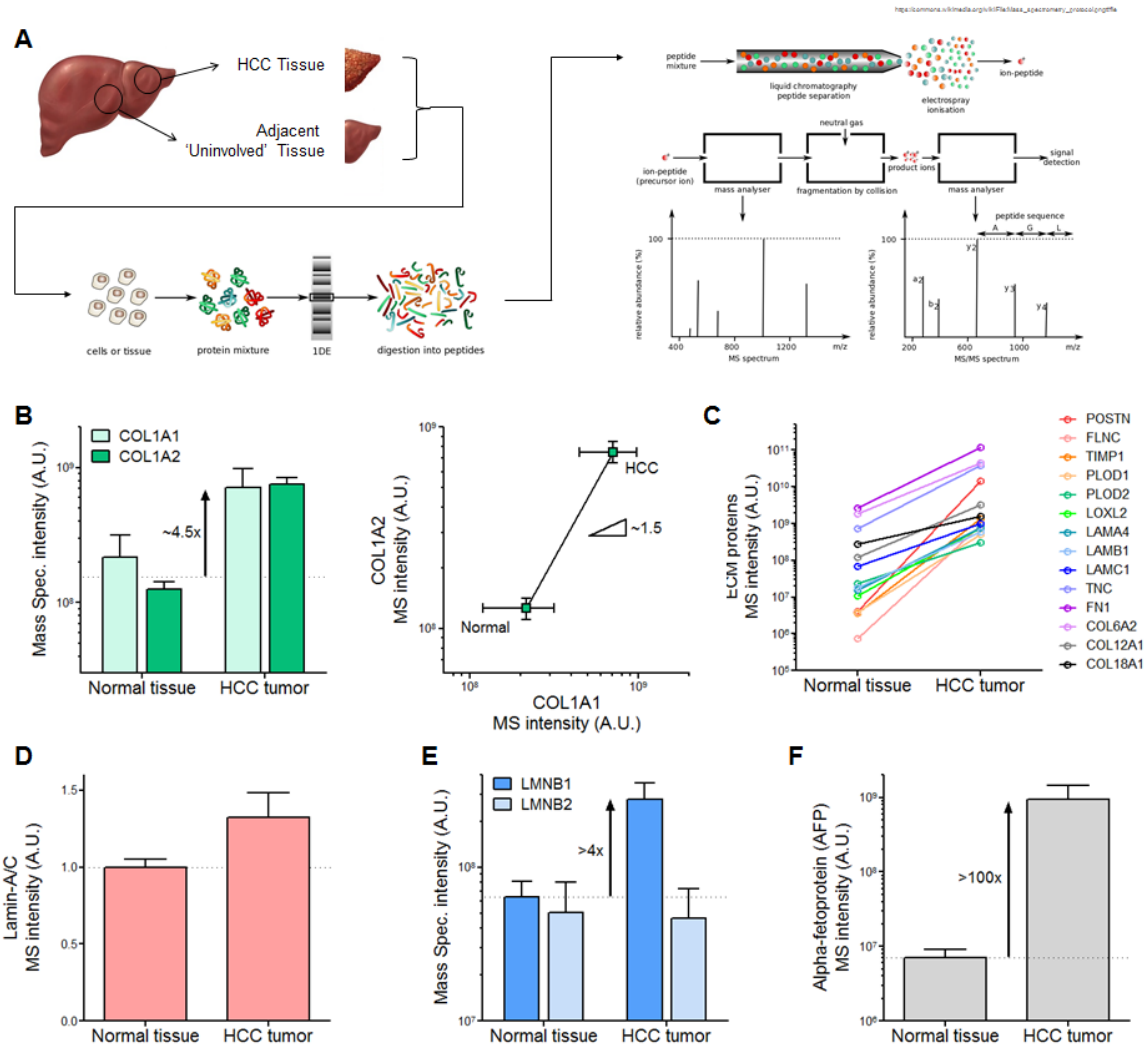

Figure 4.2. Proteomics reveals higher collagen-I and lamin-A/C levels in human HCC tumors vs adjacent tissue

(**A**) Proteomics workflow for human HCC tumors and adjacent 'uninvolved' tissue. (**B** & **C**) MS reveals elevated collagen-I levels and all other ECM proteins in human HCC tumors vs adjacent 'uninvolved' tissue. (**D**) Lamin-A/C is likewise higher in HCC tumors, consistent with increased collagenous ECM. (**E** & **F**) Lamin-B1 and AFP (a well-documented marker for HCC) are significantly elevated, as previously reported for HCC tumors.

APPENDIX A

Supplementary information for Chapter 2

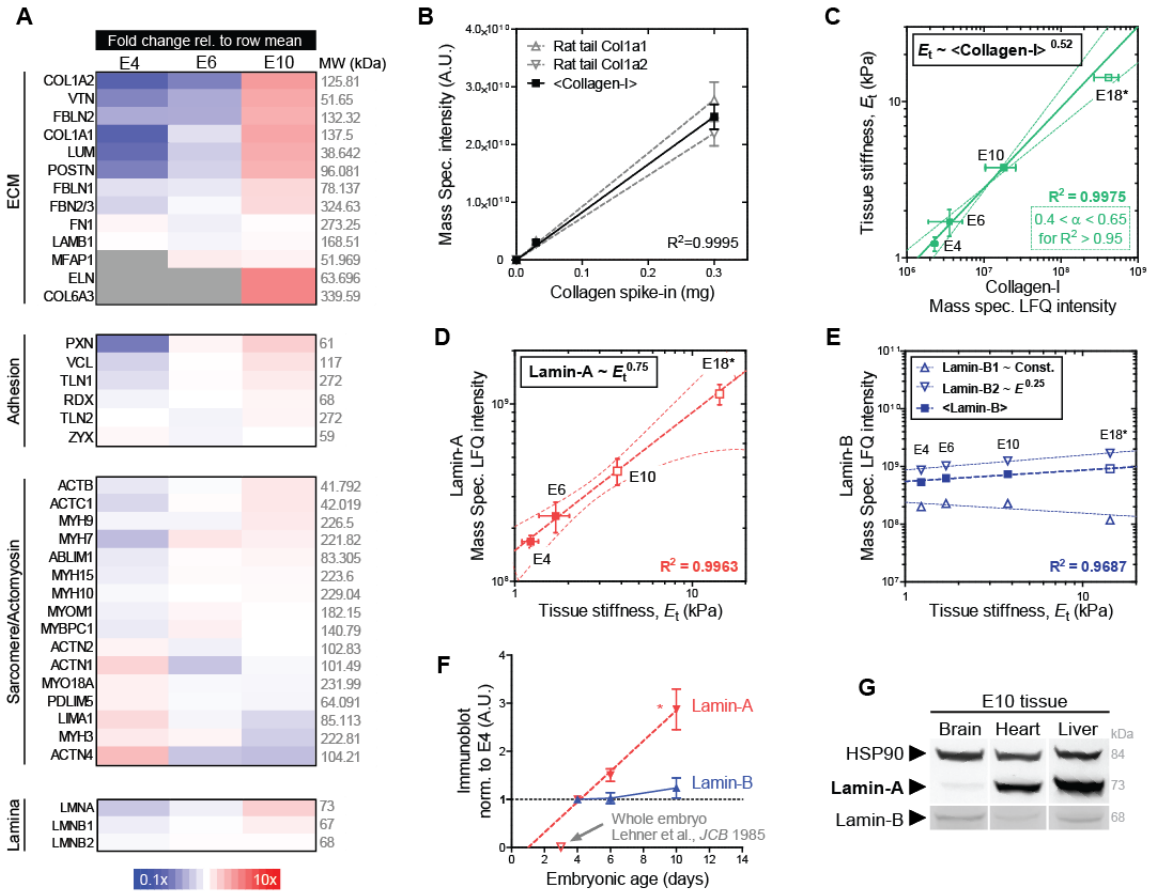

Figure A.1. Proteomic profiling of embryonic hearts reveals broad increases in proteins of the ECM, adhesion complexes, sarcomere/actomyosin assemblies, and the nuclear lamina.

(**A**) Heartmap of proteins detected by LC-MS/MS in the ECM, adhesion complexes, sarcomeres, and the nuclear lamina. Proteins were ranked based on the fold-change relative to the average. (**B**) MS measurements of collagen-I calibrated with known amounts of purified collagen. (**C**) Heart stiffness measurements by micropipette aspiration plotted against collagen-I MS intensity yield power-law scaling comparable to that found for diverse adult tissues (Swift et al., 2013). (**D**) Lamin-A MS intensity scales with heart tissue stiffness with exponent α ~ 0.75 again close to that for adult tissue proteomes (Swift et al., 2013). (**E**) Lamins-B1 & B2 remain comparatively constant throughout development and exhibit much weaker scaling (α < 0.25). (**F**) Immunoblot densitometry measurement of lamin-A and B in embryonic heart lysates at E4, E6, and E10 (n>6 hearts per lysate). Extrapolation reveals initial expression (x-intercept) at ~embryonic day 1 (E1), occurring earlier than previous reports of earliest lamin-A expression in whole embryos ~E3 (Lehner et al., 1987). (*p<0.05) (**G**) Lamin-A & B immunoblots for E10 brain and liver tissue.

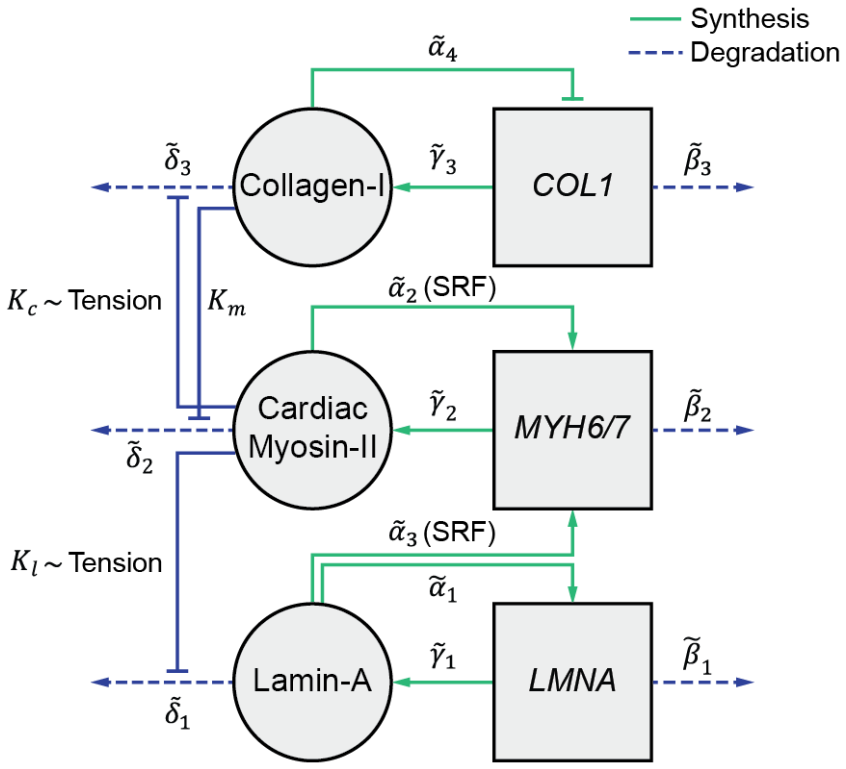

Figure A.2. 'Use it or lose it' model of tension-inhibited turnover.

Schematic diagram of a 'mechanobiological gene circuit' model that describes the tension-suppressed turnover of lamin-A, myosin-II, and collagen-I, adapted from Dingal et al. (Dingal and Discher, 2014). Squares = genes, circles = protein. Lamin-A and myosin-II protein (l and m) are weak regulators of the Serum Response Factor (SRF) pathway, which enhances transcription of many cytoskeletal proteins including myosin-II. Lamin-A also upregulates its own transcription (via RARγ) in a feedback loop. Lamin-A and collagen-I protein (l and c) turnover are dictated by $K_l \sim m^{x/n_l}$ and $K_c \sim m^{z/n_c}$, respectively, for some x and z that dictate sensitivity of degradation to myosin-generated tension. Myosin-II protein (m) turnover in turn depends on matrix elasticity E which correlates strongly with collagen-I (c, Figure 2.2E), such that $K_m \sim c^{y/n_m}$ for some y that represents the affinity for myosin degradation.

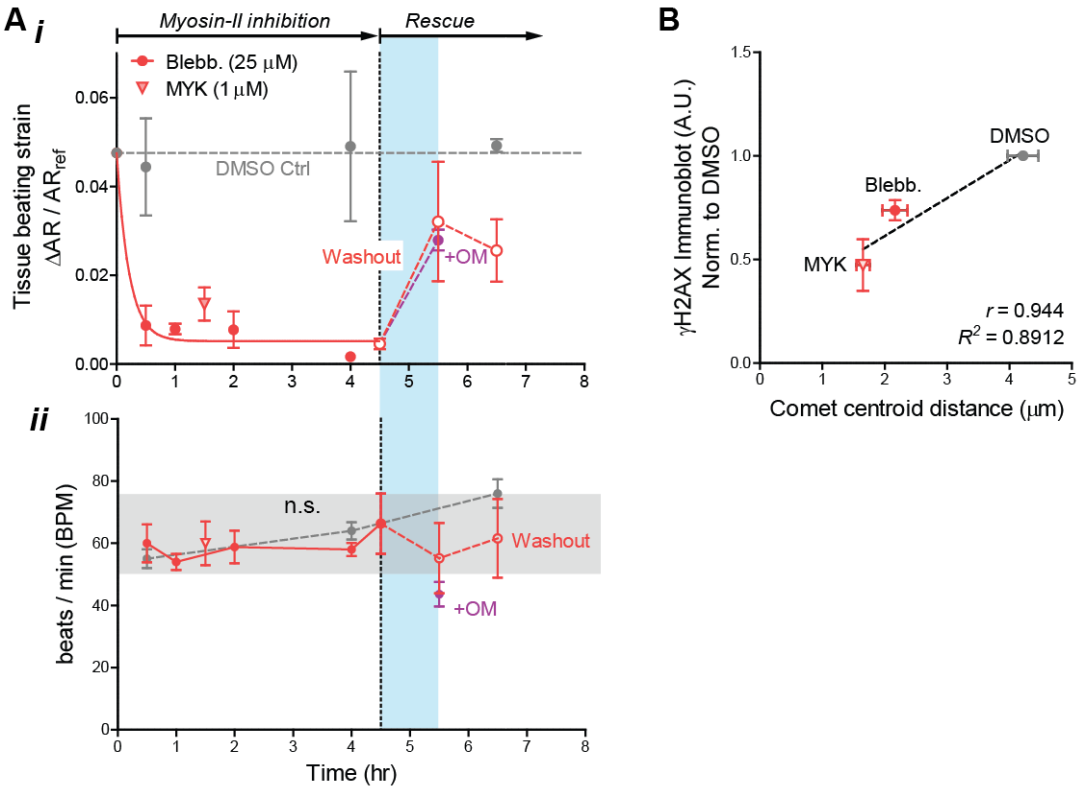

Figure A.3. Blebbistatin and MYK reversibly inhibit contractility of intact hearts within <1h and reduces DNA damage

(**A**) (***i***) Quantification of tissue beating strain $\Delta AR/AR_{ref}$ and ***(ii)*** heart rate (beats / min; BPM) in blebbistatin treated hearts. Myosin-II inhibition by blebbistatin rapidly suppresses beating (<30 min), but effects are reversible such that washout of drug with culture medium (± OM) results in near full recovery by 1h. (**B**) Densitometry quantitation of γH2AX immunoblots correlates well with quantitation of DNA breaks by electrophoretic Comet assay (r = 0.944, R^2 = 0.8912).

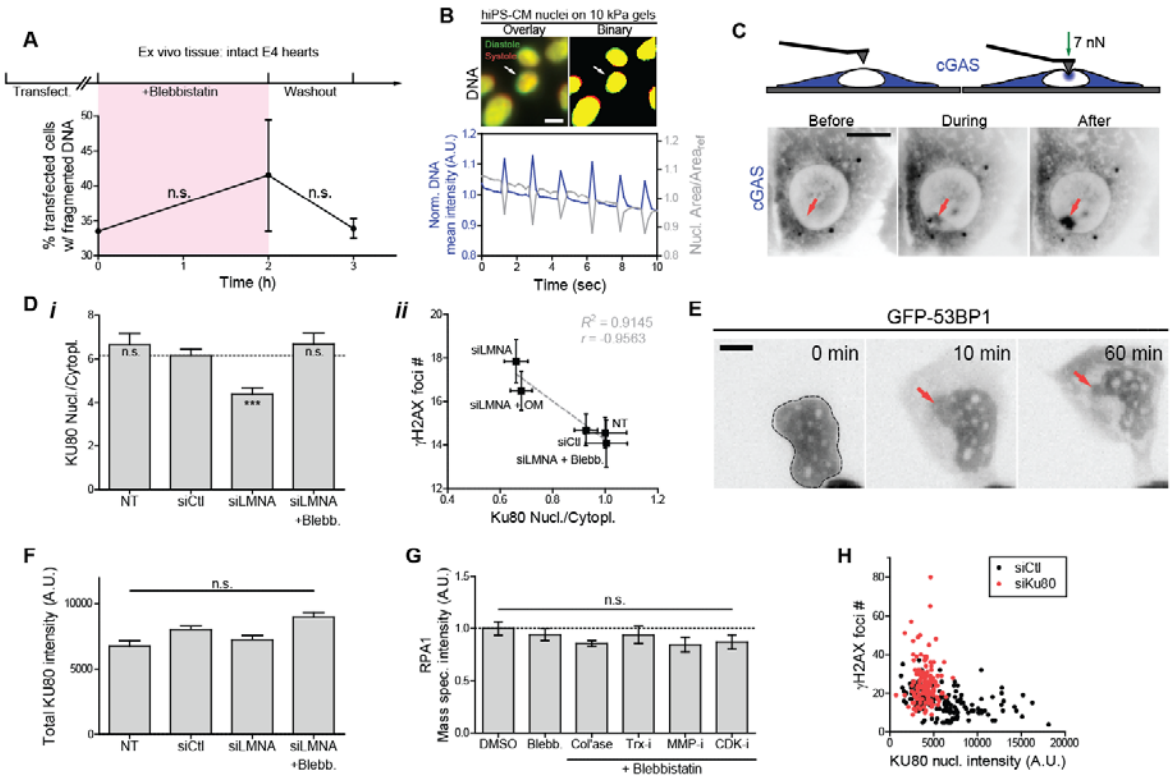

Figure A.4. Suppression of lamin-A levels in intact embryonic hearts and in beating hiPS-CMs increase rupture under high stress, causing prolonged (>1h) loss of repair factors from the nucleus and accumulation of DNA damage

(**A**) Blebbistatin treatment and washout have no significant effect on cell death/viability, as determined by %-transfected cells with fragmented DNA. (**B**) As seen with nuclei in intact embryonic hearts, 'nuclear beating' occurs in hiPS-CMs and can be quantified by changes in nucleus area and DNA mean intensity (condensation/de-condensation of DNA), which are inversely correlated. (**C**) Time-lapse images of nuclei probed with a pointed (<1 μm) Atomic Force Microscopy (AFM) tip (at ~7 nN). Nuclear rupture upon stress is evident in the rapid and stable accumulation of a cytoplasmic protein that binds DNA (GFP-cGAS). (**D**) (***i***) Nuclear/cytoplasmic KU80 immunofluorescence intensity ratio decreases with siLMNA knockdown, and **(*ii*)** anti-correlates with γH2AX foci count. (**E**) Time-lapse images of siLMNA knockdown cells transduced with GFP-53BP1 show that nuclear rupture and cytoplasmic mislocalization occur within minutes, and are maintained for at least 1h in culture indicating slow recovery. (**F**) Total (nuclear + cytoplasmic) KU80 abundance is unaffected by siLMNA or blebbistatin treatment. (**G**) RPA1 levels are unaffected by drug perturbations (per MS). (**H**) γH2AX foci count inversely correlates with KU80 nuclear immunofluorescence intensity, consistent with limited repair.

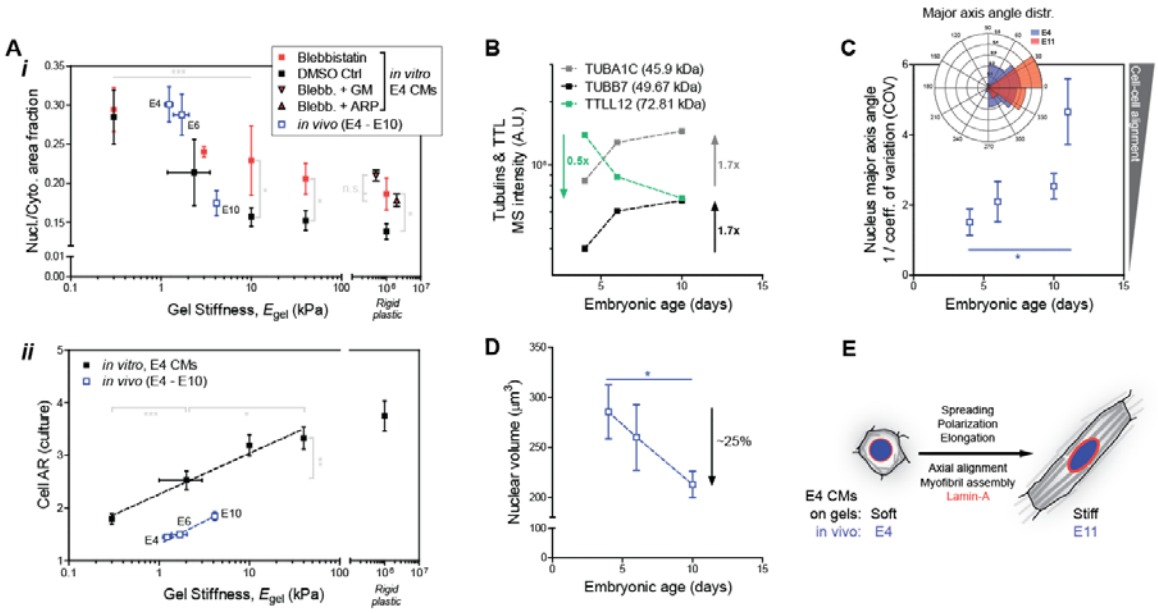

Figure A.5. Cell-on-gel morphological trends in CM size, shape, contractility, and lamin-A mirror those of *in vivo* hearts

(**A**) (***i***) Projected area of the nucleus relative to that of the cell ('Nucl./Cyto. Area fraction') decreases (***ii***) and cells elongate (increased aspect ratio, AR), as the embryonic heart stiffens and cells undergo hypertrophic growth and spreading from E4 – E10. Isolated E4 CMs cultured on gels likewise exhibit increased cell spreading and elongation on stiffer gels. (**B**) Two of the most abundantly expressed α- and β-tubulin isoforms (TUBA1C, TUBB7) increase in level from E4 to E10 and the increase is accompanied by a decrease in TTLL12, which tyrosinates and de-stabilizes microtubules (Robison et al., 2016). Trends are consistent with increased stiffness as well as with polarization/elongation of CMs during development (Fig.4D-*ii*, Fig.S4A). (**C**) Axial alignment of cells (anisotropy, quantified as 1/COV of the major axes of nuclei) increases from early (E4) to late (E11) hearts. Upper left inset: major axis angle distribution of E4 and E11 nuclei. (**D**) Nuclear volume (estimated by confocal Z-stack) decreases in development from E4 to E10. (**E**) Varying matrix stiffness alone in E4 CM cultures is sufficient to recapitulate trends in morphology and intracellular organization seen *in vivo* (from E4 to E11).

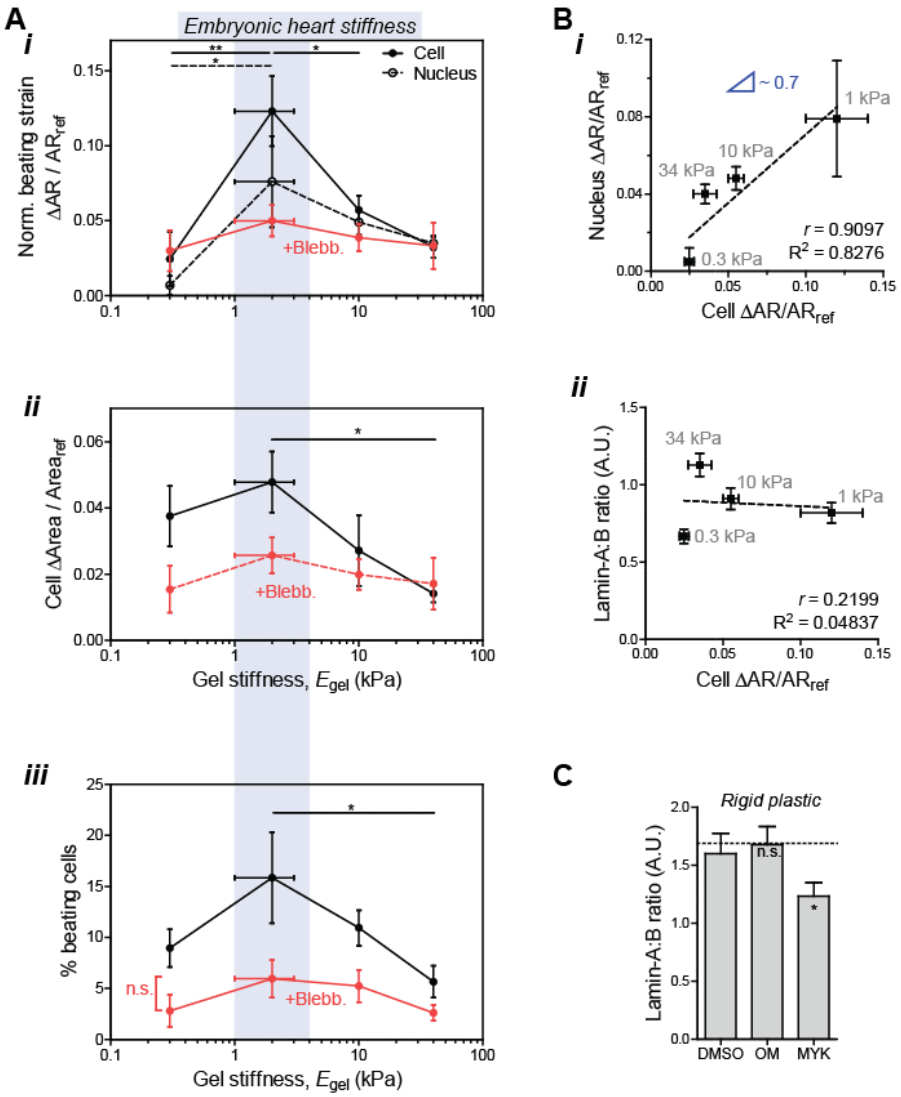

Figure A.6. Contractile beating of embryonic chick CMs exhibit an optimum on gels that match the stiffness of embryonic hearts but the increase in lamin-A levels decouples from dynamic nuclear strains

(**A**) Normalized cell and nuclear beating strains measured by (***i***) '$\Delta AR/AR_{ref}$' and (***ii***) '$\Delta Area/Area_{ref}$', and (***iii***) %-beating cells all exhibit an optimum on gels mimicking the stiffness of embryonic hearts (~2 kPa). Blebbistatin treatment abolishes mechano-sensitivity. (n>10 cells/nuclei per condition). (**B**) (***i***) Nuclear beating strain ('Nucleus $\Delta AR/AR_{ref}$') correlates well with cell beating strain ('Cell $\Delta AR/AR_{ref}$'), (***ii***) but lamin-A:B ratio does not correlate with dynamic beating. Lamin-A:B instead couples to average morphology changes in spreading area and elongation that relate to basal isometric tension. (**C**) Lamin-A:B in cells on rigid plastic decreases with MYK inhibition of cardiac myosin contractility (as with blebbistatin treatment), but remains unchanged with OM treatment.

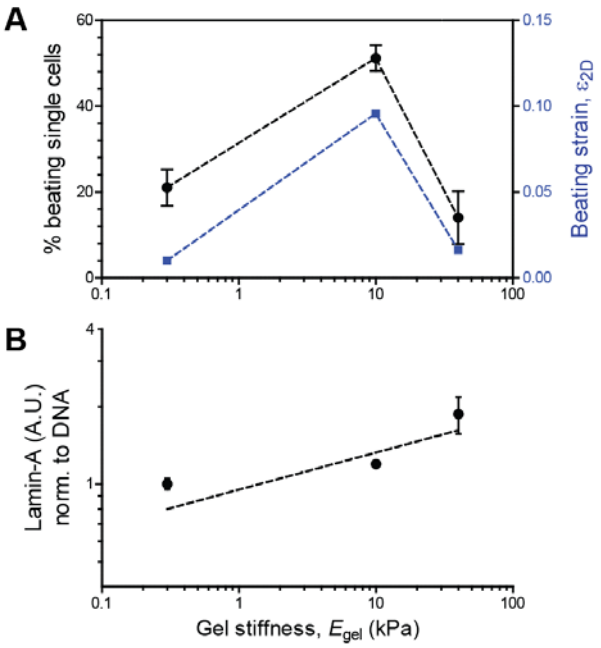

Figure A.7. Contractile beating in hiPS-CMs exhibit an optimum on 10 kPa gels but lamin-A increases monotonically from soft to stiff

(**A**) %-beating cells and beating strain (quantified using a custom Matlab code) in hiPS-CMs exhibit an optimum on 10 kPa gels that match the stiffness of mature adult hearts. (**B**) Lamin-A levels (by immunofluorescence) in hiPS-CMs increases monotonically from soft to stiff gels, appearing to decouple from dynamic beating strain.

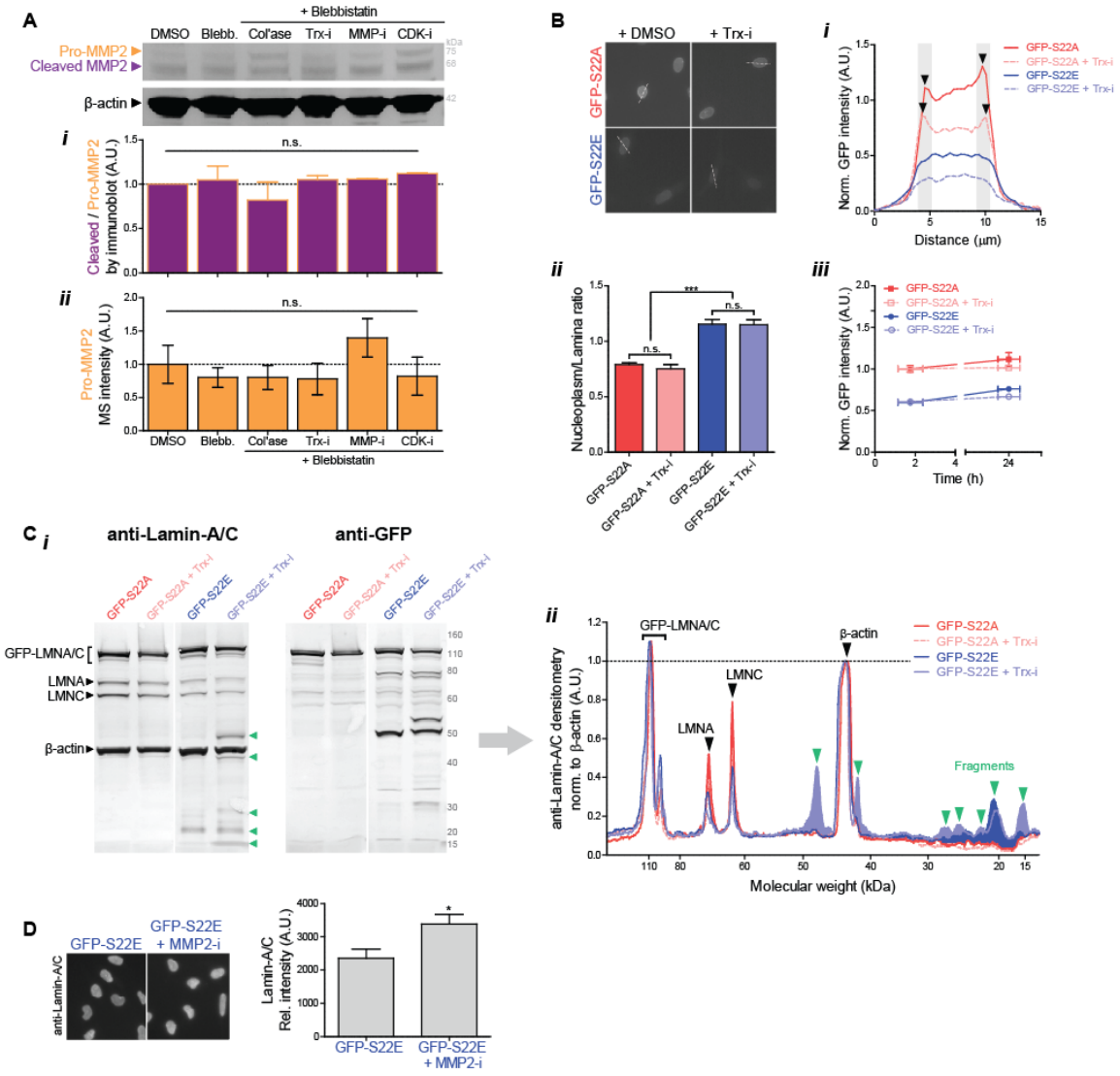

Figure A.8. Phosphorylation of lamin-A favors degradation by MMP2

(**A**) Neither the catalytic activation of MMP2 ('cleaved/pro-MMP2' fraction, as measured by immunoblot, (***i***)) nor the total abundance of pro-MMP2 (MW ~ 75 kDa, as measured by MS (***ii***)) are significantly affected by drug perturbations to contractility and/or collagen matrix. (**B**) Representative images of cells transduced with phsopho-mimetic mutants GFP-S22A and GFP-S22E, with or without protein synthesis inhibitor Trx-i. (***i***,***ii***) Line profiles across individual nuclei reveal 'non-phosphorylatable' GFP-S22A signal is far more enriched at the lamina than in the

nucleoplasm, compared to ‘constitutively phosphorylated’ GFP-S22E (n>15 nuclei). Treatment with Trx-i does not alter nucleoplasm/lamina ratio in either mutant. (***iii***) Overall fluorescence intensity of GFP-S22A is ~50% higher than that of GFP-S22E. Trx-i induces a minor ~10% decrease in either case. (**C**) (***i***) Immunoblots with anti-lamin-A/C and anti-GFP reveal multiple low-MW degradation fragment bands (green triangles) in the GFP-S22E mutant which are absent in the S22A mutant. (***ii***) Line intensity profile of anti-lamin-A/C immunoblot (*i*, left). Low-MW degradation fragments that are present in the GFP-S22E mutant but not in the GFP-S22A mutant, are shaded in blue, with green arrows indicating distinct bands. (**D**) GFP fluorescence intensity of GFP-S22E expressing cells increases upon MMP2-i treatment, consistent with inhibition of degradation.

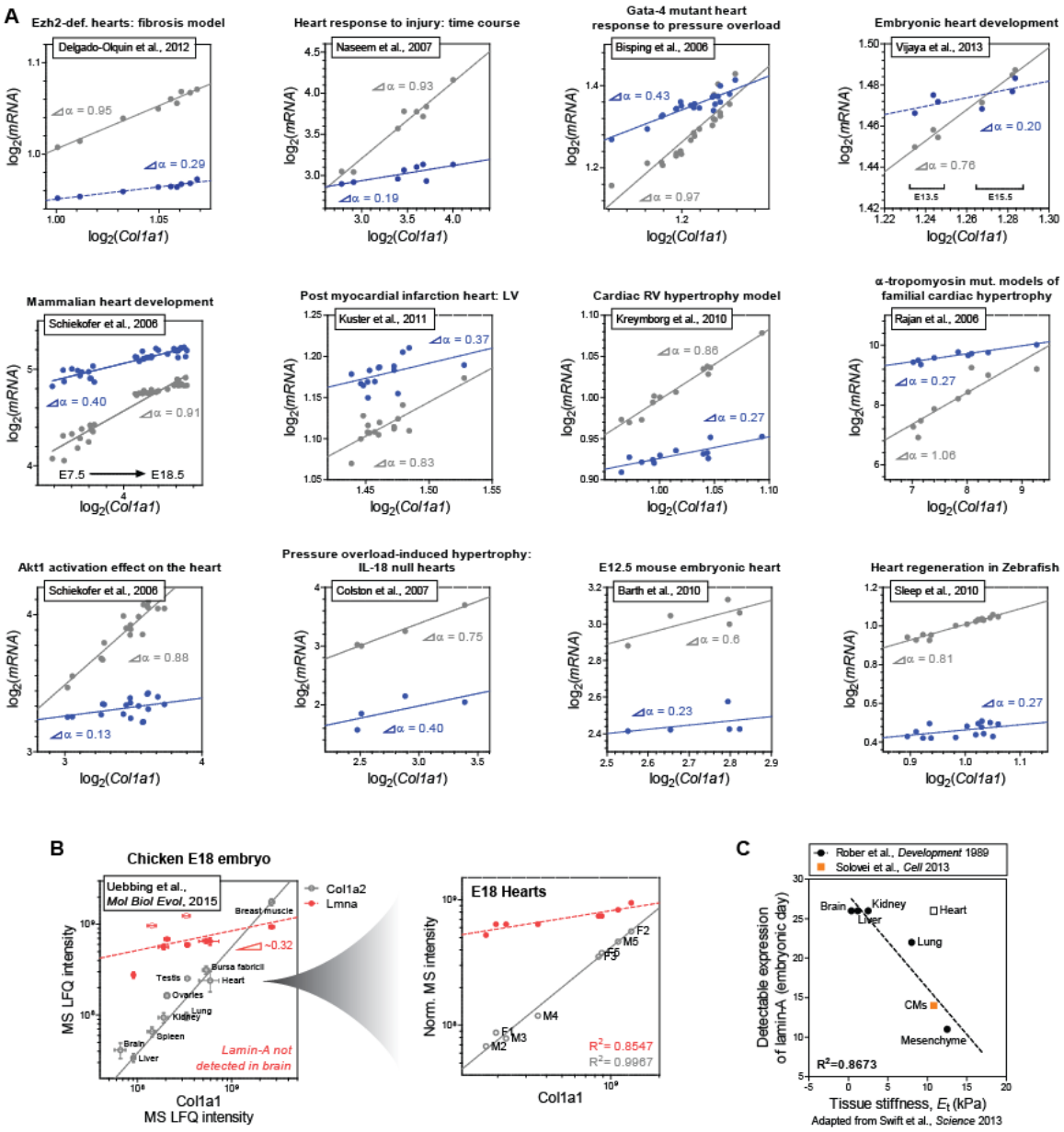

Figure A.9. Meta-analysis of 25 published transcriptomics datasets of normal and diseased hearts reveal possible feedback to gene expression and point to potential universality of lamin-A vs collagen-I scaling.

(**A**) Representative transcriptomics datasets for normal and diseased hearts. Log-log plots show normalized *mRNA* expression vs *Col1a1*. As expected for obligate heterotrimer subunits of collagen-I, *Col1a2* correlates robustly with *Col1a1*, with scaling exponent (= slope on a log-log plot), $\alpha_{Col1a2} \sim 1$. *Lmna* also increases with *Col1a1,* although with slightly weaker scaling $\alpha_{Lmna} \sim 0.3$, indicating potential feedback to gene expression. (**B**) Proteomics dataset for diverse E18 chick embryonic tissues, adapted from Uebbing et al. (Uebbing et al., 2015). Lmna again increases with Col1a1&2, with exponent $\alpha_{Lmna} \sim 0.3$. Right inset: datapoints for heart samples plotted separately reveal similar scaling. (**C**) Tissue-dependent timing of detectable lamin-A

expression (embryonic day; adapted from Rober et al. (Rober et al., 1989) and Solovei et al. (Solovei et al., 2013)) correlates inversely with stiffness E_t that the corresponding tissues eventually achieve in adult stages (adapted from Swift et al. (Swift et al., 2013)).

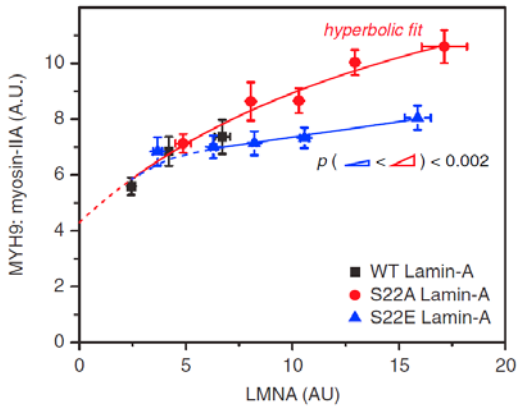

Figure A.10. Lamin-A,C phosphorylation feeds back into myosin-IIA level

Expression of increasing levels of phosphomimetic GFP-S22E-lamin-A in A549 cells with KD of endogenous lamin-A,C had minimal effect on myosin-IIA levels. In contrast, expression of an nonphosphorylatable S22A construct caused a relatively increased quantity of myosin-IIA [the x axis shows total LMNA; S22A data were fit by the hyperbolic function y = abx (1 + bx)21 + c (a = 1.3; b = 5.5; c = 4.3; R2 > 0.95); each point is averaged data from n > 20 cells; see Figures S4B–S4D for representative images and analysis of cell morphology].

			ENCODE	mRNA (microarray)	Protein (mass spec.)	
			Transcr. factor ChIP-Seq: **SRF**	*LMNA* KD in primary MSCs	Embryonic hearts (E4 - E10)	
	Gene name	Protein name	Avg(log(cluster score)) ± SEM	Fold change NT/KD ± SEM	Fold change: E10/avg	Fold change: E10/E4
SRF & Cofactors	*LMNA*	Lamin-A/C	2.28 ± 0.11	2.81 ± 0.15	1.53	2.49
	SRF	SRF	3.00 ± 0.00	1.57 ± 0.07	--	--
	MKL1	MKL1	0.00 ± 0.00	1.25 ± 0.05	--	--
	MYOCD	MYOCD	0.00 ± 0.00	1.32 ± 0.03	--	--
SRF target genes	*CALD1*	Caldesmon 1	2.53 ± 0.15	1.75 ± 0.20	1.61	2.32
	ACTC1	Actin, alpha cardiac muscle 1	2.43 ± 0.00	2.82 ± 0.83	1.25	1.79
	VCL	Vinculin	2.56 ± 0.09	1.65 ± 0.07	1.22	1.73
	ACTB	β-actin	3.00 ± 0.00	1.88 ± 0.06	1.25	1.56
	TLN1	Talin-1	2.70 ± 0.30	1.44 ± 0.11	1.22	1.63
	MYH9	Myosin-9	2.54 ± 0.46	2.74 ± 0.43	1.23	1.39
	FLNB	Filamin-B	2.36 ± 0.17	1.53 ± 0.05	1.17	1.45
	ABLIM1	Actin-binding LIM protein 1	2.44 ± 0.04	1.29 ± 0.18	1.12	1.38
	LMNB1	Lamin-B1	2.54 ± 0.04	0.93 ± 0.04	1.04	1.13
	LMNB2	Lamin-B2	0.00 ± 0.00	0.97 ± 0.05	1.18	1.40

Table 2. Serum Response Factor (SRF) target genes and cofactors increase in protein level from early to late (E4-E10) hearts as lamin-A increases.

Lamin-A is a weak regulator of the Serum Response Factor (SRF) pathway (Swift et al., 2013). Leftmost column indicates average log(cluster scores) obtained from transcription factor (SRF) ChIP-Seq data from the ENCODE database. Second column shows fold change in mRNA (non-treated/knockdown, 'NT/KD'; by microarray) resulting from *LMNA* knockdown in mesenchymal stem cells (MSCs). Two remaining columns on the right indicate fold change at the protein level in developing hearts measured by MS.

A.1 Source code for mechanobiological ‘use it or lose it’ model of tension-inhibited turnover

```
function [ fPrime ] = MBGC_odes3( t, f, K )

fPrime = zeros(6,1);

alpha_1 = K(1);
alpha_2 = K(2);
alpha_3 = K(3);
alpha_4 = K(4);

beta_1 = K(5);
beta_2 = K(6);
beta_3 = K(7);

gamma_1 = K(8);
gamma_2 = K(9);
gamma_3 = K(10);

delta_1 = K(11);
delta_2 = K(12);
delta_3 = K(13);

n_l = K(14);
n_m = K(15);
n_c = K(16);
n_f = K(17);

x = K(18);
y = K(19);
z = K(20);
k_f = K(21);
F0 = K(22);

%constants and initial conditions

L = f(1);
l = f(2);
M = f(3);
m = f(4);
C = f(5);
c = f(6);

fPrime(1) = alpha_1*l - beta_1*L;
fPrime(2) = gamma_1*L - delta_1*(l.^n_l)/((F0*m).^x + l.^n_l);
fPrime(3) = alpha_2*m + alpha_3*l - beta_2*M;
fPrime(4) = gamma_2*M - delta_2*(m.^n_m)/(c.^y + m.^n_m);
fPrime(5) = alpha_4*(c^(n_f-1))/(k_f.^n_f + c.^n_f) - beta_3*C;
fPrime(6) = gamma_3*C - delta_3*(c.^n_c)/((F0*m).^z + c.^n_c);
%put in the equations. fPrime(1) will be dw/dx in this case.

end
```

```
%% Set up IC's & parameters (constants):
fI = [0.00005; 0.00005; 0.004; 0.004; 0.004; 0.004];

K = [3.2;3.6;0;7;   3.3;3;3.1;    1;1.5;3;   7.5;6.5;5.4;
1.44;1.6;1.14;1.5;  0.27;0.45;0.55;0.89;1];

total_time = 21; % full time frame or window

figure;
for i=1:10;
    for j=1:10;
        K(18) = 0.1 + 0.01*j;
        [t,f] = ode45(@(t,f) MBGC_odes3(t,f,K),[0:0.5:total_time],fI);
        l=f(:,2);
        c=f(:,6);

        plot(l,c);
        hold on;
    end
    fI(2) = 0.005 + 0.1*i;
    plot(L,l);
    hold on;
end
    xlabel('L');
    ylabel('l');
    title('l vs L');

[t,f] = ode45(@(t,f) MBGC_odes3(t,f,K),[0:0.05:total_time],fI);
results = [t,f];

L=f(:,1);
l=f(:,2);
M=f(:,3);
m=f(:,4);
C=f(:,5);
c=f(:,6);

figure;
subplot(3,2,1);
plot(t,L);
xlabel('Embryonic age (days)');
ylabel('L');
title('L vs t');

subplot(3,2,2);
plot(t,l);
xlabel('Embryonic age (days)');
ylabel('l');
title('l vs t');

subplot(3,2,3);
plot(t,M);
xlabel('Embryonic age (days)');
ylabel('M');
```

```
title('M vs t');

subplot(3,2,4);
plot(t,m);
xlabel('Embryonic age (days)');
ylabel('m');
title('m vs t');

subplot(3,2,5);
plot(t,C);
xlabel('Embryonic age (days)');
ylabel('C');
title('C vs t');

subplot(3,2,6);
plot(t,c);
xlabel('Embryonic age (days)');
ylabel('c');
title('c vs t');

e4 = find(t==4);
e6 = find(t==6);
e10 = find(t==10);
e18 = find(t==18);

figure;
plot(c,l);
hold on;
plot(c(e4),l(e4),'MarkerSize',10, 'MarkerEdgeColor','red');
plot(c(e6),l(e6),'MarkerSize',10, 'MarkerEdgeColor','red');
plot(c(e10),l(e10),'MarkerSize',10, 'MarkerEdgeColor','red');
plot(c(e18),l(e18),'MarkerSize',10, 'MarkerEdgeColor','red');
xlabel('c');
ylabel('l');
title('l vs c');
hold off;


expmt_points =
[results(e4,:);results(e6,:);results(e10,:);,results(e18,:)];

filename = 'MBGC_ode_data.xlsx';
xlswrite(filename,results,1,'A2');
xlswrite(filename,expmt_points,1,'L2');
```

APPENDIX B

Supplementary information for Chapter 3

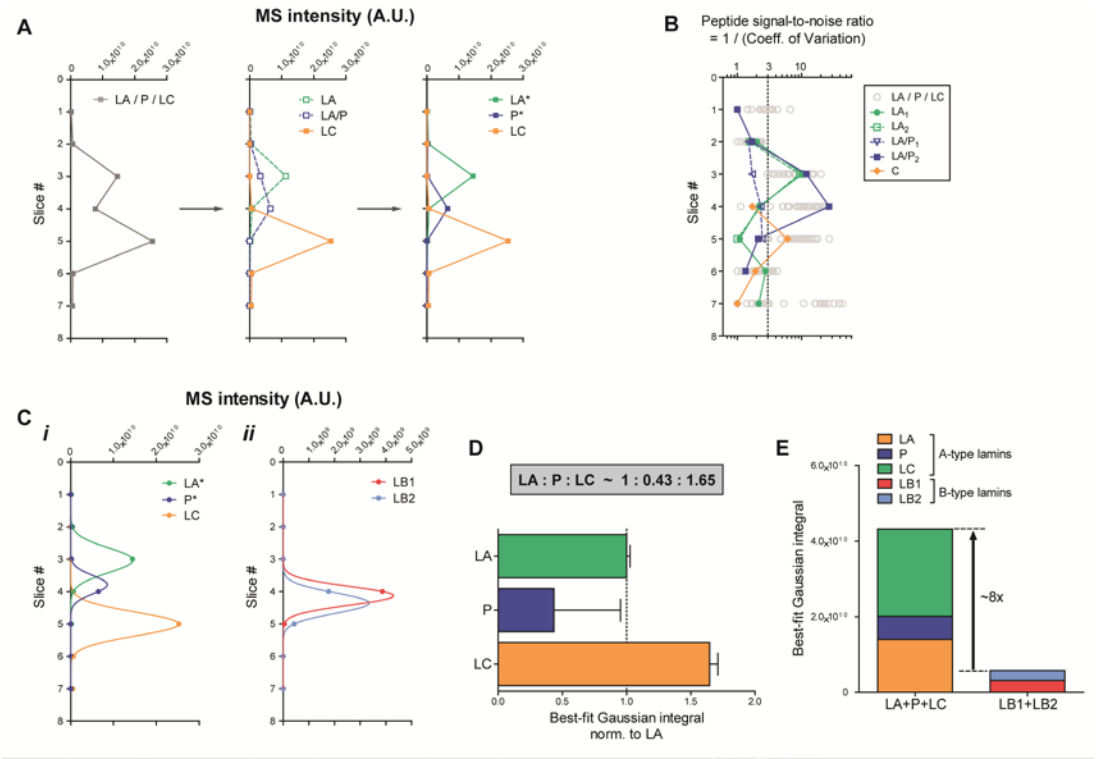

Figure B.1. A-type lamin stoichiometries measured by isoform-specific peptide intensity profiles

(**A**) Profile plot of normalized intensities of A-type lamins obtained from MaxQuant's LFQ algorithm. 'LA / P / LC' (grey) corresponds to LFQ intensity of "Prelamin-A/C" (UniProt ID: P02545), which quantifies total A-type lamin abundance without distinguishing between isoforms (leftmost plot). Line profiles specific for each isoform were constructed based on raw intensities of isoform-specific peptides (Figure 3.1B). Pair-wise intensity ratios of the isoform-specific peptides across gel slices #1~7 were used to generate adjusted profiles ('LA*' and 'P*') that account for contributions from each isoform at each gel slice range (see *Materials and Methods* for details). (**B**) MS singal-to-noise ratios of isoform-specific peptides calculated as inverse of standard Coefficient of Variance (= 1/COV = mean MS intensity / stdev). Empty grey circles = peptides shared by all three isoforms, LA, P, and LC; Isoform-specific peptide sequences: 'LA_1' = SVGGSGGGSFGDNLVTR; 'LA_2' = ASASGSGAQVGGPISSGSSASSVTVTR; 'LA/P_1' = SVTVVEDDEDEDGDDLLHHHHGSHCSSSGD; 'LA/P_2' = TVLCGTCGQPADK; 'C' = SVTVVEDDEDEDGDDLLHHHHVSGSR. (**C**) Best-fit Gaussian line plots of FEA-MS signal for (***i***) A-type lamin isoforms and (***ii***) B-type isoforms. (**D**) A-type lamin stoichiometry (LA : P : LC ~ 1 : 0.43 : 1.65) quantified by integrating the best-fit Gaussian distribution function for each isoform is consistent with that determined by summing MS intensities over all slices. (**E**) Total A : B-type lamin ratio ~ 8 quantified by integrating the best-fit Gaussian distribution function for each isoform.

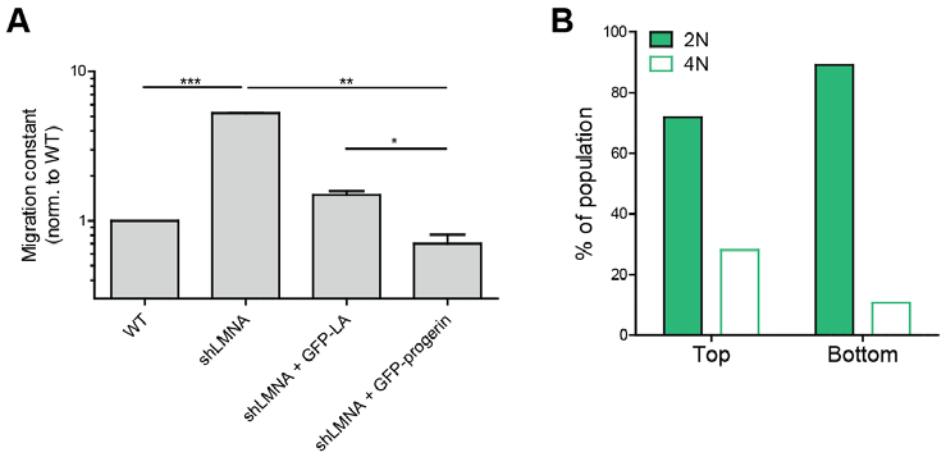

Figure B.2. Constricted migration through narrow pores decreases phosphorylation of A-type lamins.

(**A**) Migration constant (# of cells migrated to the bottom / total # of cells) quantified for WT, shLMNA, shLMNA + GFP-progerin, and shLMNA + GFP-LMNA A549 cells. *LMNA* knockdown (by shRNA) facilitates migration through narrow constrictions, but effects are rescued back to baseline levels upon transfection with GFP-LMNA. Transwell migration is further inhibited by expression of GFP-progerin. *$p < 0.05$, ** $p < 0.01$, *** $p < 0.001$. (**B**) Fraction (%) of 4N and 2N cells before (top) and after (bottom) pore migration.

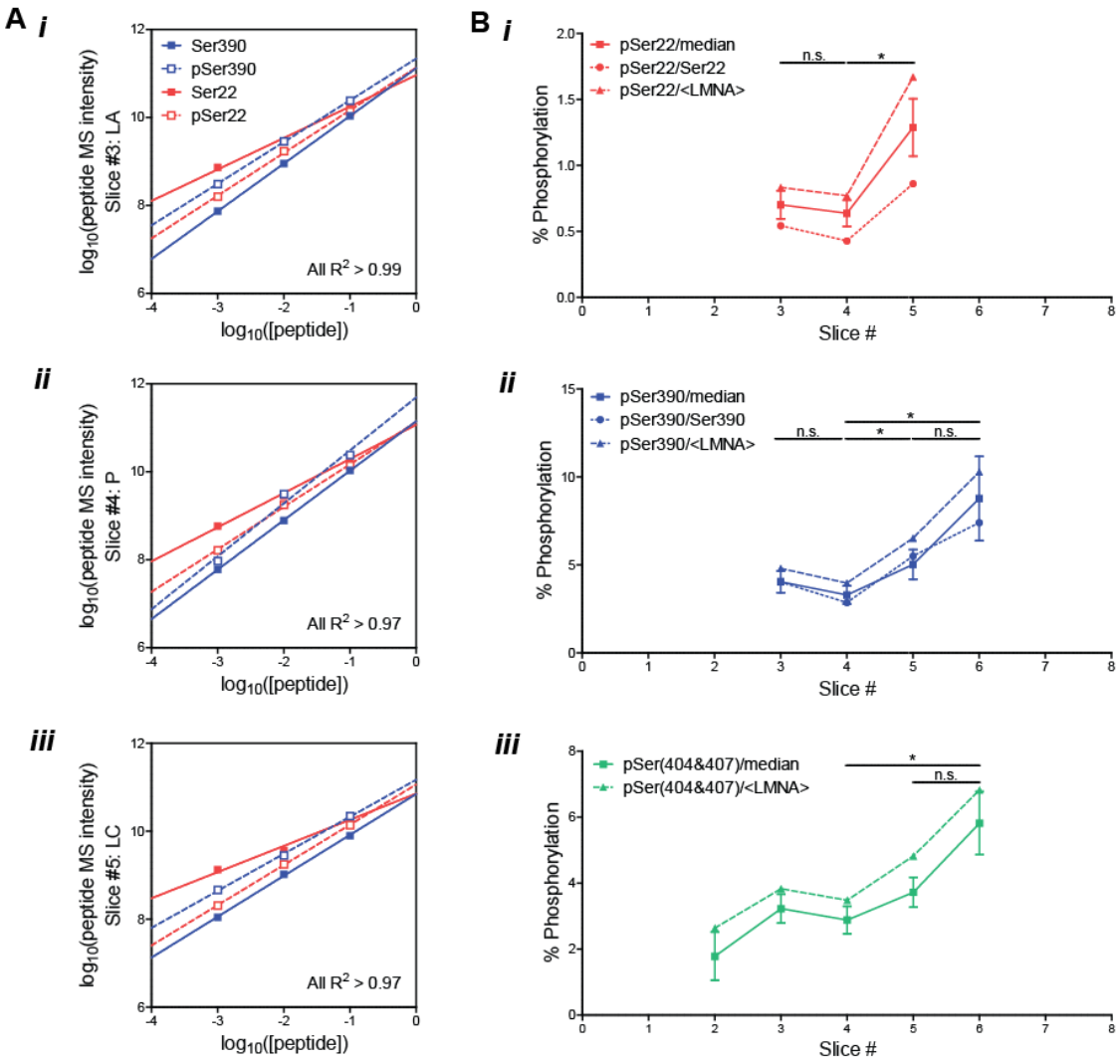

Figure B.3. Quantitation of phosphorylation stoichiometries at multiple serine residues.

(**A**) MS intensity of synthetic phospho-peptides 'pSer22' and 'pSer390' (as well as their non-phosphorylated counterparts: 'Ser22 ' and Ser390') exhibit robust linearity vs spike-in concentration (μM) over several orders of magnitude (all $R^2 > 0.97$) in slices #3, 4, and 5 corresponding to LA, P, and C peaks, respectively. (**B**) Three different normalization methods for quantifying '% phosphorylation' at (***i***) Ser22, (***ii***) Ser390, and (***iii***) Ser404&407: the ratio of phosphorylated peptide intensity divided by the median of all lamin-A/C peptides (e.g. 'pSer22/median'), the intensity of its non-phosphorylated counterpart (e.g. 'pSer22/Ser22'), and the mean intensity of all lamin-A/C peptides (e.g. 'pSer22/<LMNA>').

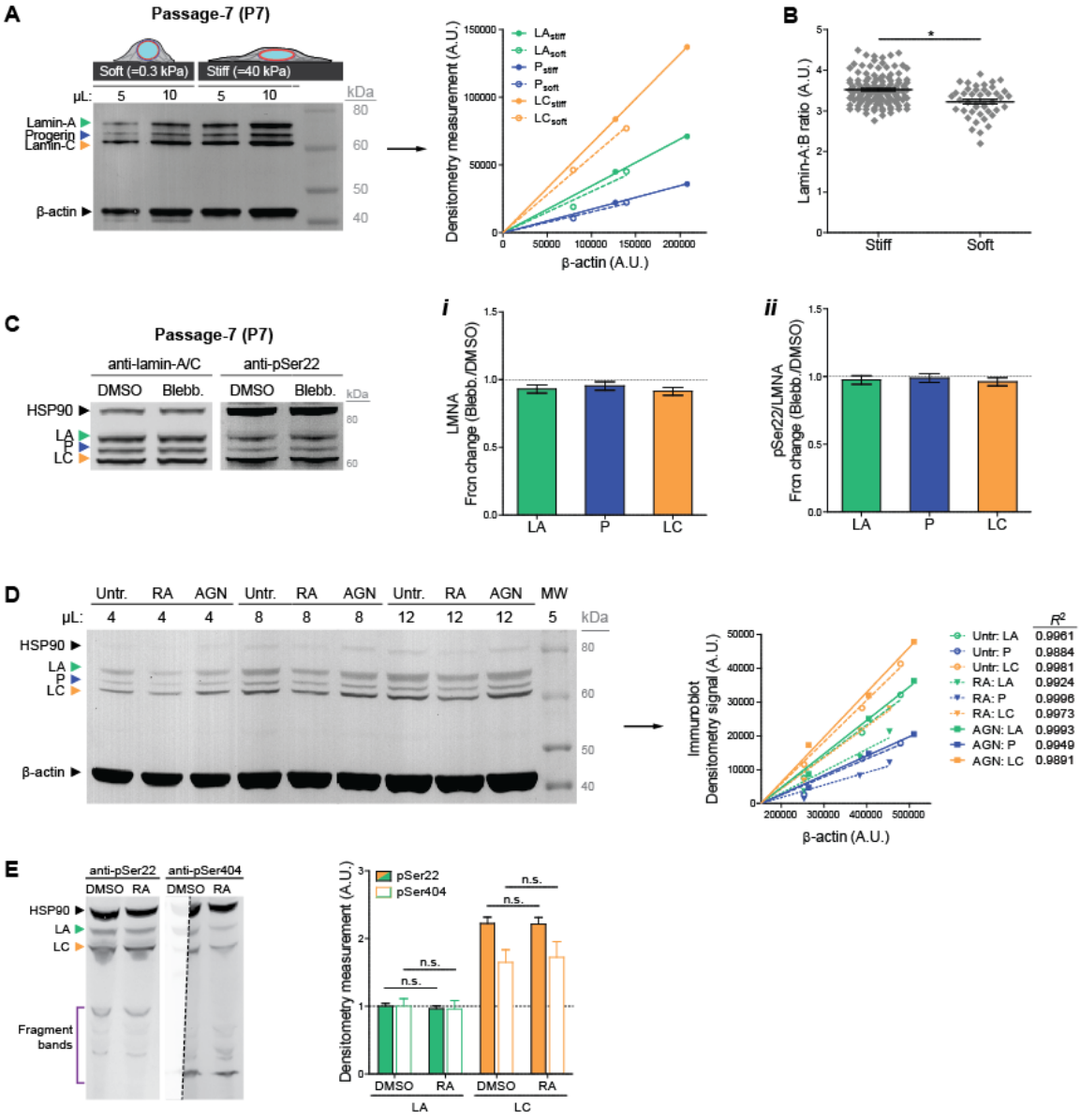

Figure B.4. Quantitative densitometry and immunofluorescence of lamin responses to matrix stiffness and retinoid compounds.

(**A**) Quantitative densitometry analysis of lamin abundance in cells cultured on soft and stiff gels, using two different sample loading volumes. Plotting densitometry signal of lamins vs housekeeping protein β-actin yields slopes that can be used to compute fold-change in levels. (**B**) Immunofluorescence quantitation of lamin-A:B ratio in early passage (P2) HGPS iPS-MSCs. (**C**) Immunoblot of DMSO vs blebbistatin treated P7 iPS-MSCs. Unlike with early passage (P2) cells, blebbistatin treatment does not result in significant changes in (***i***) LA/P/LC levels or (***ii***) normalized phosphorylation (as 'pSer22/LMNA'). (**D**) Quantitative densitometry analysis of lamin abundance in cells treated with RA or AGN, using three different sample loading volumes. Comparison of slopes (lamin densitometry signal vs housekeeping, β-actin) reveals that retinoid compounds

regulate transcription of all isoforms equally. (**E**) Immunoblot of DMSO vs RA treated human A549 cells, probed with two phosphor-serine antibodies: anti-pSer22 (left) and anti-pSer404 (right). The 'DMSO' lane in the pSer404 blot was cut in half (dashed line) for a separate immunoblot experiment/analysis, and was therefore whited-out to indicate this. Consistent with FEA-MS measurements of phosphorylation in iPS-MSCs, LC phosphorylation in A549s is ~2-fold higher than that of LA for both phsopho-sites. Low MW degradation bands are also evident in both immunoblots. Transcriptional regulation by RA does not affect phosphorylation and degradation of LA/C.

		# samples detecting phospho-peptide			# samples detecting non-phospho ctl			Detectability (%)		
LMNA	**Peptide sequence**	**LA**	**P**	**LC**	**LA**	**P**	**LC**	**LA**	**P**	**LC**
pSer18	SGAQASSTPLSPTR	0	1	1	4	4	4	0	25	25
pSer19	SGAQASSTPLSPTR	2	1	1	4	4	4	50	25	25
pSer22	SGAQASSTPLSPTR	1	1	1	4	4	4	25	25	25
pSer390	LRLSPSPTSQR	1	1	2	4	4	4	25	25	50
pSer404,407	ASSHSSQTQGGGSVTK	4	4	4	0	0	0	100	100	100
LMNB1	**Peptide sequence**	**LB1**			**LB1**			**LB1**		
pSer23	AGGPTTPLSPTR	0			4			0		
pSer391	LSPSPSSR	0			4			0		
pSer393	LSPSPSSR	0			4			0		
LMNB2	**Peptide sequence**	**LB2**			**LB2**			**LB2**		
pSer37	AGGPATPLSPTR	0			4			0		
pSer405	LSPSPSSR	0			4			0		
pSer407	LSPSPSSR	0			4			0		

Table 3. MS detects multiple phosphorylated lamin-A/C peptides but none for lamin-B1/B2 at analogous sites

APPENDIX C

Standard laboratory protocols and reagents used

C.1 Immunoblotting

Cell pellets were rinsed with PBS and suspended in ice-cold 1x NuPAGE LDS buffer (Invitrogen; diluted 1:4 in 1x RIPA buffer, plus 1% protease inhibitor cocktail (Sigma), 1% β-mercaptoethanol (Sigma)), and lysed by sonication on ice (10 x 3s pulses using a probe sonicator, at intermediate power setting). Lysed samples were then heated to ~80 °C for 10 min and centrifuged at maximum RPM for 30 min at 4°C. SDS-PAGE gels (NuPAGE 4-12% Bis-Tris; Invitrogen) were loaded with 5 – 15 µL of lysate per lane. Each sample was loaded in duplicates or triplicates (with varying loading volumes) for quantitative analysis. Lysates were diluted with additional 1x NuPAGE LDS buffer if necessary. Gel electrophoresis was run for 10 min at 100 V and 1 hr at 160 V. Electrophoresis-separated samples were then transferred to a polyvinylidene fluoride membrane using an iBlot Gel Transfer Device (Invitrogen). The membrane was blocked with 5% non-fat dry milk in TTBS buffer (Tris-buffered saline, BioRad; with 0.1% Tween-20), washed x3 in TTBS, then incubated with primary antibodies against: LMNA (CST, #4777), HSP90 (Abcam, #ab13495), β-actin (Santa Cruz, #sc-47778), and/or LMNA pSer22 (CST, #2026), LMNA pSer404 (EMD Millipore, ABT1387) diluted in TBS to final concentrations of ~1 µg/ml and incubated at 4 °C overnight. After washing x3 with TTBS, the membrane was incubated with 1:2000 diluted secondary Ab: anti-mouse/rabbit HRP-conjugated IgG (GE Healthcare), at RT for 1.5 hrs. The membrane was washed x3 again with TTBS and developed using ChromoSensor (GenScript) for ~3 min at RT. Immunoblot images were obtained using a HP Scanjet 4850. Quantitative densitometry analysis was performed using ImageJ (NIH).

C.2 Immunofluorescence imaging

Cells were first rinsed with pre-warmed PBS, fixed with 4% paraformaldehyde (PFA, Fisher) for 15 min, washed x3 with PBS, and permeabilized with 0.5% Triton-X (Fisher) in PBS for 10 min. Fixed and permeabilized cells were then blocked with 5% BSA in PBS for a minimum of 1.5 hrs. Samples were then incubated overnight with primary antibody solution in 0.5% BSA solution with gentle shaking at 4 °C. The primary antibodies used were: LMNA (1:500, CST, #4777), LMNB (1:500, Santa Cruz, #sc-6217), and γH2AX (EMD Millipore, #05-636). Samples were then

washed x3 in 0.1% BSA in PBS and incubated with the corresponding secondary antibodies at 1:500 dilution for 1.5 hrs at RT (Alexa Fluor 488, 546 and 647 nm; Invitrogen). Immunostained cells on gels or glass coverslips were mounted with mounting media (Invitrogen ProLong Gold Antifade Reagent). Epifluorescence imaging was performed using an Olympus IX71 with a digital EMCCD camera (Cascade 512B, Photometrics) and a 40×/0.6 NA objective. Confocal imaging was done in Leica TCS SP8 system with either a 63×/1.4 NA oil-immersion or 40×/1.2 NA water-immersion objective. Image analysis was done with ImageJ.

C.3 Synthesis of soft and stiff polyacrylamide (PA) gels for cell culture

Circular glass coverslips (Fisher Scientific; 18 mm) were first cleaned in boiling ethanol then subsequently in RCA solution (H_2O : H_2O_2 : NH_4OH = 2:1:1 by vol.) for 10 min each. The cleaned coverslips were then functionalized in ATCS solution (chloroform with 0.1% allytrichlorosilane (Sigma) plus 0.1% trimethylamine (Sigma)) for 1 hr. Fresh gel precursor solution for soft-stiff PA gels were prepared as previously described **(Swift et al., 2013)**. 1% ammonium persulphate (APS, Sigma) and 0.1% N,N,N',N'-tetramethylethylenediamine (TEMED, Sigma) and were added to the precursor solutions to initiate gel polymerization, and 20 µl of the resulting mixture were added to each cleaned coverslip. The solutions were then covered with larger coverslips (Fisher Scientific; 25 mm) and incubated to allow for polymerization at RT for ~45 min. Polymerized gels were rinsed x3 with PBS and the large coverslips were gently removed. To coat the gel with collagen-I, Sulfo-SANPAH cross-linker (50 µg/ml in 50 mM HEPES, G-Biosciences) was applied over the whole gel surface and photoactivated under 365nm UV light for 10 min. Excess Sulfo-SANPAH was washed away with PBS and collagen-I solution (0.2 mg/ml in 50mM HEPES) was then added and incubated overnight at RT with gentle shaking.

BIBLIOGRAPHY

Aebi, U., J. Cohn, L. Buhle, and L. Gerace. 1986. The nuclear lamina is a meshwork of intermediate-type filaments. *Nature*. 323:560-564.

Akopyan, K., H. Silva Cascales, E. Hukasova, A.T. Saurin, E. Mullers, H. Jaiswal, D.A. Hollman, G.J. Kops, R.H. Medema, and A. Lindqvist. 2014. Assessing kinetics from fixed cells reveals activation of the mitotic entry network at the S/G2 transition. *Molecular cell*. 53:843-853.

Alam, S.G., D. Lovett, D.I. Kim, K.J. Roux, R.B. Dickinson, and T.P. Lele. 2015. The nucleus is an intracellular propagator of tensile forces in NIH 3T3 fibroblasts. *Journal of cell science*. 128:1901-1911.

Baghirova, S., B.G. Hughes, M. Poirier, M.Y. Kondo, and R. Schulz. 2016. Nuclear matrix metalloproteinase-2 in the cardiomyocyte and the ischemic-reperfused heart. *Journal of molecular and cellular cardiology*. 94:153-161.

Barrett, A.J. 2004. Bioinformatics of proteases in the MEROPS database. *Current opinion in drug discovery & development*. 7:334-341.

Barrett, T., S.E. Wilhite, P. Ledoux, C. Evangelista, I.F. Kim, M. Tomashevsky, K.A. Marshall, K.H. Phillippy, P.M. Sherman, M. Holko, A. Yefanov, H. Lee, N. Zhang, C.L. Robertson, N. Serova, S. Davis, and A. Soboleva. 2013. NCBI GEO: archive for functional genomics data sets--update. *Nucleic acids research*. 41:D991-995.

Bengtsson, L., and H. Otto. 2008. LUMA interacts with emerin and influences its distribution at the inner nuclear membrane. *Journal of cell science*. 121:536-548.

Benson, E.K., S.W. Lee, and S.A. Aaronson. 2010. Role of progerin-induced telomere dysfunction in HGPS premature cellular senescence. *Journal of cell science*. 123:2605-2612.

Bergo, M.O., H.D. Lieu, B.J. Gavino, P. Ambroziak, J.C. Otto, P.J. Casey, Q.M. Walker, and S.G. Young. 2004. On the physiological importance of endoproteolysis of CAAX proteins: heart-specific RCE1 knockout mice develop a lethal cardiomyopathy. *The Journal of biological chemistry*. 279:4729-4736.

Bertacchini, J., F. Beretti, V. Cenni, M. Guida, F. Gibellini, L. Mediani, O. Marin, N.M. Maraldi, A. de Pol, G. Lattanzi, L. Cocco, and S. Marmiroli. 2013. The protein kinase Akt/PKB regulates both prelamin A degradation and Lmna gene expression. *FASEB journal : official publication of the Federation of American Societies for Experimental Biology*. 27:2145-2155.

Bione, S., E. Maestrini, S. Rivella, M. Mancini, S. Regis, G. Romeo, and D. Toniolo. 1994. Identification of a novel X-linked gene responsible for Emery-Dreifuss muscular dystrophy. *Nature genetics*. 8:323-327.

Bollen, I.A.E., M. Schuldt, M. Harakalova, A. Vink, F.W. Asselbergs, J.R. Pinto, M. Kruger, D.W.D. Kuster, and J. van der Velden. 2017. Genotype-specific pathogenic effects in human dilated cardiomyopathy. *The Journal of physiology*. 595:4677-4693.

Bone, C.R., and D.A. Starr. 2016. Nuclear migration events throughout development. *Journal of cell science*. 129:1951-1961.

Bonne, G., M.R. Di Barletta, S. Varnous, H.M. Becane, E.H. Hammouda, L. Merlini, F. Muntoni, C.R. Greenberg, F. Gary, J.A. Urtizberea, D. Duboc, M. Fardeau, D. Toniolo, and K. Schwartz. 1999. Mutations in the gene encoding lamin A/C cause autosomal dominant Emery-Dreifuss muscular dystrophy. *Nature genetics*. 21:285-288.

Booth-Gauthier, E.A., V. Du, M. Ghibaudo, A.D. Rape, K.N. Dahl, and B. Ladoux. 2013. Hutchinson-Gilford progeria syndrome alters nuclear shape and reduces cell motility in three dimensional model substrates. *Integrative biology : quantitative biosciences from nano to macro*. 5:569-577.

Booth, E.A., S.T. Spagnol, T.A. Alcoser, and K.N. Dahl. 2015. Nuclear stiffening and chromatin softening with progerin expression leads to an attenuated nuclear response to force. *Soft matter*. 11:6412-6418.

Boudou, T., W.R. Legant, A. Mu, M.A. Borochin, N. Thavandiran, M. Radisic, P.W. Zandstra, J.A. Epstein, K.B. Margulies, and C.S. Chen. 2012. A microfabricated platform to measure and manipulate the mechanics of engineered cardiac microtissues. *Tissue engineering. Part A*. 18:910-919.

Broers, J.L., H.J. Kuijpers, C. Ostlund, H.J. Worman, J. Endert, and F.C. Ramaekers. 2005. Both lamin A and lamin C mutations cause lamina instability as well as loss of internal nuclear lamin organization. *Experimental cell research*. 304:582-592.

Broers, J.L., Y. Raymond, M.K. Rot, H. Kuijpers, S.S. Wagenaar, and F.C. Ramaekers. 1993. Nuclear A-type lamins are differentially expressed in human lung cancer subtypes. *The American journal of pathology*. 143:211-220.

Brower, G.L., J.D. Gardner, M.F. Forman, D.B. Murray, T. Voloshenyuk, S.P. Levick, and J.S. Janicki. 2006. The relationship between myocardial extracellular matrix remodeling and ventricular function. *European journal of cardio-thoracic surgery : official journal of the European Association for Cardio-thoracic Surgery*. 30:604-610.

Burke, B., and C.L. Stewart. 2013. The nuclear lamins: flexibility in function. *Nature reviews. Molecular cell biology*. 14:13-24.

Burma, S., B.P. Chen, M. Murphy, A. Kurimasa, and D.J. Chen. 2001. ATM phosphorylates histone H2AX in response to DNA double-strand breaks. *The Journal of biological chemistry*. 276:42462-42467.

Burridge, P.W., G. Keller, J.D. Gold, and J.C. Wu. 2012. Production of de novo cardiomyocytes: human pluripotent stem cell differentiation and direct reprogramming. *Cell stem cell*. 10:16-28.

Burtner, C.R., and B.K. Kennedy. 2010. Progeria syndromes and ageing: what is the connection? *Nature reviews. Molecular cell biology*. 11:567-578.

Butcher, J.T., T.C. McQuinn, D. Sedmera, D. Turner, and R.R. Markwald. 2007. Transitions in early embryonic atrioventricular valvular function correspond with changes in cushion biomechanics that are predictable by tissue composition. *Circulation research*. 100:1503-1511.

Butin-Israeli, V., S.A. Adam, A.E. Goldman, and R.D. Goldman. 2012. Nuclear lamin functions and disease. *Trends in genetics : TIG*. 28:464-471.

Buxboim, A., J. Irianto, J. Swift, A. Athirasala, J.W. Shin, F. Rehfeldt, and D.E. Discher. 2017. Coordinated increase of nuclear tension and lamin-A with matrix stiffness outcompetes lamin-B receptor that favors soft tissue phenotypes. *Molecular biology of the cell*. 28:3333-3348.

Buxboim, A., J. Swift, J. Irianto, K.R. Spinler, P.C. Dingal, A. Athirasala, Y.R. Kao, S. Cho, T. Harada, J.W. Shin, and D.E. Discher. 2014. Matrix elasticity regulates lamin-A,C phosphorylation and turnover with feedback to actomyosin. *Current biology : CB*. 24:1909-1917.

Cao, K., C.D. Blair, D.A. Faddah, J.E. Kieckhaefer, M. Olive, M.R. Erdos, E.G. Nabel, and F.S. Collins. 2011. Progerin and telomere dysfunction collaborate to trigger cellular senescence in normal human fibroblasts. *The Journal of clinical investigation*. 121:2833-2844.

Cao, K., B.C. Capell, M.R. Erdos, K. Djabali, and F.S. Collins. 2007. A lamin A protein isoform overexpressed in Hutchinson-Gilford progeria syndrome interferes with mitosis in progeria and normal cells. *Proceedings of the National Academy of Sciences of the United States of America*. 104:4949-4954.

Capell, B.C., M.R. Erdos, J.P. Madigan, J.J. Fiordalisi, R. Varga, K.N. Conneely, L.B. Gordon, C.J. Der, A.D. Cox, and F.S. Collins. 2005. Inhibiting farnesylation of progerin prevents the characteristic nuclear blebbing of Hutchinson-Gilford progeria syndrome. *Proceedings of the National Academy of Sciences of the United States of America*. 102:12879-12884.

Captur, G., E. Arbustini, G. Bonne, P. Syrris, K. Mills, K. Wahbi, S.A. Mohiddin, W.J. McKenna, S. Pettit, C.Y. Ho, A. Muchir, P. Gissen, P.M. Elliott, and J.C. Moon. 2018. Lamin and the heart. *Heart*. 104:468-479.

Cenni, V., C. Capanni, M. Columbaro, M. Ortolani, M.R. D'Apice, G. Novelli, M. Fini, S. Marmiroli, E. Scarano, N.M. Maraldi, S. Squarzoni, S. Prencipe, and G. Lattanzi. 2011. Autophagic degradation of farnesylated prelamin A as a therapeutic approach to lamin-linked progeria. *European journal of histochemistry : EJH*. 55:e36.

Chancellor, T.J., J. Lee, C.K. Thodeti, and T. Lele. 2010. Actomyosin tension exerted on the nucleus through nesprin-1 connections influences endothelial cell adhesion, migration, and cyclic strain-induced reorientation. *Biophysical journal*. 99:115-123.

Chang, L., and R.D. Goldman. 2004. Intermediate filaments mediate cytoskeletal crosstalk. *Nature reviews. Molecular cell biology*. 5:601-613.

Chin, L., Y. Xia, D.E. Discher, and P.A. Janmey. 2016. Mechanotransduction in cancer. *Current opinion in chemical engineering*. 11:77-84.

Cho, N.W., R.L. Dilley, M.A. Lampson, and R.A. Greenberg. 2014. Interchromosomal homology searches drive directional ALT telomere movement and synapsis. *Cell*. 159:108-121.

Cho, S., A. Abbas, J. Irianto, I.L. Ivanovska, Y. Xia, M. Tewari, and D.E. Discher. 2018. Progerin phosphorylation in interphase is lower and less mechanosensitive than lamin-A,C in iPS-derived mesenchymal stem cells. *Nucleus*. 9:230-245.

Cho, S., J. Irianto, and D.E. Discher. 2017. Mechanosensing by the nucleus: From pathways to scaling relationships. *The Journal of cell biology*.

Chopra, A., M.E. Murray, F.J. Byfield, M.G. Mendez, R. Halleluyan, D.J. Restle, D. Raz-Ben Aroush, P.A. Galie, K. Pogoda, R. Bucki, C. Marcinkiewicz, G.D. Prestwich, T.I. Zarembinski, C.S. Chen, E. Pure, J.Y. Kresh, and P.A. Janmey. 2014. Augmentation of integrin-mediated mechanotransduction by hyaluronic acid. *Biomaterials*. 35:71-82.

Choquet, D., D.P. Felsenfeld, and M.P. Sheetz. 1997. Extracellular matrix rigidity causes strengthening of integrin-cytoskeleton linkages. *Cell*. 88:39-48.

Chow, K.H., R.E. Factor, and K.S. Ullman. 2012. The nuclear envelope environment and its cancer connections. *Nature reviews. Cancer*. 12:196-209.

Constantinescu, D., H.L. Gray, P.J. Sammak, G.P. Schatten, and A.B. Csoka. 2006. Lamin A/C expression is a marker of mouse and human embryonic stem cell differentiation. *Stem cells*. 24:177-185.

Cremer, T., and C. Cremer. 2001. Chromosome territories, nuclear architecture and gene regulation in mammalian cells. *Nature reviews. Genetics*. 2:292-301.

Crisp, M., Q. Liu, K. Roux, J.B. Rattner, C. Shanahan, B. Burke, P.D. Stahl, and D. Hodzic. 2006. Coupling of the nucleus and cytoplasm: role of the LINC complex. *The Journal of cell biology*. 172:41-53.

Csoka, A.B., S.B. English, C.P. Simkevich, D.G. Ginzinger, A.J. Butte, G.P. Schatten, F.G. Rothman, and J.M. Sedivy. 2004. Genome-scale expression profiling of Hutchinson-Gilford progeria syndrome reveals widespread transcriptional misregulation leading to mesodermal/mesenchymal defects and accelerated atherosclerosis. *Aging cell*. 3:235-243.

Dahl, K.N., A.J. Ribeiro, and J. Lammerding. 2008. Nuclear shape, mechanics, and mechanotransduction. *Circulation research*. 102:1307-1318.

Dahl, K.N., P. Scaffidi, M.F. Islam, A.G. Yodh, K.L. Wilson, and T. Misteli. 2006. Distinct structural and mechanical properties of the nuclear lamina in Hutchinson-Gilford progeria syndrome. *Proceedings of the National Academy of Sciences of the United States of America*. 103:10271-10276.

Dasbiswas, K., S. Majkut, D.E. Discher, and S.A. Safran. 2015. Substrate stiffness-modulated registry phase correlations in cardiomyocytes map structural order to coherent beating. *Nature communications*. 6:6085.

Davies, B.S., L.G. Fong, S.H. Yang, C. Coffinier, and S.G. Young. 2009. The posttranslational processing of prelamin A and disease. *Annual review of genomics and human genetics*. 10:153-174.

Davis, J., L.C. Davis, R.N. Correll, C.A. Makarewich, J.A. Schwanekamp, F. Moussavi-Harami, D. Wang, A.J. York, H. Wu, S.R. Houser, C.E. Seidman, J.G. Seidman, M. Regnier, J.M. Metzger, J.C. Wu, and J.D. Molkentin. 2016. A Tension-Based Model Distinguishes Hypertrophic versus Dilated Cardiomyopathy. *Cell*. 165:1147-1159.

de La Rosa, J., J.M. Freije, R. Cabanillas, F.G. Osorio, M.F. Fraga, M.S. Fernández-García, R. Rad, V. Fanjul, A.P. Ugalde, and Q. Liang. 2013a. Prelamin A causes progeria through cell-extrinsic mechanisms and prevents cancer invasion. *Nature communications*. 4:2268.

de la Rosa, J., J.M. Freije, R. Cabanillas, F.G. Osorio, M.F. Fraga, M.S. Fernandez-Garcia, R. Rad, V. Fanjul, A.P. Ugalde, Q. Liang, H.M. Prosser, A. Bradley, J. Cadinanos, and C. Lopez-Otin. 2013b. Prelamin A causes progeria through cell-extrinsic mechanisms and prevents cancer invasion. *Nature communications*. 4:2268.

De Vos, W.H., F. Houben, M. Kamps, A. Malhas, F. Verheyen, J. Cox, E.M. Manders, V.L. Verstraeten, M.A. van Steensel, C.L. Marcelis, A. van den Wijngaard, D.J. Vaux, F.C. Ramaekers, and J.L. Broers. 2011. Repetitive disruptions of the nuclear envelope invoke temporary loss of cellular compartmentalization in laminopathies. *Human molecular genetics*. 20:4175-4186.

Dechat, T., B. Korbei, O.A. Vaughan, S. Vlcek, C.J. Hutchison, and R. Foisner. 2000. Lamina-associated polypeptide 2alpha binds intranuclear A-type lamins. *Journal of cell science*. 113 Pt 19:3473-3484.

del Rio, A., R. Perez-Jimenez, R. Liu, P. Roca-Cusachs, J.M. Fernandez, and M.P. Sheetz. 2009. Stretching single talin rod molecules activates vinculin binding. *Science*. 323:638-641.

Denais, C.M., R.M. Gilbert, P. Isermann, A.L. McGregor, M. te Lindert, B. Weigelin, P.M. Davidson, P. Friedl, K. Wolf, and J. Lammerding. 2016. Nuclear envelope rupture and repair during cancer cell migration. *Science*. 352:353-358.

Dey, P. 2010. Cancer nucleus: morphology and beyond. *Diagnostic cytopathology*. 38:382-390.

di Masi, A., M.R. D'Apice, R. Ricordy, C. Tanzarella, and G. Novelli. 2008. The R527H mutation in LMNA gene causes an increased sensitivity to ionizing radiation. *Cell cycle*. 7:2030-2037.

Dingal, P.C., A.M. Bradshaw, S. Cho, M. Raab, A. Buxboim, J. Swift, and D.E. Discher. 2015. Fractal heterogeneity in minimal matrix models of scars modulates stiff-niche stem-cell responses via nuclear exit of a mechanorepressor. *Nature materials*. 14:951-960.

Dingal, P.C., and D.E. Discher. 2014. Systems mechanobiology: tension-inhibited protein turnover is sufficient to physically control gene circuits. *Biophysical journal*. 107:2734-2743.

Discher, D.E., P. Janmey, and Y.L. Wang. 2005. Tissue cells feel and respond to the stiffness of their substrate. *Science*. 310:1139-1143.

Discher, D.E., D.J. Mooney, and P.W. Zandstra. 2009. Growth factors, matrices, and forces combine and control stem cells. *Science*. 324:1673-1677.

Dittmer, T.A., and T. Misteli. 2011. The lamin protein family. *Genome biology*. 12:222.

Dou, Z., C. Xu, G. Donahue, T. Shimi, J.A. Pan, J. Zhu, A. Ivanov, B.C. Capell, A.M. Drake, P.P. Shah, J.M. Catanzaro, M.D. Ricketts, T. Lamark, S.A. Adam, R. Marmorstein, W.X. Zong, T. Johansen, R.D. Goldman, P.D. Adams, and S.L. Berger. 2015. Autophagy mediates degradation of nuclear lamina. *Nature*. 527:105-109.

Dupont, S., L. Morsut, M. Aragona, E. Enzo, S. Giulitti, M. Cordenonsi, F. Zanconato, J. Le Digabel, M. Forcato, S. Bicciato, N. Elvassore, and S. Piccolo. 2011. Role of YAP/TAZ in mechanotransduction. *Nature*. 474:179-183.

Eckersley-Maslin, M.A., J.H. Bergmann, Z. Lazar, and D.L. Spector. 2013. Lamin A/C is expressed in pluripotent mouse embryonic stem cells. *Nucleus*. 4:53-60.

Elosegui-Artola, A., I. Andreu, A.E.M. Beedle, A. Lezamiz, M. Uroz, A.J. Kosmalska, R. Oria, J.Z. Kechagia, P. Rico-Lastres, A.L. Le Roux, C.M. Shanahan, X. Trepat, D. Navajas, S. Garcia-Manyes, and P. Roca-Cusachs. 2017. Force Triggers YAP Nuclear Entry by Regulating Transport across Nuclear Pores. *Cell*. 171:1397-1410 e1314.

Engler, A.J., C. Carag-Krieger, C.P. Johnson, M. Raab, H.Y. Tang, D.W. Speicher, J.W. Sanger, J.M. Sanger, and D.E. Discher. 2008. Embryonic cardiomyocytes beat best on a matrix with heart-like elasticity: scar-like rigidity inhibits beating. *Journal of cell science*. 121:3794-3802.

Engler, A.J., S. Sen, H.L. Sweeney, and D.E. Discher. 2006. Matrix elasticity directs stem cell lineage specification. *Cell*. 126:677-689.

Enyedi, B., M. Jelcic, and P. Niethammer. 2016. The Cell Nucleus Serves as a Mechanotransducer of Tissue Damage-Induced Inflammation. *Cell*. 165:1160-1170.

Eriksson, M., W.T. Brown, L.B. Gordon, M.W. Glynn, J. Singer, L. Scott, M.R. Erdos, C.M. Robbins, T.Y. Moses, P. Berglund, A. Dutra, E. Pak, S. Durkin, A.B. Csoka, M. Boehnke, T.W. Glover, and F.S. Collins. 2003. Recurrent de novo point mutations in lamin A cause Hutchinson-Gilford progeria syndrome. *Nature*. 423:293-298.

Fatkin, D., C. MacRae, T. Sasaki, M.R. Wolff, M. Porcu, M. Frenneaux, J. Atherton, H.J. Vidaillet, Jr., S. Spudich, U. De Girolami, J.G. Seidman, C. Seidman, F. Muntoni, G. Muehle, W. Johnson, and B. McDonough. 1999. Missense mutations in the rod domain of the lamin A/C gene as causes of dilated cardiomyopathy and conduction-system disease. *The New England journal of medicine*. 341:1715-1724.

Flynn, B.P., A.P. Bhole, N. Saeidi, M. Liles, C.A. Dimarzio, and J.W. Ruberti. 2010. Mechanical strain stabilizes reconstituted collagen fibrils against enzymatic degradation by mammalian collagenase matrix metalloproteinase 8 (MMP-8). *PloS one*. 5:e12337.

Friedrich, B.M., A. Buxboim, D.E. Discher, and S.A. Safran. 2011. Striated acto-myosin fibers can reorganize and register in response to elastic interactions with the matrix. *Biophysical journal*. 100:2706-2715.

Geiger, B., J.P. Spatz, and A.D. Bershadsky. 2009. Environmental sensing through focal adhesions. *Nature reviews. Molecular cell biology*. 10:21-33.

Gennes, P.G.d. 1979. Scaling concepts in polymer physics. Cornell University Press, Ithaca, N.Y. 324 p. pp.

Gerace, L., and G. Blobel. 1980. The nuclear envelope lamina is reversibly depolymerized during mitosis. *Cell*. 19:277-287.

Gjorevski, N., A.S. Piotrowski, V.D. Varner, and C.M. Nelson. 2015. Dynamic tensile forces drive collective cell migration through three-dimensional extracellular matrices. *Scientific reports*. 5:11458.

Goldman, R.D., Y. Gruenbaum, R.D. Moir, D.K. Shumaker, and T.P. Spann. 2002. Nuclear lamins: building blocks of nuclear architecture. *Genes & development*. 16:533-547.

Goldman, R.D., D.K. Shumaker, M.R. Erdos, M. Eriksson, A.E. Goldman, L.B. Gordon, Y. Gruenbaum, S. Khuon, M. Mendez, R. Varga, and F.S. Collins. 2004. Accumulation of mutant lamin A causes progressive changes in nuclear architecture in Hutchinson-Gilford progeria syndrome. *Proceedings of the National Academy of Sciences of the United States of America*. 101:8963-8968.

González-Cruz, R.D., J.S. Sadick, V.C. Fonseca, and E.M. Darling. 2018. Nuclear Lamin Protein C Is Linked to Lineage-Specific, Whole-Cell Mechanical Properties. *Cellular and molecular bioengineering*.

Gonzalez-Suarez, I., A.B. Redwood, and S. Gonzalo. 2009a. Loss of A-type lamins and genomic instability. *Cell cycle*. 8:3860-3865.

Gonzalez-Suarez, I., A.B. Redwood, S.M. Perkins, B. Vermolen, D. Lichtensztejin, D.A. Grotsky, L. Morgado-Palacin, E.J. Gapud, B.P. Sleckman, T. Sullivan, J. Sage, C.L. Stewart, S. Mai, and S. Gonzalo. 2009b. Novel roles for A-type lamins in telomere biology and the DNA damage response pathway. *The EMBO journal*. 28:2414-2427.

Gonzalo, S., R. Kreienkamp, and P. Askjaer. 2017. Hutchinson-Gilford Progeria Syndrome: A premature aging disease caused by LMNA gene mutations. *Ageing research reviews*. 33:18-29.

Goodwin, J.S., K.R. Drake, C.L. Remmert, and A.K. Kenworthy. 2005. Ras diffusion is sensitive to plasma membrane viscosity. *Biophysical journal*. 89:1398-1410.

Gordon, L.B., W.T. Brown, and F.S. Collins. 1993. Hutchinson-Gilford Progeria Syndrome. *In* GeneReviews((R)). M.P. Adam, H.H. Ardinger, R.A. Pagon, S.E. Wallace, L.J.H. Bean, K. Stephens, and A. Amemiya, editors, Seattle (WA).

Gordon, L.B., M.E. Kleinman, D.T. Miller, D.S. Neuberg, A. Giobbie-Hurder, M. Gerhard-Herman, L.B. Smoot, C.M. Gordon, R. Cleveland, B.D. Snyder, B. Fligor, W.R. Bishop, P. Statkevich, A. Regen, A. Sonis, S. Riley, C. Ploski, A. Correia, N. Quinn, N.J. Ullrich, A. Nazarian, M.G. Liang, S.Y. Huh, A. Schwartzman, and M.W. Kieran. 2012. Clinical trial of a farnesyltransferase inhibitor in children with Hutchinson-Gilford progeria syndrome. *Proceedings of the National Academy of Sciences of the United States of America*. 109:16666-16671.

Gotic, I., M. Leschnik, U. Kolm, M. Markovic, B.J. Haubner, K. Biadasiewicz, B. Metzler, C.L. Stewart, and R. Foisner. 2010. Lamina-associated polypeptide 2alpha loss impairs heart function and stress response in mice. *Circulation research*. 106:346-353.

Gruenbaum, Y., and R. Foisner. 2015. Lamins: nuclear intermediate filament proteins with fundamental functions in nuclear mechanics and genome regulation. *Annual review of biochemistry*. 84:131-164.

Gruenbaum, Y., A. Margalit, R.D. Goldman, D.K. Shumaker, and K.L. Wilson. 2005. The nuclear lamina comes of age. *Nature reviews. Molecular cell biology*. 6:21-31.

Grundy, G.J., S.L. Rulten, Z. Zeng, R. Arribas-Bosacoma, N. Iles, K. Manley, A. Oliver, and K.W. Caldecott. 2013. APLF promotes the assembly and activity of non-homologous end joining protein complexes. *The EMBO journal*. 32:112-125.

Guelen, L., L. Pagie, E. Brasset, W. Meuleman, M.B. Faza, W. Talhout, B.H. Eussen, A. de Klein, L. Wessels, W. de Laat, and B. van Steensel. 2008. Domain organization of human chromosomes revealed by mapping of nuclear lamina interactions. *Nature*. 453:948-951.

Guilluy, C., L.D. Osborne, L. Van Landeghem, L. Sharek, R. Superfine, R. Garcia-Mata, and K. Burridge. 2014. Isolated nuclei adapt to force and reveal a mechanotransduction pathway in the nucleus. *Nature cell biology*. 16:376-381.

Gutierrez-Fernandez, A., C. Soria-Valles, F.G. Osorio, J. Gutierrez-Abril, C. Garabaya, A. Aguirre, A. Fueyo, M.S. Fernandez-Garcia, X.S. Puente, and C. Lopez-Otin. 2015. Loss of MT1-MMP causes cell senescence and nuclear defects which can be reversed by retinoic acid. *The EMBO journal*. 34:1875-1888.

Halder, G., S. Dupont, and S. Piccolo. 2012. Transduction of mechanical and cytoskeletal cues by YAP and TAZ. *Nature reviews. Molecular cell biology*. 13:591-600.

Hales, B.F. 2005. DNA repair disorders causing malformations. *Current opinion in genetics & development*. 15:234-240.

Hampoelz, B., Y. Azou-Gros, R. Fabre, O. Markova, P.H. Puech, and T. Lecuit. 2011. Microtubule-induced nuclear envelope fluctuations control chromatin dynamics in Drosophila embryos. *Development*. 138:3377-3386.

Haque, F., D.J. Lloyd, D.T. Smallwood, C.L. Dent, C.M. Shanahan, A.M. Fry, R.C. Trembath, and S. Shackleton. 2006. SUN1 interacts with nuclear lamin A and cytoplasmic nesprins to provide a physical connection between the nuclear lamina and the cytoskeleton. *Molecular and cellular biology*. 26:3738-3751.

Haque, F., D. Mazzeo, J.T. Patel, D.T. Smallwood, J.A. Ellis, C.M. Shanahan, and S. Shackleton. 2010. Mammalian SUN protein interaction networks at the inner nuclear membrane and their role in laminopathy disease processes. *The Journal of biological chemistry*. 285:3487-3498.

Harada, T., J. Swift, J. Irianto, J.W. Shin, K.R. Spinler, A. Athirasala, R. Diegmiller, P.C. Dingal, I.L. Ivanovska, and D.E. Discher. 2014. Nuclear lamin stiffness is a barrier to 3D migration, but softness can limit survival. *The Journal of cell biology*. 204:669-682.

Harr, J.C., T.R. Luperchio, X. Wong, E. Cohen, S.J. Wheelan, and K.L. Reddy. 2015. Directed targeting of chromatin to the nuclear lamina is mediated by chromatin state and A-type lamins. *The Journal of cell biology*. 208:33-52.

Heald, R., and F. McKeon. 1990. Mutations of phosphorylation sites in lamin A that prevent nuclear lamina disassembly in mitosis. *Cell*. 61:579-589.

Henderson, J.T., G. Shannon, A.I. Veress, and C.P. Neu. 2013. Direct measurement of intranuclear strain distributions and RNA synthesis in single cells embedded within native tissue. *Biophysical journal*. 105:2252-2261.

Hennekam, R.C. 2006. Hutchinson-Gilford progeria syndrome: review of the phenotype. *American journal of medical genetics. Part A*. 140:2603-2624.

Hernandez, L., K.J. Roux, E.S. Wong, L.C. Mounkes, R. Mutalif, R. Navasankari, B. Rai, S. Cool, J.W. Jeong, H. Wang, H.S. Lee, S. Kozlov, M. Grunert, T. Keeble, C.M. Jones, M.D. Meta, S.G. Young, I.O. Daar, B. Burke, A.O. Perantoni, and C.L. Stewart. 2010. Functional coupling between the extracellular matrix and nuclear lamina by Wnt signaling in progeria. *Developmental cell*. 19:413-425.

Higo, T., A.T. Naito, T. Sumida, M. Shibamoto, K. Okada, S. Nomura, A. Nakagawa, T. Yamaguchi, T. Sakai, A. Hashimoto, Y. Kuramoto, M. Ito, S. Hikoso, H. Akazawa, J.K. Lee, I. Shiojima, P.J. McKinnon, Y. Sakata, and I. Komuro. 2017. DNA single-strand break-induced DNA damage response causes heart failure. *Nature communications*. 8:15104.

Hirschy, A., F. Schatzmann, E. Ehler, and J.C. Perriard. 2006. Establishment of cardiac cytoarchitecture in the developing mouse heart. *Developmental biology*. 289:430-441.

Ho, C.Y., D.E. Jaalouk, M.K. Vartiainen, and J. Lammerding. 2013. Lamin A/C and emerin regulate MKL1-SRF activity by modulating actin dynamics. *Nature*. 497:507-511.

Huang, D.L., N.A. Bax, C.D. Buckley, W.I. Weis, and A.R. Dunn. 2017. Vinculin forms a directionally asymmetric catch bond with F-actin. *Science*. 357:703-706.

Ihalainen, T.O., L. Aires, F.A. Herzog, R. Schwartlander, J. Moeller, and V. Vogel. 2015. Differential basal-to-apical accessibility of lamin A/C epitopes in the nuclear lamina regulated by changes in cytoskeletal tension. *Nature materials*. 14:1252-1261.

Ingber, D.E. 2006. Cellular mechanotransduction: putting all the pieces together again. *FASEB journal : official publication of the Federation of American Societies for Experimental Biology*. 20:811-827.

Irianto, J., C.R. Pfeifer, R.R. Bennett, Y. Xia, I.L. Ivanovska, A.J. Liu, R.A. Greenberg, and D.E. Discher. 2016a. Nuclear constriction segregates mobile nuclear proteins away from chromatin. *Molecular biology of the cell*.

Irianto, J., C.R. Pfeifer, I.L. Ivanovska, J. Swift, and D.E. Discher. 2016b. Nuclear lamins in cancer. *Cellular and molecular bioengineering*. 9:258-267.

Irianto, J., Y. Xia, C.R. Pfeifer, A. Athirasala, J. Ji, C. Alvey, M. Tewari, R. Bennett, S. Harding, A. Liu, R.A. Greenberg, and D.E. Discher. 2016c. DNA damage follows repair factor depletion and portends genome variation in cancer cells after pore migration. *Current biology : CB*. *In press*.

Irianto, J., Y. Xia, C.R. Pfeifer, A. Athirasala, J. Ji, C. Alvey, M. Tewari, R.R. Bennett, S.M. Harding, A.J. Liu, R.A. Greenberg, and D.E. Discher. 2017. DNA Damage Follows Repair Factor Depletion and Portends Genome Variation in Cancer Cells after Pore Migration. *Current biology : CB*. 27:210-223.

Isermann, P., and J. Lammerding. 2013. Nuclear mechanics and mechanotransduction in health and disease. *Current biology : CB*. 23:R1113-1121.

Ivanovska, I.L., J. Swift, K. Spinler, D. Dingal, S. Cho, and D.E. Discher. 2017. Cross-linked matrix rigidity and soluble retinoids synergize in nuclear lamina regulation of stem cell differentiation. *Molecular biology of the cell*. 28:2010-2022.

Jacot, J.G., A.D. McCulloch, and J.H. Omens. 2008. Substrate stiffness affects the functional maturation of neonatal rat ventricular myocytes. *Biophysical journal*. 95:3479-3487.

Jahn, D., S. Schramm, M. Schnolzer, C.J. Heilmann, C.G. de Koster, W. Schutz, R. Benavente, and M. Alsheimer. 2012. A truncated lamin A in the Lmna -/- mouse line: implications for the understanding of laminopathies. *Nucleus*. 3:463-474.

Jung, H.J., C. Coffinier, Y. Choe, A.P. Beigneux, B.S. Davies, S.H. Yang, R.H. Barnes, 2nd, J. Hong, T. Sun, S.J. Pleasure, S.G. Young, and L.G. Fong. 2012. Regulation of prelamin A but not lamin C by miR-9, a brain-specific microRNA. *Proceedings of the National Academy of Sciences of the United States of America*. 109:E423-431.

Katz, Z.B., A.L. Wells, H.Y. Park, B. Wu, S.M. Shenoy, and R.H. Singer. 2012. beta-Actin mRNA compartmentalization enhances focal adhesion stability and directs cell migration. *Genes & development*. 26:1885-1890.

Kaufmann, S.H., M. Mabry, R. Jasti, and J.H. Shaper. 1991. Differential expression of nuclear envelope lamins A and C in human lung cancer cell lines. *Cancer research*. 51:581-586.

Khatau, S.B., C.M. Hale, P.J. Stewart-Hutchinson, M.S. Patel, C.L. Stewart, P.C. Searson, D. Hodzic, and D. Wirtz. 2009. A perinuclear actin cap regulates nuclear shape. *Proceedings of the National Academy of Sciences of the United States of America*. 106:19017-19022.

Kim, D.H., S. Cho, and D. Wirtz. 2014a. Tight coupling between nucleus and cell migration through the perinuclear actin cap. *Journal of cell science*. 127:2528-2541.

Kim, D.H., B. Li, F. Si, J.M. Phillip, D. Wirtz, and S.X. Sun. 2015. Volume regulation and shape bifurcation in the cell nucleus. *Journal of cell science*. 128:3375-3385.

Kim, D.H., and D. Wirtz. 2015. Cytoskeletal tension induces the polarized architecture of the nucleus. *Biomaterials*. 48:161-172.

Kim, J.S., J. Min, A.K. Recknagel, M. Riccio, and J.T. Butcher. 2011. Quantitative three-dimensional analysis of embryonic chick morphogenesis via microcomputed tomography. *Anatomical record*. 294:1-10.

Kim, M.S., S.M. Pinto, D. Getnet, R.S. Nirujogi, S.S. Manda, R. Chaerkady, A.K. Madugundu, D.S. Kelkar, R. Isserlin, S. Jain, J.K. Thomas, B. Muthusamy, P. Leal-Rojas, P. Kumar, N.A. Sahasrabuddhe, L. Balakrishnan, J. Advani, B. George, S. Renuse, L.D. Selvan, A.H. Patil, V. Nanjappa, A. Radhakrishnan, S. Prasad, T. Subbannayya, R. Raju, M. Kumar, S.K. Sreenivasamurthy, A. Marimuthu, G.J. Sathe, S. Chavan, K.K. Datta, Y. Subbannayya, A. Sahu, S.D. Yelamanchi, S. Jayaram, P. Rajagopalan, J. Sharma, K.R. Murthy, N. Syed, R. Goel, A.A. Khan, S. Ahmad, G. Dey, K. Mudgal, A. Chatterjee, T.C. Huang, J. Zhong, X. Wu, P.G. Shaw, D. Freed, M.S. Zahari, K.K. Mukherjee, S. Shankar, A. Mahadevan, H. Lam, C.J. Mitchell, S.K. Shankar, P. Satishchandra, J.T. Schroeder, R. Sirdeshmukh, A. Maitra, S.D. Leach, C.G. Drake, M.K. Halushka, T.S. Prasad, R.H. Hruban, C.L. Kerr, G.D. Bader, C.A. Iacobuzio-Donahue, H. Gowda, and A. Pandey. 2014b. A draft map of the human proteome. *Nature*. 509:575-581.

Kochin, V., T. Shimi, E. Torvaldson, S.A. Adam, A. Goldman, C.G. Pack, J. Melo-Cardenas, S.Y. Imanishi, R.D. Goldman, and J.E. Eriksson. 2014. Interphase phosphorylation of lamin A. *Journal of cell science*. 127:2683-2696.

Korfali, N., G.S. Wilkie, S.K. Swanson, V. Srsen, J. de Las Heras, D.G. Batrakou, P. Malik, N. Zuleger, A.R. Kerr, L. Florens, and E.C. Schirmer. 2012. The nuclear envelope proteome differs notably between tissues. *Nucleus*. 3:552-564.

Koser, D.E., A.J. Thompson, S.K. Foster, A. Dwivedy, E.K. Pillai, G.K. Sheridan, H. Svoboda, M. Viana, L.D. Costa, J. Guck, C.E. Holt, and K. Franze. 2016. Mechanosensing is critical for axon growth in the developing brain. *Nature neuroscience*.

Kramann, R., R.K. Schneider, D.P. DiRocco, F. Machado, S. Fleig, P.A. Bondzie, J.M. Henderson, B.L. Ebert, and B.D. Humphreys. 2015. Perivascular Gli1+ progenitors are key contributors to injury-induced organ fibrosis. *Cell stem cell*. 16:51-66.

Krieg, M., Y. Arboleda-Estudillo, P.H. Puech, J. Kafer, F. Graner, D.J. Muller, and C.P. Heisenberg. 2008. Tensile forces govern germ-layer organization in zebrafish. *Nature cell biology*. 10:429-436.

Kubben, N., J.W. Voncken, J. Demmers, C. Calis, G. van Almen, Y. Pinto, and T. Misteli. 2010. Identification of differential protein interactors of lamin A and progerin. *Nucleus*. 1:513-525.

Kubben, N., J.W. Voncken, G. Konings, M. van Weeghel, M.M. van den Hoogenhof, M. Gijbels, A. van Erk, K. Schoonderwoerd, B. van den Bosch, V. Dahlmans, C. Calis, S.M. Houten, T. Misteli, and Y.M. Pinto. 2011. Post-natal myogenic and adipogenic developmental: defects and metabolic impairment upon loss of A-type lamins. *Nucleus*. 2:195-207.

Kumar, A., M. Mazzanti, M. Mistrik, M. Kosar, G.V. Beznoussenko, A.A. Mironov, M. Garre, D. Parazzoli, G.V. Shivashankar, G. Scita, J. Bartek, and M. Foiani. 2014. ATR mediates a checkpoint at the nuclear envelope in response to mechanical stress. *Cell*. 158:633-646.

Lahmers, S., Y. Wu, D.R. Call, S. Labeit, and H. Granzier. 2004. Developmental control of titin isoform expression and passive stiffness in fetal and neonatal myocardium. *Circulation research*. 94:505-513.

Lammerding, J., L.G. Fong, J.Y. Ji, K. Reue, C.L. Stewart, S.G. Young, and R.T. Lee. 2006. Lamins A and C but not lamin B1 regulate nuclear mechanics. *The Journal of biological chemistry*. 281:25768-25780.

Lammerding, J., J. Hsiao, P.C. Schulze, S. Kozlov, C.L. Stewart, and R.T. Lee. 2005. Abnormal nuclear shape and impaired mechanotransduction in emerin-deficient cells. *The Journal of cell biology*. 170:781-791.

Larrieu, D., S. Britton, M. Demir, R. Rodriguez, and S.P. Jackson. 2014. Chemical inhibition of NAT10 corrects defects of laminopathic cells. *Science*. 344:527-532.

Le, H.Q., S. Ghatak, C.Y. Yeung, F. Tellkamp, C. Gunschmann, C. Dieterich, A. Yeroslaviz, B. Habermann, A. Pombo, C.M. Niessen, and S.A. Wickstrom. 2016. Mechanical regulation of transcription controls Polycomb-mediated gene silencing during lineage commitment. *Nature cell biology*. 18:864-875.

Lee, Y.K., Y.M. Lau, Z.J. Cai, W.H. Lai, L.Y. Wong, H.F. Tse, K.M. Ng, and C.W. Siu. 2017. Modeling Treatment Response for Lamin A/C Related Dilated Cardiomyopathy in Human Induced Pluripotent Stem Cells. *Journal of the American Heart Association*. 6.

Lehner, C.F., R. Stick, H.M. Eppenberger, and E.A. Nigg. 1987. Differential expression of nuclear lamin proteins during chicken development. *The Journal of cell biology*. 105:577-587.

Li, C.X., N.P. Talele, S. Boo, A. Koehler, E. Knee-Walden, J.L. Balestrini, P. Speight, A. Kapus, and B. Hinz. 2017. MicroRNA-21 preserves the fibrotic mechanical memory of mesenchymal stem cells. *Nature materials*. 16:379-389.

Li, Y., J.S. Chu, K. Kurpinski, X. Li, D.M. Bautista, L. Yang, K.L. Sung, and S. Li. 2011. Biophysical regulation of histone acetylation in mesenchymal stem cells. *Biophysical journal*. 100:1902-1909.

Liu, B., J. Wang, K.M. Chan, W.M. Tjia, W. Deng, X. Guan, J.D. Huang, K.M. Li, P.Y. Chau, D.J. Chen, D. Pei, A.M. Pendas, J. Cadinanos, C. Lopez-Otin, H.F. Tse, C. Hutchison, J. Chen, Y. Cao, K.S. Cheah, K. Tryggvason, and Z. Zhou. 2005. Genomic instability in laminopathy-based premature aging. *Nature medicine*. 11:780-785.

Liu, G.H., B.Z. Barkho, S. Ruiz, D. Diep, J. Qu, S.L. Yang, A.D. Panopoulos, K. Suzuki, L. Kurian, C. Walsh, J. Thompson, S. Boue, H.L. Fung, I. Sancho-Martinez, K. Zhang, J. Yates, 3rd, and J.C. Izpisua Belmonte. 2011. Recapitulation of premature ageing with iPSCs from Hutchinson-Gilford progeria syndrome. *Nature*. 472:221-225.

Liu, Y., A. Rusinol, M. Sinensky, Y. Wang, and Y. Zou. 2006. DNA damage responses in progeroid syndromes arise from defective maturation of prelamin A. *Journal of cell science*. 119:4644-4649.

Lloyd, D.J., R.C. Trembath, and S. Shackleton. 2002. A novel interaction between lamin A and SREBP1: implications for partial lipodystrophy and other laminopathies. *Human molecular genetics*. 11:769-777.

Lo Cicero, A., A.L. Jaskowiak, A.L. Egesipe, J. Tournois, B. Brinon, P.R. Pitrez, L. Ferreira, A. de Sandre-Giovannoli, N. Levy, and X. Nissan. 2016. A High Throughput Phenotypic Screening reveals compounds that counteract premature osteogenic differentiation of HGPS iPS-derived mesenchymal stem cells. *Scientific reports*. 6:34798.

Lovett, D.B., N. Shekhar, J.A. Nickerson, K.J. Roux, and T.P. Lele. 2013. Modulation of Nuclear Shape by Substrate Rigidity. *Cellular and molecular bioengineering*. 6:230-238.

Maharana, S., K.V. Iyer, N. Jain, M. Nagarajan, Y. Wang, and G.V. Shivashankar. 2016. Chromosome intermingling-the physical basis of chromosome organization in differentiated cells. *Nucleic acids research*. 44:5148-5160.

Majkut, S., T. Idema, J. Swift, C. Krieger, A. Liu, and D.E. Discher. 2013. Heart-specific stiffening in early embryos parallels matrix and myosin expression to optimize beating. *Current biology : CB*. 23:2434-2439.

Margalit, A., M. Segura-Totten, Y. Gruenbaum, and K.L. Wilson. 2005. Barrier-to-autointegration factor is required to segregate and enclose chromosomes within the nuclear envelope and assemble the nuclear lamina. *Proceedings of the National Academy of Sciences of the United States of America*. 102:3290-3295.

Marganski, W.A., M. Dembo, and Y.L. Wang. 2003. Measurements of cell-generated deformations on flexible substrata using correlation-based optical flow. *Methods in enzymology*. 361:197-211.

Martinsen, B.J. 2005. Reference guide to the stages of chick heart embryology. *Developmental dynamics : an official publication of the American Association of Anatomists*. 233:1217-1237.

McClintock, D., D. Ratner, M. Lokuge, D.M. Owens, L.B. Gordon, F.S. Collins, and K. Djabali. 2007. The mutant form of lamin A that causes Hutchinson-Gilford progeria is a biomarker of cellular aging in human skin. *PloS one*. 2:e1269.

Meshorer, E., D. Yellajoshula, E. George, P.J. Scambler, D.T. Brown, and T. Misteli. 2006. Hyperdynamic plasticity of chromatin proteins in pluripotent embryonic stem cells. *Developmental cell*. 10:105-116.

Mih, J.D., A. Marinkovic, F. Liu, A.S. Sharif, and D.J. Tschumperlin. 2012. Matrix stiffness reverses the effect of actomyosin tension on cell proliferation. *Journal of cell science*. 125:5974-5983.

Moir, R.D., M. Yoon, S. Khuon, and R.D. Goldman. 2000. Nuclear lamins A and B1: different pathways of assembly during nuclear envelope formation in living cells. *The Journal of cell biology*. 151:1155-1168.

Moiseeva, O., S. Lopes-Paciencia, G. Huot, F. Lessard, and G. Ferbeyre. 2016. Permanent farnesylation of lamin A mutants linked to progeria impairs its phosphorylation at serine 22 during interphase. *Aging*. 8:366-381.

Muchir, A., G. Bonne, A.J. van der Kooi, M. van Meegen, F. Baas, P.A. Bolhuis, M. de Visser, and K. Schwartz. 2000. Identification of mutations in the gene encoding lamins A/C in autosomal dominant limb girdle muscular dystrophy with atrioventricular conduction disturbances (LGMD1B). *Human molecular genetics*. 9:1453-1459.

Munjal, A., J.M. Philippe, E. Munro, and T. Lecuit. 2015. A self-organized biomechanical network drives shape changes during tissue morphogenesis. *Nature*. 524:351-355.

Murphy, A.J., J. Pierce, C. de Caestecker, J. Libes, D. Neblett, M. de Caestecker, A.O. Perantoni, S. Tanigawa, J.R. Anderson, J.S. Dome, A. Das, T.J. Carroll, and H.N. Lovvorn, 3rd. 2014. Aberrant activation, nuclear localization, and phosphorylation of Yes-associated protein-1 in the embryonic kidney and Wilms tumor. *Pediatric blood & cancer*. 61:198-205.

Muslimovic, A., S. Nystrom, Y. Gao, and O. Hammarsten. 2009. Numerical analysis of etoposide induced DNA breaks. *PloS one*. 4:e5859.

Naeem, A.S., Y. Zhu, W.L. Di, S. Marmiroli, and R.F. O'Shaughnessy. 2015. AKT1-mediated Lamin A/C degradation is required for nuclear degradation and normal epidermal terminal differentiation. *Cell death and differentiation*. 22:2123-2132.

Naetar, N., S. Ferraioli, and R. Foisner. 2017. Lamins in the nuclear interior - life outside the lamina. *Journal of cell science*. 130:2087-2096.

Narula, N., V. Favalli, P. Tarantino, M. Grasso, A. Pilotto, R. Bellazzi, A. Serio, F.I. Gambarin, P. Charron, B. Meder, Y. Pinto, P.M. Elliott, J. Mogensen, M. Bolognesi, M. Bollati, and E. Arbustini. 2012. Quantitative expression of the mutated lamin A/C gene in patients with cardiolaminopathy. *Journal of the American College of Cardiology*. 60:1916-1920.

Neelam, S., T.J. Chancellor, Y. Li, J.A. Nickerson, K.J. Roux, R.B. Dickinson, and T.P. Lele. 2015. Direct force probe reveals the mechanics of nuclear homeostasis in the mammalian cell. *Proceedings of the National Academy of Sciences of the United States of America*. 112:5720-5725.

Okumura, K., K. Nakamachi, Y. Hosoe, and N. Nakajima. 2000. Identification of a novel retinoic acid-responsive element within the lamin A/C promoter. *Biochemical and biophysical research communications*. 269:197-202.

Osmanagic-Myers, S., T. Dechat, and R. Foisner. 2015. Lamins at the crossroads of mechanosignaling. *Genes & development*. 29:225-237.

Osorio, F.G., C.L. Navarro, J. Cadinanos, I.C. Lopez-Mejia, P.M. Quiros, C. Bartoli, J. Rivera, J. Tazi, G. Guzman, I. Varela, D. Depetris, F. de Carlos, J. Cobo, V. Andres, A. De Sandre-Giovannoli, J.M. Freije, N. Levy, and C. Lopez-Otin. 2011. Splicing-directed therapy in a new mouse model of human accelerated aging. *Science translational medicine*. 3:106ra107.

Paddy, M.R., A.S. Belmont, H. Saumweber, D.A. Agard, and J.W. Sedat. 1990. Interphase nuclear envelope lamins form a discontinuous network that interacts with only a fraction of the chromatin in the nuclear periphery. *Cell*. 62:89-106.

Pajerowski, J.D., K.N. Dahl, F.L. Zhong, P.J. Sammak, and D.E. Discher. 2007. Physical plasticity of the nucleus in stem cell differentiation. *Proceedings of the National Academy of Sciences of the United States of America*. 104:15619-15624.

Pasapera, A.M., I.C. Schneider, E. Rericha, D.D. Schlaepfer, and C.M. Waterman. 2010. Myosin II activity regulates vinculin recruitment to focal adhesions through FAK-mediated paxillin phosphorylation. *The Journal of cell biology*. 188:877-890.

Paszek, M.J., N. Zahir, K.R. Johnson, J.N. Lakins, G.I. Rozenberg, A. Gefen, C.A. Reinhart-King, S.S. Margulies, M. Dembo, D. Boettiger, D.A. Hammer, and V.M. Weaver. 2005. Tensional homeostasis and the malignant phenotype. *Cancer cell*. 8:241-254.

Pelham, R.J., Jr., and Y. Wang. 1997. Cell locomotion and focal adhesions are regulated by substrate flexibility. *Proceedings of the National Academy of Sciences of the United States of America*. 94:13661-13665.

Pellegrini, C., M. Columbaro, C. Capanni, M.R. D'Apice, C. Cavallo, M. Murdocca, G. Lattanzi, and S. Squarzoni. 2015. All-trans retinoic acid and rapamycin normalize Hutchinson Gilford progeria fibroblast phenotype. *Oncotarget*. 6:29914-29928.

Peters, B.A., B.G. Kermani, O. Alferov, M.R. Agarwal, M.A. McElwain, N. Gulbahce, D.M. Hayden, Y.T. Tang, R.Y. Zhang, R. Tearle, B. Crain, R. Prates, A. Berkeley, S. Munne, and R. Drmanac. 2015. Detection and phasing of single base de novo mutations in biopsies from human in vitro fertilized embryos by advanced whole-genome sequencing. *Genome research*. 25:426-434.

Pfeifer, C.R., Y. Xia, K. Zhu, D. Liu, J. Irianto, S.M. Harding, R.A. Greenberg, and D.E. Discher. 2017. Cell cycle repression and DNA repair defects follow constricted migration. *bioRxiv*.

Poh, Y.C., S.P. Shevtsov, F. Chowdhury, D.C. Wu, S. Na, M. Dundr, and N. Wang. 2012. Dynamic force-induced direct dissociation of protein complexes in a nuclear body in living cells. *Nature communications*. 3:866.

Poleshko, A., P.P. Shah, M. Gupta, A. Babu, M.P. Morley, L.J. Manderfield, J.L. Ifkovits, D. Calderon, H. Aghajanian, J.E. Sierra-Pagan, Z. Sun, Q. Wang, L. Li, N.C. Dubois, E.E. Morrisey, M.A. Lazar, C.L. Smith, J.A. Epstein, and R. Jain. 2017. Genome-Nuclear Lamina Interactions Regulate Cardiac Stem Cell Lineage Restriction. *Cell*. 171:573-587 e514.

Prudova, A., U. auf dem Keller, G.S. Butler, and C.M. Overall. 2010. Multiplex N-terminome analysis of MMP-2 and MMP-9 substrate degradomes by iTRAQ-TAILS quantitative proteomics. *Molecular & cellular proteomics : MCP*. 9:894-911.

Przybyla, L., J.N. Lakins, and V.M. Weaver. 2016. Tissue Mechanics Orchestrate Wnt-Dependent Human Embryonic Stem Cell Differentiation. *Cell stem cell*. 19:462-475.

Puente, B.N., W. Kimura, S.A. Muralidhar, J. Moon, J.F. Amatruda, K.L. Phelps, D. Grinsfelder, B.A. Rothermel, R. Chen, J.A. Garcia, C.X. Santos, S. Thet, E. Mori, M.T. Kinter, P.M. Rindler, S. Zacchigna, S. Mukherjee, D.J. Chen, A.I. Mahmoud, M. Giacca, P.S. Rabinovitch, A. Aroumougame, A.M. Shah, L.I. Szweda, and H.A. Sadek. 2014. The oxygen-rich postnatal environment induces cardiomyocyte cell-cycle arrest through DNA damage response. *Cell*. 157:565-579.

Pugh, G.E., P.J. Coates, E.B. Lane, Y. Raymond, and R.A. Quinlan. 1997. Distinct nuclear assembly pathways for lamins A and C lead to their increase during quiescence in Swiss 3T3 cells. *Journal of cell science*. 110 (Pt 19):2483-2493.

Raab, M., M. Gentili, H. de Belly, H.R. Thiam, P. Vargas, A.J. Jimenez, F. Lautenschlaeger, R. Voituriez, A.M. Lennon-Dumenil, N. Manel, and M. Piel. 2016. ESCRT III repairs nuclear envelope ruptures during cell migration to limit DNA damage and cell death. *Science*. 352:359-362.

Rajala, G.M., J.H. Kalbfleisch, and S. Kaplan. 1976. Evidence that blood pressure controls heart rate in the chick embryo prior to neural control. *Journal of embryology and experimental morphology*. 36:685-695.

Rajan, S., S.S. Williams, G. Jagatheesan, R.P. Ahmed, G. Fuller-Bicer, A. Schwartz, B.J. Aronow, and D.F. Wieczorek. 2006. Microarray analysis of gene expression during early stages of mild and severe cardiac hypertrophy. *Physiological genomics*. 27:309-317.

Reddel, C.J., and A.S. Weiss. 2004. Lamin A expression levels are unperturbed at the normal and mutant alleles but display partial splice site selection in Hutchinson-Gilford progeria syndrome. *Journal of medical genetics*. 41:715-717.

Redwood, A.B., S.M. Perkins, R.P. Vanderwaal, Z. Feng, K.J. Biehl, I. Gonzalez-Suarez, L. Morgado-Palacin, W. Shi, J. Sage, J.L. Roti-Roti, C.L. Stewart, J. Zhang, and S. Gonzalo. 2011. A dual role for A-type lamins in DNA double-strand break repair. *Cell cycle*. 10:2549-2560.

Rhinn, M., and P. Dolle. 2012. Retinoic acid signalling during development. *Development*. 139:843-858.

Ribeiro, A.J., Y.S. Ang, J.D. Fu, R.N. Rivas, T.M. Mohamed, G.C. Higgs, D. Srivastava, and B.L. Pruitt. 2015. Contractility of single cardiomyocytes differentiated from pluripotent stem cells depends on physiological shape and substrate stiffness. *Proceedings of the National Academy of Sciences of the United States of America*. 112:12705-12710.

Rober, R.A., K. Weber, and M. Osborn. 1989. Differential timing of nuclear lamin A/C expression in the various organs of the mouse embryo and the young animal: a developmental study. *Development*. 105:365-378.

Robison, P., M.A. Caporizzo, H. Ahmadzadeh, A.I. Bogush, C.Y. Chen, K.B. Margulies, V.B. Shenoy, and B.L. Prosser. 2016. Detyrosinated microtubules buckle and bear load in contracting cardiomyocytes. *Science*. 352:aaf0659.

Rodriguez, J., F. Calvo, J.M. Gonzalez, B. Casar, V. Andres, and P. Crespo. 2010. ERK1/2 MAP kinases promote cell cycle entry by rapid, kinase-independent disruption of retinoblastoma-lamin A complexes. *The Journal of cell biology*. 191:967-979.

Rodriguez, S., F. Coppede, H. Sagelius, and M. Eriksson. 2009. Increased expression of the Hutchinson-Gilford progeria syndrome truncated lamin A transcript during cell aging. *European journal of human genetics : EJHG*. 17:928-937.

Rozario, T., and D.W. DeSimone. 2010. The extracellular matrix in development and morphogenesis: a dynamic view. *Developmental biology*. 341:126-140.

Sawada, Y., M. Tamada, B.J. Dubin-Thaler, O. Cherniavskaya, R. Sakai, S. Tanaka, and M.P. Sheetz. 2006. Force sensing by mechanical extension of the Src family kinase substrate p130Cas. *Cell*. 127:1015-1026.

Scaffidi, P., and T. Misteli. 2005. Reversal of the cellular phenotype in the premature aging disease Hutchinson-Gilford progeria syndrome. *Nature medicine*. 11:440-445.

Scaffidi, P., and T. Misteli. 2008. Lamin A-dependent misregulation of adult stem cells associated with accelerated ageing. *Nature cell biology*. 10:452-459.

Schirmer, E.C., L. Florens, T. Guan, J.R. Yates, 3rd, and L. Gerace. 2003. Nuclear membrane proteins with potential disease links found by subtractive proteomics. *Science*. 301:1380-1382.

Sen, S., and S. Kumar. 2009. Cell-Matrix De-Adhesion Dynamics Reflect Contractile Mechanics. *Cellular and molecular bioengineering*. 2:218-230.

Serebryannyy, L., and T. Misteli. 2017. Protein sequestration at the nuclear periphery as a potential regulatory mechanism in premature aging. *The Journal of cell biology*.

Shanbhag, N.M., I.U. Rafalska-Metcalf, C. Balane-Bolivar, S.M. Janicki, and R.A. Greenberg. 2010. ATM-dependent chromatin changes silence transcription in cis to DNA double-strand breaks. *Cell*. 141:970-981.

Shao, X., Q. Li, A. Mogilner, A.D. Bershadsky, and G.V. Shivashankar. 2015. Mechanical stimulation induces formin-dependent assembly of a perinuclear actin rim. *Proceedings of the National Academy of Sciences of the United States of America*. 112:E2595-2601.

Shimi, T., M. Kittisopikul, J. Tran, A.E. Goldman, S.A. Adam, Y. Zheng, K. Jaqaman, and R.D. Goldman. 2015. Structural organization of nuclear lamins A, C, B1, and B2 revealed by superresolution microscopy. *Molecular biology of the cell*. 26:4075-4086.

Shin, J.W., A. Buxboim, K.R. Spinler, J. Swift, D.A. Christian, C.A. Hunter, C. Leon, C. Gachet, P.C. Dingal, I.L. Ivanovska, F. Rehfeldt, J.A. Chasis, and D.E. Discher. 2014. Contractile forces sustain and polarize hematopoiesis from stem and progenitor cells. *Cell stem cell*. 14:81-93.

Shoulders, M.D., and R.T. Raines. 2009. Collagen structure and stability. *Annual review of biochemistry*. 78:929-958.

Shukla, P.C., K.K. Singh, A. Quan, M. Al-Omran, H. Teoh, F. Lovren, L. Cao, Rovira, II, Y. Pan, C. Brezden-Masley, B. Yanagawa, A. Gupta, C.X. Deng, J.G. Coles, H. Leong-Poi, W.L. Stanford, T.G. Parker, M.D. Schneider, T. Finkel, and S. Verma. 2011. BRCA1 is an essential regulator of heart function and survival following myocardial infarction. *Nature communications*. 2:593.

Singh, M., C.R. Hunt, R.K. Pandita, R. Kumar, C.R. Yang, N. Horikoshi, R. Bachoo, S. Serag, M.D. Story, J.W. Shay, S.N. Powell, A. Gupta, J. Jeffery, S. Pandita, B.P. Chen, D. Deckbar, M. Lobrich, Q. Yang, K.K. Khanna, H.J. Worman, and T.K. Pandita. 2013. Lamin A/C depletion enhances DNA damage-induced stalled replication fork arrest. *Molecular and cellular biology*. 33:1210-1222.

Siu, C.W., Y.K. Lee, J.C. Ho, W.H. Lai, Y.C. Chan, K.M. Ng, L.Y. Wong, K.W. Au, Y.M. Lau, J. Zhang, K.W. Lay, A. Colman, and H.F. Tse. 2012. Modeling of lamin A/C mutation premature cardiac aging using patient-specific induced pluripotent stem cells. *Aging*. 4:803-822.

Solovei, I., A.S. Wang, K. Thanisch, C.S. Schmidt, S. Krebs, M. Zwerger, T.V. Cohen, D. Devys, R. Foisner, L. Peichl, H. Herrmann, H. Blum, D. Engelkamp, C.L. Stewart, H. Leonhardt, and B. Joffe. 2013. LBR and lamin A/C sequentially tether peripheral heterochromatin and inversely regulate differentiation. *Cell*. 152:584-598.

Song, J., H. Tan, A.J. Perry, T. Akutsu, G.I. Webb, J.C. Whisstock, and R.N. Pike. 2012. PROSPER: an integrated feature-based tool for predicting protease substrate cleavage sites. *PloS one*. 7:e50300.

Soubeyrand, S., L. Pope, and R.J. Hache. 2010. Topoisomerase IIalpha-dependent induction of a persistent DNA damage response in response to transient etoposide exposure. *Molecular oncology*. 4:38-51.

Stephens, A.D., E.J. Banigan, S.A. Adam, R.D. Goldman, and J.F. Marko. 2017. Chromatin and lamin A determine two different mechanical response regimes of the cell nucleus. *Molecular biology of the cell*. 28:1984-1996.

Stewart, C., and B. Burke. 1987. Teratocarcinoma stem cells and early mouse embryos contain only a single major lamin polypeptide closely resembling lamin B. *Cell*. 51:383-392.

Sullivan, T., D. Escalante-Alcalde, H. Bhatt, M. Anver, N. Bhat, K. Nagashima, C.L. Stewart, and B. Burke. 1999. Loss of A-type lamin expression compromises nuclear envelope integrity leading to muscular dystrophy. *The Journal of cell biology*. 147:913-920.

Sun, S., M.Z. Xu, R.T. Poon, P.J. Day, and J.M. Luk. 2010. Circulating Lamin B1 (LMNB1) biomarker detects early stages of liver cancer in patients. *Journal of proteome research*. 9:70-78.

Sun, Y., K.M. Yong, L.G. Villa-Diaz, X. Zhang, W. Chen, R. Philson, S. Weng, H. Xu, P.H. Krebsbach, and J. Fu. 2014. Hippo/YAP-mediated rigidity-dependent motor neuron differentiation of human pluripotent stem cells. *Nature materials*. 13:599-604.

Swift, J., I.L. Ivanovska, A. Buxboim, T. Harada, P.C. Dingal, J. Pinter, J.D. Pajerowski, K.R. Spinler, J.W. Shin, M. Tewari, F. Rehfeldt, D.W. Speicher, and D.E. Discher. 2013. Nuclear lamin-A scales with tissue stiffness and enhances matrix-directed differentiation. *Science*. 341:1240104.

Taber, L.A., H. Sun, E.B. Clark, and B.B. Keller. 1994. Epicardial strains in embryonic chick ventricle at stages 16 through 24. *Circulation research*. 75:896-903.

Taimen, P., K. Pfleghaar, T. Shimi, D. Moller, K. Ben-Harush, M.R. Erdos, S.A. Adam, H. Herrmann, O. Medalia, F.S. Collins, A.E. Goldman, and R.D. Goldman. 2009. A progeria mutation reveals functions for lamin A in nuclear assembly, architecture, and chromosome organization. *Proceedings of the National Academy of Sciences of the United States of America*. 106:20788-20793.

Tajik, A., Y. Zhang, F. Wei, J. Sun, Q. Jia, W. Zhou, R. Singh, N. Khanna, A.S. Belmont, and N. Wang. 2016. Transcription upregulation via force-induced direct stretching of chromatin. *Nature materials*.

Tamiello, C., M.A. Kamps, A. van den Wijngaard, V.L. Verstraeten, F.P. Baaijens, J.L. Broers, and C.C. Bouten. 2013. Soft substrates normalize nuclear morphology and prevent nuclear rupture in fibroblasts from a laminopathy patient with compound heterozygous LMNA mutations. *Nucleus*. 4:61-73.

Tammaro, M., P. Barr, B. Ricci, and H. Yan. 2013. Replication-dependent and transcription-dependent mechanisms of DNA double-strand break induction by the topoisomerase 2-targeting drug etoposide. *PloS one*. 8:e79202.

Taylor, M.R., D. Slavov, A. Gajewski, S. Vlcek, L. Ku, P.R. Fain, E. Carniel, A. Di Lenarda, G. Sinagra, M.M. Boucek, J. Cavanaugh, S.L. Graw, P. Ruegg, J. Feiger, X. Zhu, D.A. Ferguson, M.R. Bristow, J. Gotzmann, R. Foisner, L. Mestroni, and G. Familial Cardiomyopathy Registry Research. 2005. Thymopoietin (lamina-associated polypeptide 2) gene mutation associated with dilated cardiomyopathy. *Human mutation*. 26:566-574.

Theret, D.P., M.J. Levesque, M. Sato, R.M. Nerem, and L.T. Wheeler. 1988. The application of a homogeneous half-space model in the analysis of endothelial cell micropipette measurements. *Journal of biomechanical engineering*. 110:190-199.

Torvaldson, E., V. Kochin, and J.E. Eriksson. 2015. Phosphorylation of lamins determine their structural properties and signaling functions. *Nucleus*. 6:166-171.

Trichet, L., J. Le Digabel, R.J. Hawkins, S.R. Vedula, M. Gupta, C. Ribrault, P. Hersen, R. Voituriez, and B. Ladoux. 2012. Evidence of a large-scale mechanosensing mechanism for cellular adaptation to substrate stiffness. *Proceedings of the National Academy of Sciences of the United States of America*. 109:6933-6938.

Turgay, Y., M. Eibauer, A.E. Goldman, T. Shimi, M. Khayat, K. Ben-Harush, A. Dubrovsky-Gaupp, K.T. Sapra, R.D. Goldman, and O. Medalia. 2017. The molecular architecture of lamins in somatic cells. *Nature*. 543:261-264.

Tzatzalos, E., O.J. Abilez, P. Shukla, and J.C. Wu. 2016. Engineered heart tissues and induced pluripotent stem cells: Macro- and microstructures for disease modeling, drug screening, and translational studies. *Advanced drug delivery reviews*. 96:234-244.

Uebbing, S., A. Konzer, L. Xu, N. Backstrom, B. Brunstrom, J. Bergquist, and H. Ellegren. 2015. Quantitative Mass Spectrometry Reveals Partial Translational Regulation for Dosage Compensation in Chicken. *Molecular biology and evolution*. 32:2716-2725.

Uhler, C., and G.V. Shivashankar. 2017. Regulation of genome organization and gene expression by nuclear mechanotransduction. *Nature reviews. Molecular cell biology*. 18:717-727.

Ulrich, T.A., E.M. de Juan Pardo, and S. Kumar. 2009. The mechanical rigidity of the extracellular matrix regulates the structure, motility, and proliferation of glioma cells. *Cancer research*. 69:4167-4174.

van der Rest, M., and R. Garrone. 1991. Collagen family of proteins. *FASEB journal : official publication of the Federation of American Societies for Experimental Biology*. 5:2814-2823.

Vanneste, E., T. Voet, C. Le Caignec, M. Ampe, P. Konings, C. Melotte, S. Debrock, M. Amyere, M. Vikkula, F. Schuit, J.P. Fryns, G. Verbeke, T. D'Hooghe, Y. Moreau, and J.R. Vermeesch. 2009. Chromosome instability is common in human cleavage-stage embryos. *Nature medicine*. 15:577-583.

Vargas, J.D., E.M. Hatch, D.J. Anderson, and M.W. Hetzer. 2012. Transient nuclear envelope rupturing during interphase in human cancer cells. *Nucleus*. 3:88-100.

Vartiainen, M.K., S. Guettler, B. Larijani, and R. Treisman. 2007. Nuclear actin regulates dynamic subcellular localization and activity of the SRF cofactor MAL. *Science*. 316:1749-1752.

Versaevel, M., T. Grevesse, and S. Gabriele. 2012. Spatial coordination between cell and nuclear shape within micropatterned endothelial cells. *Nature communications*. 3:671.

Vidak, S., and R. Foisner. 2016. Molecular insights into the premature aging disease progeria. *Histochemistry and cell biology*. 145:401-417.

Vidak, S., N. Kubben, T. Dechat, and R. Foisner. 2015. Proliferation of progeria cells is enhanced by lamina-associated polypeptide 2alpha (LAP2alpha) through expression of extracellular matrix proteins. *Genes & development*. 29:2022-2036.

Vizcaino, J.A., A. Csordas, N. del-Toro, J.A. Dianes, J. Griss, I. Lavidas, G. Mayer, Y. Perez-Riverol, F. Reisinger, T. Ternent, Q.W. Xu, R. Wang, and H. Hermjakob. 2016. 2016 update of the PRIDE database and its related tools. *Nucleic acids research*. 44:D447-456.

Wang, L., W. Yang, W. Ju, P. Wang, X. Zhao, E.C. Jenkins, W.T. Brown, and N. Zhong. 2012. A proteomic study of Hutchinson-Gilford progeria syndrome: Application of 2D-chromotography in a premature aging disease. *Biochemical and biophysical research communications*. 417:1119-1126.

Wang, N., and D.E. Ingber. 1994. Control of cytoskeletal mechanics by extracellular matrix, cell shape, and mechanical tension. *Biophysical journal*. 66:2181-2189.

Wang, S., R. Sekiguchi, W.P. Daley, and K.M. Yamada. 2017. Patterned cell and matrix dynamics in branching morphogenesis. *The Journal of cell biology*. 216:559-570.

Wang, S., E. Stoops, U. Cp, B. Markus, A. Reuveny, E. Ordan, and T. Volk. 2018. Mechanotransduction via the LINC complex regulates DNA replication in myonuclei. *The Journal of cell biology*.

West, G., J. Gullmets, L. Virtanen, S.P. Li, A. Keinanen, T. Shimi, M. Mauermann, T. Helio, M. Kaartinen, L. Ollila, J. Kuusisto, J.E. Eriksson, R.D. Goldman, H. Herrmann, and P. Taimen. 2016. Deleterious assembly of the lamin A/C mutant p.S143P causes ER stress in familial dilated cardiomyopathy. *Journal of cell science*. 129:2732-2743.

Wheaton, K., D. Campuzano, W. Ma, M. Sheinis, B. Ho, G.W. Brown, and S. Benchimol. 2017. Progerin-Induced Replication Stress Facilitates Premature Senescence in Hutchinson-Gilford Progeria Syndrome. *Molecular and cellular biology*. 37.

Wilson, K.L., and R. Foisner. 2010. Lamin-binding Proteins. *Cold Spring Harbor perspectives in biology*. 2:a000554.

Woessner, J.F., Jr., R.I. Bashey, and R.J. Boucek. 1967. Collagen development in heart and skin of the chick embryo. *Biochimica et biophysica acta*. 140:329-338.

Wolberg, W.H., W.N. Street, and O.L. Mangasarian. 1999. Importance of nuclear morphology in breast cancer prognosis. *Clinical cancer research : an official journal of the American Association for Cancer Research*. 5:3542-3548.

Worman, H.J. 2012. Nuclear lamins and laminopathies. *The Journal of pathology*. 226:316-325.

Worman, H.J., and G. Bonne. 2007. "Laminopathies": a wide spectrum of human diseases. *Experimental cell research*. 313:2121-2133.

Wozniak, M.A., and C.S. Chen. 2009. Mechanotransduction in development: a growing role for contractility. *Nature reviews. Molecular cell biology*. 10:34-43.

Xie, W., A. Chojnowski, T. Boudier, J.S. Lim, S. Ahmed, Z. Ser, C. Stewart, and B. Burke. 2016. A-type Lamins Form Distinct Filamentous Networks with Differential Nuclear Pore Complex Associations. *Current biology : CB*. 26:2651-2658.

Xie, Y., A. Mustafa, A. Yerzhan, D. Merzhakupova, P. Yerlan, N.O. A, X. Wang, Y. Huang, and L. Miao. 2017. Nuclear matrix metalloproteinases: functions resemble the evolution from the intracellular to the extracellular compartment. *Cell death discovery*. 3:17036.

Yahalom-Ronen, Y., D. Rajchman, R. Sarig, B. Geiger, and E. Tzahor. 2015. Reduced matrix rigidity promotes neonatal cardiomyocyte dedifferentiation, proliferation and clonal expansion. *eLife*. 4.

Yang, C., M.W. Tibbitt, L. Basta, and K.S. Anseth. 2014a. Mechanical memory and dosing influence stem cell fate. *Nature materials*. 13:645-652.

Yang, X., L. Pabon, and C.E. Murry. 2014b. Engineering adolescence: maturation of human pluripotent stem cell-derived cardiomyocytes. *Circulation research*. 114:511-523.

Yang, Y., E. Candelario-Jalil, J.F. Thompson, E. Cuadrado, E.Y. Estrada, A. Rosell, J. Montaner, and G.A. Rosenberg. 2010. Increased intranuclear matrix metalloproteinase activity in neurons interferes with oxidative DNA repair in focal cerebral ischemia. *Journal of neurochemistry*. 112:134-149.

Yang, Y.L., L.M. Leone, and L.J. Kaufman. 2009. Elastic moduli of collagen gels can be predicted from two-dimensional confocal microscopy. *Biophysical journal*. 97:2051-2060.

Zaidel-Bar, R., R. Milo, Z. Kam, and B. Geiger. 2007. A paxillin tyrosine phosphorylation switch regulates the assembly and form of cell-matrix adhesions. *Journal of cell science*. 120:137-148.

Zhang, J., Q. Lian, G. Zhu, F. Zhou, L. Sui, C. Tan, R.A. Mutalif, R. Navasankari, Y. Zhang, H.F. Tse, C.L. Stewart, and A. Colman. 2011. A human iPSC model of Hutchinson Gilford Progeria reveals vascular smooth muscle and mesenchymal stem cell defects. *Cell stem cell*. 8:31-45.

Zhang, Q., C. Bethmann, N.F. Worth, J.D. Davies, C. Wasner, A. Feuer, C.D. Ragnauth, Q. Yi, J.A. Mellad, D.T. Warren, M.A. Wheeler, J.A. Ellis, J.N. Skepper, M. Vorgerd, B. Schlotter-Weigel, P.L. Weissberg, R.G. Roberts, M. Wehnert, and C.M. Shanahan. 2007. Nesprin-1 and -2 are involved in the pathogenesis of Emery Dreifuss muscular dystrophy and are critical for nuclear envelope integrity. *Human molecular genetics*. 16:2816-2833.

Zimowska, M., M. Swierczynska, and M.A. Ciemerych. 2013. Nuclear MMP-9 role in the regulation of rat skeletal myoblasts proliferation. *Biology of the cell*. 105:334-344.

Zou, L., Y. Luo, M. Chen, G. Wang, M. Ding, C.C. Petersen, R. Kang, F. Dagnaes-Hansen, Y. Zeng, N. Lv, Q. Ma, D.Q. Le, F. Besenbacher, L. Bolund, T.G. Jensen, J. Kjems, W.T. Pu,

and C. Bunger. 2013. A simple method for deriving functional MSCs and applied for osteogenesis in 3D scaffolds. *Scientific reports*. 3:2243.